Statistical Field Estimation and Scale Estimation for Complex Coastal Regions and Archipelagos

by

Arpit Agarwal

Submitted to the Department of Mechanical Engineering
in partial fulfillment of the requirements for the degree of

Master of Science in Mechanical Engineering

at the

MASSACHUSETTS INSTITUTE OF TECHNOLOGY

May 2009

© Massachusetts Institute of Technology 2009. All rights reserved.

Author .....
Department of Mechanical Engineering
May 20, 2009

Certified by .....
Pierre F. J. Lermusiaux
Associate Professor
Thesis Supervisor

Accepted by .....
David E. Hardt
Chairman, Department Committee on Graduate Thesis

Statistical Field Estimation and Scale Estimation for Complex Coastal Regions and Archipelagos

by

Arpit Agarwal

Submitted to the Department of Mechanical Engineering
on May 20, 2009, in partial fulfillment of the
requirements for the degree of
Master of Science in Mechanical Engineering

Abstract

A fundamental requirement in realistic computational geophysical fluid dynamics is the optimal estimation of gridded fields and of spatial-temporal scales directly from the spatially irregular and multivariate data sets that are collected by varied instruments and sampling schemes. In this work, we derive and utilize new schemes for the mapping and dynamical inference of ocean fields in complex multiply-connected domains, study the computational properties of our new mapping schemes, and derive and investigate new schemes for adaptive estimation of spatial and temporal scales.

Objective Analysis (OA) is the statistical estimation of fields using the Bayesian-based Gauss-Markov theorem, i.e. the update step of the Kalman Filter. The existing multi-scale OA approach of the Multidisciplinary Simulation, Estimation and Assimilation System consists of the successive utilization of Kalman update steps, one for each scale and for each correlation across scales. In the present work, the approach is extended to field mapping in complex, multiply-connected, coastal regions and archipelagos. A reasonably accurate correlation function often requires an estimate of the distance between data and model points, without going across complex landforms. New methods for OA based on estimating the length of optimal shortest sea paths using the Level Set Method (LSM) and Fast Marching Method (FMM) are derived, implemented and utilized in general idealized and realistic ocean cases. Our new methodologies could improve widely-used gridded databases such as the climatological gridded fields of the World Ocean Atlas (WOA) since these oceanic maps were computed without accounting for coastline constraints. A new FMM-based methodology for the estimation of absolute velocity under geostrophic balance in complicated domains is also outlined. Our new schemes are compared with other approaches, including the use of stochastically forced differential equations (SDE). We find that our FMM-based scheme for complex, multiply-connected, coastal regions is more efficient and accurate than the SDE approach. We also show that the field maps obtained using our FMM-based scheme do not require postprocessing (smoothing) of fields. The computational properties of the new mapping schemes are studied in detail. We find that higher-order schemes improve the accuracy of distance estimates. We also show

that the covariance matrices we estimate are not necessarily positive definite because the Weiner Khinchin and Bochner relationships for positive definiteness are only valid for convex simply-connected domains. Several approaches to overcome this issue are discussed and qualitatively evaluated. The solutions we propose include introducing a small process noise or reducing the covariance matrix based on the dominant singular value decomposition. We have also developed and utilized novel methodologies for the adaptive estimation of spatial-temporal scales from irregularly spaced ocean data. The three novel methodologies are based on the use of structure functions, short term Fourier transform and second generation wavelets. To our knowledge, this is the first time that adaptive methodologies for the spatial-temporal scale estimation are proposed. The ultimate goal of all these methods would be to create maps of spatial and temporal scales that evolve as new ocean data are fed to the scheme. This would potentially be a significant advance to the ocean community for better understanding and sampling of ocean processes.

Thesis Supervisor: Pierre F. J. Lermusiaux
Title: Associate Professor

Acknowledgments

I would like to express my sincere gratitude to Prof. Pierre F. J. Lermusiaux for his valuable guidance and suggestions throughout the course of this research work. Apart from being very supportive, he has helped tremendously with the proofreading of this document. I am highly indebted to research scientists Dr. Patrick J. Haley and Wayne G. Leslie for providing me with data, computational codes and very helpful inputs. I am very thankful to Oleg G. Logoutov for sharing his ideas and methods. I am sincerely thankful to Prof. Harry Asada for discussions on Objective Analysis and scale estimation methodologies during my course (2.160) project. I would like to thank Jinshan Xu (post doctoral student), Lisa Burton, Eric Heubel, Themis Sapsis and Mattheus Ueckermann (graduate students in the MSEAS group) for providing me with valuable suggestions through friendly discussions. In particular, I would like to thank Eric Heubel for helping me in MATLAB codes and in creating plots, and Mattheus Ueckermann for helping me with latex and for suggesting corrections in my thesis. We are grateful to the Office of Naval Research for research support under grants N00014-07-1-1061 and N00014-08-1-1097 (ONR6.1), N00014-07-1-0473 (PhilEx) and S05-06 (PLUSNet) to the Massachusetts Institute of Technology. I am very grateful to the whole Philex and PLUSNet teams for their fruitful collaborations. In particular, I thank crews, operators and support personnel of the Melville ship (Prof. Arnold L. Gordon, Lamont-Doherty Earth Observatory of Columbia University), gliders (University of Washington - Applied Physics Laboratory: Craig Lee, Bruce Howe, Marc Stewart) and kayaks (MIT LAMSS group under the guidance of Prof. Henrik Schmidt) for their work and the critical data they provided. Finally, I would like to thank my parents and siblings for providing me with the moral support without which this work would not have been possible.

Contents

List of Figures

List of Tables

Chapter 1

Introduction and Motivation

The statistical estimation theory of Objective Analysis (OA) was introduced by Gandin (1965) to the field of meteorology and was extended to oceanography by Bretherton et al. (1976). The theory is based on the Gauss-Markov theorem (Plackett, 1950), and it provides a sound basis for interpolating irregularly spaced data onto a computational grid. Upto details of the set-up, which are specific to the oceanic and atmospheric fields, the OA scheme is equivalent to utilize the Kalman update steps of the Kalman Filter to grid the irregularly-spaced data. Specifically, the data is gridded based on the specified prior field estimate and error covariance matrices. The OA methodology has been well formulated for open oceans without any landforms (convex simply-connected domains), but the OA in complex coastal regions (multiply-connected domains) is one of the 'last' mapping problems which remains to be studied in detail. This is one of the main research question of the present work.

Our OA research is carried out within the Multidisciplinary Simulation, Estimation and Assimilation System (MSEAS) group. MSEAS (http://mseas.mit.edu) consists of a set of mathematical models and computational methods for ocean predictions and dynamical diagnostics, for optimization and control of autonomous ocean observation systems, and for data assimilation and data-model comparisons. It is used for basic and fundamental research and for realistic simulations and predictions in varied regions of the world's ocean, recently including monitoring (Lermusiaux, 2007), naval exercises including real-time acoustic-ocean predictions (Xu et al., 2008)

and environmental management (Cossarini et al., 2009). Several different models are included in the MSEAS, including a new free-surface primitive-equation dynamical model which uses two-way nesting free-surface and open boundary condition schemes (Haley et al., 2008). This new free-surface code is based on the primitive-equation model of the Harvard Ocean Prediction System (HOPS). Additionally, barotropic tides are calculated from an inverse tidal model (Logoutov, 2008).

In MSEAS, the Kalman updates for data gridding are carried out successively, from the largest scale (uniform mean prior) to the smallest scale, using a sequential processing of observations and scale separation. In a two-scale version, a two-staged OA approach (Lermusiaux, 1997, 1999a) maps the scarcely available data onto oceanic fields in two steps: the larger and the smaller scale steps. The two main requirements for the Objective Analysis based on a Kalman update (also called the Gauss Markov estimation theory) are the statistical description of the field being estimated and the observational noise covariance. While observational noise statistics is dependent on the measurement sensor, the knowledge of the field statistics does not come easily in oceanography due to the scarcity of observations. A description of field statistics is often provided by a simple analytical correlation function which depends on the spatial separation distance and the spatial-temporal scales (Carter and Robinson, 1987). Other schemes also utilize dynamical models to construct covariances.

Our research study on Objective Analysis for coastal regions has been motivated by the Philippines Straits Dynamics Experiment (PhilEx) sponsored by the Office of Naval Research. The goal of PhilEx is to enhance understanding of the oceanographic processes and features arising in and around straits, and to improve the capability to predict the inherent spatial and temporal variability of these regions using models and advanced data assimilation techniques. There are several examples of Objective Analysis in coastal regions (Hessler, 1984, Stacey et al., 1988, Paris et al., 2002), but the methodologies employed in these examples do not satisfy coastline constraints (e.g. there should be no direct relationship across landforms).

New methodologies for field (e.g. temperature, salinity, biology, and velocity) mapping in complex multiply-connected coastal domains and archipelagos are derived

and demonstrated in this work. These methodologies will likely be very useful in improving the World Ocean Atlas (WOA) climatologies in complex multiply-connected domains. The WOA provides global ocean climatology containing monthly, seasonal and annual means of temperature (T) and salinity (S) fields at standard ocean depths. The temperature and salinity climatologies presented as part of the WOA (Levitus, 1982), which is also termed as 'Levitus Climatology' and its atlas updates in 1994 (Levitus and Boyer, 1994, Levitus et al., 1994), 1998 (Antonov et al., 1998a,b,c, Boyer et al., 1998a,b,c), 2001 (Stephens et al., 2002, Boyer et al., 2002) and 2005 (Locarnini et al., 2006, Antonov et al., 2006, Garcia et al., 2006a,b) have proven to be valuable tools for studying the hydrographic structures of the World's oceans. The WOA climatologies have been very useful for providing initial and boundary conditions to ocean circulation models. As its MSEAS counterpart, the OA procedure for 'Levitus Climatology' requires the use of an analytical correlation function to determine the covariance (or weight function, as described by Levitus (1982)). If the "straight Euclidean distance" (the straight line distance between two points) is used in such analytical correlation functions, the distance estimate is inappropriate for complex multiply-connected domains, as this "straight Euclidean distance" goes across land and so violate the coastline constraints. An appropriate measure of distance to be used in the correlation function for OA in such complex multiply-connected regions should be longer. It is nonetheless the length of the optimal shortest sea path i.e., the shortest path without going across complex landforms.

Such an optimal shortest sea path in complex multiply-connected regions can be obtained using the following numerical techniques: the Level set method (LSM) (Osher and Sethian, 1988, Sethian, 1999b) and the Fast Marching Method (FMM) (Sethian, 1996, 1999b). These methods model the propagation of evolving boundaries using appropriate PDE's. They have been applied in both the Philippines Archipelago and Dabob Bay (WA, USA) regions. They are also compared to the SDE approach proposed by Lynch and McGillicuddy (2001). Other optimization methods for path planning, for example Dikjstra's algorithm (Bertsimas and Tsitsiklis, 1997) and Bresenham line algorithm (Bresenham, 1965) could also be used for mapping in complex

domains, but our FMM and LSM schemes are shown to be computationally more efficient and more accurate. The optimal path length can also be used in conjunction with the methodology proposed by Lermusiaux et al. for three-dimensional, multivariate and multi-scale spatial mapping of geophysical fields and their dominant errors (Lermusiaux et al., 1998, 2000, Lermusiaux, 2002) in coastal regions. This method reduces the dimension of the error covariance matrices by focusing on the error subspace formed by dominant eigen-decomposition of the a-priori covariance (Lermusiaux and Robinson, 1999).

The new LSM and FMM schemes are also used in this work to estimate the minimum vertical area along any path between two islands. Vertical areas across landforms are needed to compute the transport streamfunction along the island coastlines, which minimizes the inter island transport. Such estimates of the transport streamfunction will aid in the computation of absolute velocity under geostrophic balance (Wunsch, 1996) in complex domains with islands.

Computational properties of the new mapping schemes are also investigated in detail. To reduce the computational cost and to understand the impact of the individual data, sequential processing of observations (Parrish and Cohn, 1985, Cho et al., 1996) is discussed utilized. By definition, the prior covariance matrix should be positive definite. According to the Wiener-Khinchin and Bochner theorem (Papoulis, 1991, Yaglom, 2004, Dolloff et al., 2006), the covariance matrix based on analytical correlation function will be positive definite if a Fourier transform (or the spectral density of the correlation function) is non-negative for all frequencies. These theorems are valid only for convex simply-connected domains. In our complex multiply-connected domains, the covariance matrix may become negative due to: a. Numerical error in the computation of the optimal path length using our new FMM/LSM based schemes b. The presence of landforms. These issues may lead to divergence problems (Brown and Hwang, 1997) of field mapping schemes. Therefore, the following two questions were resolved and investigated: a). What are the computational errors in optimal path lengths computed using the FMM/LSM and how can they be reduced? b). What are the computational issues including non-positive definite covariances that arise in a

multiply-connected coastal domain and how can they be remedied? These computational studies were indispensable for the development of our novel FMM/LSM based scheme for complex multiply-connected domains.

Apart from the OA research, another major question for ocean studies is the estimation of spatial and temporal scales from irregular ocean field measurements. Such scale estimation is potentially a significant advance to the ocean community for better understanding and sampling of ocean processes. The issue is that this is a challenging problem, especially because of the irregular properties of the data but also due to the multi-scale turbulent and/or intermittent ocean dynamics. The knowledge of the spatial-temporal scales is linked to our OA results: it provides a direct estimate of parameters needed for the analytical correlation function. These scales can also be used to obtain a measure of the internal Rossby radius of deformation, another relevant length scale in atmospheric and ocean sciences. The internal Rossby radius is the length scale at which rotational effects become as important as buoyancy effects.

We have proposed and implemented novel methods for adaptive spatial-temporal scale estimation from irregular field measurements. The ultimate goal of these new methods would be to create maps of spatial and temporal scales that evolve as ocean data are collected or are fed to to the scale estimation scheme, all without having to map the data. Denman and Freeland (1985) proposed an approach for estimating scales using the so-called structure function. We have further developed this approach, which is based on using the structure function and the non-linear least square fitting methods, to obtain adaptive scale estimates that vary in space and time. If the signal is stationary, i.e. the scales do not change with time, then the Fourier analysis can be very useful tool for scale estimation. Fourier analysis is valid only for stationary signals, but short term Fourier transforms (STFT) can be used for non-stationary signals as well, even though it has some resolution problems. We have proposed a new method for adaptive scale estimation based on STFT and have illustrated the method using chirp signal data. Wavelet Analysis is another approach which helps in overcoming the resolution issues, and which can potentially be very useful for adaptive scale estimation. However, the limitation of classic wavelet analysis and STFT is in

dealing with the irregularly sampled ocean data. Using adaptive methods based on second generation wavelets (Sweldens, 1998, Jansen and Oonincx, 2005), which are applicable to irregularly sampled and non-dyadic data sets, to learn the largest and the most energetic scales from the irregularly spaced ocean data is discussed and exemplified using a chirp signal data set.

In Chapter 2, we review the two staged multi-scale static field mapping approach from MSEAS and the Objective Analysis scheme used for 'Levitus Climatology'. In Chapter 3, we derive and utilize the new OA methodologies based on the Level Set Method and the Fast Marching Method and compare them to existing schemes including the OA based on the stochastically forced differential equations. A new optimization approach is proposed for computing the transport streamfunction and absolute velocity under geostrophic balance by minimizing the inter-island transport. In Chapter 4, applications of our new methodologies, for the complex regions of Dabob Bay and Philippines Archipelago are presented. In Chapter 5, we study the computational properties of our new mapping schemes. Chapter 6 introduces our novel methodologies for adaptive scale estimation including the use of the structure function, the use of STFT and the use of second generation wavelets. Chapter 7 consists of a summary and conclusions.

Chapter 2

Objective Analysis Approach

The multi-scale OA approach from MSEAS (Section 2.1) and the approach for 'Levitus Climatology' (Section 2.2) for field mapping are summarized in this Chapter. These approaches, which require the computation of Euclidean distance, are well established for mapping heterogeneous, multivariate, irregular data (Gandin, 1965, Bretherton et al., 1976, Carter and Robinson, 1987, Daley, 1993) in open oceans without islands or archipelagos as well as in atmospheric sciences.

2.1 Multi-scale static field estimation: MSEAS Objective Analysis

The two staged OA approach (Lermusiaux, 1997, 1999a) in MSEAS, utilizes the Gauss-Markov or minimum error variance criterion (Plackett, 1950) to map observations to the numerical grid. Let us denote the vector of numerical grid point locations as $\mathbf{x}$ and the vector of measurement locations as $\mathbf{X}$, then the OA estimate of the field ($\psi^{\mathbf{OA}}$) based on the background field ($\bar{\psi}$,$\bar{\mathbf{d}}$) is given by:

$$\begin{aligned} \psi^{\mathbf{OA}} &= \bar{\psi} + Cor(\mathbf{x},\mathbf{X})[Cor(\mathbf{X},\mathbf{X}) + \mathbf{R}]^{-1}[\mathbf{d} - \bar{\mathbf{d}}] \\ &= \bar{\psi} + \mathbf{K}[\mathbf{d} - \bar{\mathbf{d}}] \end{aligned} \tag{2.1}$$

where, $\bar{\mathbf{d}} = \mathbf{H}\bar{\psi}$, $\mathbf{H}$ is the observation matrix, $\mathbf{d}$ is the sensor data vector, $\mathbf{R}$ is the observational error covariance matrix, and Gain ($\mathbf{K}$) is given by:

$$\mathbf{K} = Cor(\mathbf{x}, \mathbf{X})[Cor(\mathbf{X}, \mathbf{X}) + \mathbf{R}]^{-1} \tag{2.2}$$

The error covariance of the estimated field is given by:

$$\begin{aligned} \mathbf{P^{OA}} &= E[(\mathbf{x} - E[\mathbf{x}])(\mathbf{x} - E[\mathbf{x}])^T] \\ &= Cor(\mathbf{x}, \mathbf{x}) - Cor(\mathbf{x}, \mathbf{X})[Cor(\mathbf{X}, \mathbf{X}) + \mathbf{R}]^{-1} Cor(\mathbf{X}, \mathbf{x}) \\ &= Cor(\mathbf{x}, \mathbf{x}) - \mathbf{K} Cor(\mathbf{X}, \mathbf{x}). \end{aligned} \tag{2.3}$$

A comparison between the MSEAS update equations (OA) and the Kalman filter update equations is made in Table 2.1.

Kalman Filter Update Equations	MSEAS Update equations (OA)
Kalman gain: $\mathrm{K_t}=\mathrm{P_{t\|t-1}H_t}^{\mathrm{T}}[\mathrm{H_tP_{t\|t-1}H_t}^{\mathrm{T}}+\mathrm{R_t}]^{-1}$	OA estimator: $Gain = Cor(\mathbf{x}, \mathbf{X})[Cor(\mathbf{X}, \mathbf{X}) + \mathbf{R}]^{-1}$
State estimate update equation: $\hat{x}_t = \hat{x}_{t\|t-1} + K_t(y_t - H_t\hat{x}_{t\|t-1})$	State estimate update equation: $\psi^{OA} = \bar{\psi} + Gain[\mathbf{d} - \bar{\mathbf{d}}]$.
Error Covariance equation: $P_t = (I - K_tH_t)P_{t\|t-1}$	Error Covariance equation: $\mathbf{P}^{OA} = Cor(\mathbf{x}, \mathbf{x}) - Gain \times Cor(\mathbf{X}, \mathbf{x})$

Table 2.1: Comparison between the Kalman Filter and MSEAS OA update equations

Thus, the update equations of OA are equivalent to the update equations of the discrete Kalman filter (KF) algorithm where the background error correlation matrix for the field-to-data points, Cor($\mathbf{x}$,$\mathbf{X}$), and the background correlation matrix at the data points, Cor($\mathbf{X}$,$\mathbf{X}$), are directly related to the KF a priori error covariance matrix $P_{t|t-1}$ i.e. Cor($\mathbf{x}$,$\mathbf{X}$) = $P_{t|t-1}H_t^T$ and Cor($\mathbf{X}$,$\mathbf{X}$) = $H_tP_{t|t-1}H_t^T$ (H_t is the observation matrix). The matrix $\mathbf{R}$ represents the error covariance for the sensor data $\mathbf{d}$ at the data points. This matrix is often chosen diagonal with a uniform non-dimensional error variance ϵ^2, i.e. $\mathbf{R} = \epsilon^2 I$. In MSEAS, the correlation matrices are often generated

from the following isotropic function:

$$Cor(r) = \left(1 - \frac{r^2}{L_0^2}\right) exp\left[-0.5 \times (\frac{r^2}{L_e^2} + \frac{\Delta t^2}{\tau^2})\right] \tag{2.4}$$

Here, Δt is the difference between the observation and the estimation time and τ is the decorrelation time scale. The parameters L_0 and L_e are the zero-crossing and the e-folding length scales. The scalar r is the spatial separation distance. The Euclidean distance does not satisfy coastline constraints. So, the use of the optimal distance (the minimum distance between two points without going across complex landforms) is proposed. LSM or FMM can be utilized to obtain such optimal distance between any two points in a complex (for example, multi-island) multiply-connected coastal region. These methods are efficient and accurate solvers for optimal distances in multiply-connected complex domains and satisfy coastline constraints.

The MSEAS OA is carried out in two stages. In the first stage, the largest dynamical scales are mapped onto computational grid using the parameters $(\tau,\ L_0,\ L_e)_{\mathrm{LS}}$. The background field for this stage is often chosen to be constant and equal to the horizontal mean of all the observations. In the second stage, the smaller scales are mapped using the coefficients $(\tau,\ L_0,\ L_e)_{\mathrm{ME}}$ often corresponding to the most energetic (meso) scales. The background field for this stage is the first stage OA. The block diagram for the two staged MSEAS OA is shown in Figure C-1. A major assumption in this OA approach is that the errors in the largest and the most energetic stages are statistically independent. The accuracy of the field estimates obtained using OA also depends on the spatial and time scale parameters used in the analytical correlation function, as well as the correlation function itself.

2.2 Objective Analysis approach for the 'Levitus Climatology'

The objective analysis scheme used for 'Levitus Climatology' (Levitus, 1982, Locarnini et al., 2006, Antonov et al., 2006, Garcia et al., 2006a,b) has its origins in the

work of Cressman (1959) and Barnes (1964). This scheme is based on adding "corrections", which are computed as a distance-weighted mean of all grid point difference values, to the first-guess field. Initially, the World Ocean Atlas 1994 (WOA94) used the Barnes (1973) scheme which requires only a single "correction" to the first-guess field at each grid point in comparison to the successive correction method of Cressman (1959) and Barnes (1964). This was done to reduce the computing time. Barnes (1994) suggests using the multi-pass analysis when computing time is not an issue. The analysis scheme used in WOA98, WOA01 and WOA05 is a three-pass "correction" scheme. The inputs to this analysis scheme are one-degree square means of the observed data values, and a first-guess field. The difference between the observed mean and the first-guess field is then computed. An influence radius is specified next and a correction to the first-guess value at all the grid points is computed as a distance-weighted mean of all the grid point difference values that lie within the area around the grid point defined by the influence radius. Mathematically, the correction factor derived by Barnes (1964) is given by:

$$C_{i,j} = \frac{\sum_{s=1}^{d} W_s Q_s}{\sum_{s=1}^{d} W_s} \tag{2.5}$$

where,

(i, j) - coordinates of a grid point in east-west and north-south directions respectively;

$C_{i,j}$ - correction factor at the grid point coordinates (i, j);

d - the number of data points that fall within the area around point (i, j) defined by the influence radius;

Q_s - difference between the observed mean and the first-guess at the S^{th} data point in the influence area;

$W_s = exp(-Er^2/R^2)$ (for $r \leq R$; $W_s = 0$ for $r > R$) $\equiv$ Correlation weight;

r - distance of observation from grid point;

R - influence radius;

$E = 4$.

At each grid point, the analyzed value $G_{i,j}$ is the sum of the first guess $F_{i,j}$ and

the correction $C_{i,j}$. The expression is:

$$G_{i,j} = F_{i,j} + C_{i,j} \tag{2.6}$$

If there is no data within the area defined by the influence radius, the correction is zero and the analyzed value of the field is the same as the first-guess. The analysis scheme is set up such that the inference radius can be varied in each iteration. To progressively analyze the smaller scale phenomena with each iteration, the analysis begins with a large inference radius which is decreased gradually with each iteration.

Equation 2.6 can also be expressed in the matrix form, which is given by

$$\mathbf{G} = \mathbf{F} + [diag(\mathbf{W}\mathbf{e}_d)]^{-1}\mathbf{W}\mathbf{Q} \tag{2.7}$$

Here n is the number of model points, the analyzed field $\mathbf{G}$ and the first guess $\mathbf{F}$ are n-by-1 vectors, the correlation weight matrix $\mathbf{W}$ is a n-by-d matrix, the difference between the observed mean and the first-guess at the data point $\mathbf{Q}$ is a d-by-1 vector and $\mathbf{e}_d$ is a d-by-1 vector with unit entities. The operation diag($\mathbf{v}$) creates a diagonal matrix i.e. it puts the vector $\mathbf{v}$ on the main diagonal.

Analogous to the Kalman Gain ($\mathbf{K}$) from the Gauss Markov criterion ($K = Cor(\mathbf{x}, \mathbf{X})[Cor(\mathbf{X}, \mathbf{X}) + \mathbf{R}]^{-1}$), Equations 2.7 and 2.1 show that a similar Gain matrix ($K_L = [diag(\mathbf{W}\mathbf{e}_d)]^{-1}\mathbf{W}$) can be defined for the Levitus methodology. While the multi-scale OA approach in MSEAS is based on Gauss Markov estimation theory, the Levitus OA is based on estimating the field by computing the distance-weighted mean of all grid point difference values (between the mean and first-guess field) in the inference radius and then adding it to the first-guess field. Thus, the choice of first guess-field is very important in the 'Levitus OA' analysis. On the other hand, in Gauss Markov estimation, the first-guess field is often the mean of the data values and the correction is made in the Kalman update step by computing the difference between the data and the interpolated value of the first-guess on the data location. The Gauss Markov estimation theory also requires the knowledge of error covariance of the observation noise ($\mathbf{R}$).

The above approaches for MSEAS OA and 'Levitus Climatology', which are based on computing the covariance or the weight factors by providing Euclidean distance as an input to the correlation function, are valid only for open oceans. New methodologies based on computing the length of the optimal path using the Level Set Method and the Fast Marching Method are discussed in Chapter 3.

Chapter 3

OA methodologies in complex coastal regions and archipelagos

This chapter describes the new methodologies for Objective Analysis in complex multiply-connected coastal regions and compares them to previous methods. The new methodologies are based on finding the length of the optimal path using the Level Set Method and the Fast Marching Method, as described in Section 3.1. In Section 3.2, we discuss other methods including the methodology proposed by Lynch and McGillicuddy (2001) based on using the stochastically forced differential equation (SDE) for the field and the methodology based on using the SDE for the covariance (Logoutov, Lermusiaux, personal communication). An improved version of the optimization methodology proposed by Haley and Lermusiaux (2009), for estimating the inter-island transport and for estimating the absolute velocity under geostrophic balance in multiply-connected coastal regions is presented in Section 3.3.

3.1 Novel Objective Analysis Methodologies based on optimal path length

The optimal path in a domain having complex multiply-connected islands and archipelagos is defined as the shortest path between two points without going across

landforms. Optimization method like Dijkstra's algorithm (Bertsimas and Tsitsiklis, 1997) can be utilized to obtain the optimal path length. Apart from being computationally expensive, Dijkstra's method is also inaccurate. The accuracy of FMM and LSM is illustrated in Figure C-2 where it is compared to the optimization method (Dijkstra's method with norm p = 2) for optimal distance computations in a complex domain (Takei, 2006). Another classic method for approximately computing the optimal path length is the Bresenham line algorithm (Bresenham, 1965). This algorithm is used for computer control of a digital plotter. In the oceanic context, the modified Bresenham line algorithm can be used to obtain the length of the optimal path. The modified algorithm is explained using Figure C-3, which has a complex island in the domain. To compute the length of the optimal path between the points A and B in Figure C-3, a straight line connecting the two points is drawn. Since the optimal path does not go across landforms, the straight line path is modified such that it goes along the boundary of the island upon hitting the island. The optimal path between the points A and B is drawn in Figure C-3. The limitation of the Bresenham algorithm, apart from being computationally expensive, is that the optimal path length computed using this algorithm is discontinuous. Again, this is illustrated in Figure C-3. The straight line between points A and C does not intersect the complex island, and therefore the straight line path is the optimal path. However, it is clearly observed from Figure C-3 that the length of the optimal path, which is computed from the Bresenham line algorithm, between points A and B is significantly larger than the length of the optimal path between points A and C. Since, points B and C are not very far from each other, the length of the true optimal path between points A and B and between points A and C should not differ significantly. This example clearly illustrates the limitation of the Bresenham line algorithm for computing the optimal path in the oceanic context.

We propose to utilize the methodology based on using level sets for computing the length of the optimal path. The novel Objective Analysis methodology based on computing the length of the optimal path using the Level Set Method is discussed in Section 3.1.1 and the methodology based on using the Fast Marching Method is

discussed in Section 3.1.2. These methods can efficiently and accurately compute the optimal path length.

3.1.1 Objective Analysis using the Level Set Method (LSM)

A level set of a real-valued function ϕ of n variables is a set of the form:

$$\{(x_1, ..., x_n) | \phi(x_1, ..., x_n) = c\} \tag{3.1}$$

where, c is a constant. That is, a level set is the set where the function ϕ takes on a given constant value c.

Osher and Sethian (1988), Sethian (1999b) proposed a numerical technique, which is called the Level Set Method, to implicitly represent and model the propagation of evolving interfaces under the influence of a given velocity field using appropriate partial differential equations (PDE's). An initial value formulation describing the interface motion is now discussed. The initial position of interfaces are given by level sets of the function ϕ. The evolution of this function ϕ is linked to the propagation of the interface through a time-dependent level set equation. Interfaces can be represented explicitly (parametrized interfaces i.e. interfaces given by $\mathbf{x} = \mathbf{x}(\mathrm{s})$, where s is the parameter) or implicitly (interfaces given by zero level set i.e. $\phi(\mathbf{x}) = 0$). Using the implicit representation $\phi(\mathbf{x})$, where $\mathbf{x}$ is the position vector, the convection equation can be solved to propagate level sets by a velocity field $\mathbf{v}$:

$$\phi_t + \mathbf{v}.\nabla\phi = 0 \tag{3.2}$$

In many cases, one is interested only in the motion normal to the boundary. Therefore, the velocity $\mathbf{v}$ can be represented using the scalar speed function F and the normal direction $\mathbf{n}$. Thus.

$$\mathbf{v} = F\mathbf{n} = F\frac{\nabla\phi}{|\nabla\phi|} \tag{3.3}$$

The hyperbolic, non-linear (Hamilton-Jacobi equation) level set equation, obtained from Equations 3.2 and 3.3, is given by:

$$\phi_t + F|\nabla\phi| = 0 \tag{3.4}$$

The following first order upwinded finite difference approximation can be used to numerically solve the level set equation (2-dimensional in space) (Osher and Sethian, 1988, Sethian, 1999b):

$$\phi_{i,j}^{n+1} = \phi_{i,j}^{n} - \Delta t[max(F,0)\nabla_{i,j}^{+} + min(F,0)\nabla_{i,j}^{-}]$$

where,

$$\begin{aligned}
\nabla_{i,j}^{+} &= [max(D^{-x}\phi_{i,j}^{n},0)^2 + min(D^{+x}\phi_{i,j}^{n},0)^2 + \\
&\quad max(D^{-y}\phi_{i,j}^{n},0)^2 + min(D^{+y}\phi_{i,j}^{n},0)^2]^{1/2} \\
\nabla_{i,j}^{-} &= [min(D^{-x}\phi_{i,j}^{n},0)^2 + max(D^{+x}\phi_{i,j}^{n},0)^2 + \\
&\quad min(D^{-y}\phi_{i,j}^{n},0)^2 + max(D^{+y}\phi_{i,j}^{n},0)^2]^{1/2}
\end{aligned} \tag{3.5}$$

Here, D^{-x} is the first order backward difference operator in the x-direction; D^{+x} is the first order forward difference operator in x-direction, etc. Mathematically, these operators are given by:

$$D^{-x}\phi_{i,j} = \frac{\phi_{i,j} - \phi_{i-1,j}}{\Delta x}; \qquad D^{+x}\phi_{i,j} = \frac{\phi_{i+1,j} - \phi_{i,j}}{\Delta x} \tag{3.6}$$

The level set equation is an initial value problem which tracks the evolution of the level sets ϕ=constant assuming F is given by the specifics of the evolution of the ϕ for a particular problem.

If the scalar speed function of the front F is non-negative, then the steady state boundary value problem, known as the Eikonal equation, can be formulated to evaluate the arrival time function T($\mathbf{x}$). The Eikonal equation representing the time T($\mathbf{x}$)

for the "frontal interface" to reach the position $\mathbf{x}$ from its initial position is given by:

$$F|\nabla T| = 1 \tag{3.7}$$

The Eikonal equation simply states that the gradient of the arrival time function is inversely proportional to the speed of the front. To solve the Eikonal equation, a time dependent problem is proposed. The time evolved steady state solution of the resultant Hamilton-Jacobi equation is the Eikonal equation. Mathematically, this is written as:

$$T_t + F|\nabla T| = 1 \stackrel{steady}{\longrightarrow} F|\nabla T| = 1 \tag{3.8}$$

This Hamilton-Jacobi equation (Equation 3.8 (Left)) can be discretized using the numerical scheme for the Level Set equation. The steady state solution of this Hamilton-Jacobi equation will be the solution of the Eikonal equation (Equation 3.8 (Right)).

The Level Set Method has been used in a wide variety of applications which include the arrival time problems in the control theory, generation of minimal surfaces, flame propagation, fluid interfaces, shape reconstruction etc. In the oceanic context, the method can be used to determine the optimal distance defined here as the minimum distance between two points without going across complex landforms.

Numerics and operation count for the LSM: MATLAB code has been developed for Objective Analysis using the Level Set Method. For estimating the optimal distance, the scalar speed function F is set to 0 for the grid points on the land and 1 for the grid points on the water. The level set T($\mathbf{x}$), which is the arrival time function, also represents the optimal distance from the starting position to the position vector $\mathbf{x}$ for the above speed function F. The above OA approach, which is based on computing the evolution of all the level sets and not simply the zero level set corresponding to the front itself, has an operation count of O(N^3) in two dimensions for N^2 grid points (Sethian, 1999b). Thus, it is a computationally expensive technique since an extra dimension has been added to the problem.

A modified approach named 'Fast Marching level set method', which significantly

reduces the operation count, is described in the next section. Roughly speaking, the two possible ways to view these solution techniques are either iteration towards the solution, or direct construction of the stationary solution T. While LSM constructs the solution to the Eikonal equation (Equation 3.7) by iterating towards the solution, FMM is based on direct construction of the stationary solution T.

3.1.2 Objective Analysis using the Fast Marching Method (FMM)

The Fast Marching Method (FMM) for monotonically advancing fronts, which has been proposed by Sethian (1996, 1999b), is described in this section. This method leads to an extremely fast scheme for solving the Eikonal equation (Equation 3.7). The Level set method, which is described in Section 3.1.1, relies on computing the evolution of all level sets by solving an initial value partial differential equation using numerical techniques from hyperbolic conservation laws. As an alternative, an efficient modification is to perform the work only in the neighborhood of the zero level set, as this is known as the 'narrow band approach'. The basic idea of this alternative approach is to tag the grid points as either "alive", "land mines" or "far away" depending on whether they are inside the band, near its boundary, or outside the band, respectively. The work is performed only on *alive* points, and the band is reconstructed once the land mine points are reached.

FMM, which allows boundary value problems to be solved without iterations, is now discussed in detail. The method is applicable to monotonically advancing fronts (i.e. the front speed ($F \geq 0$ or $F \leq 0$) which are governed by the level set equation (Equation 3.8). The steady state form of the level set equation is the Eikonal equation (Equation 3.7) which says that the gradient of the arrival time surface is inversely proportional to the speed of the front. For the two dimensional case, the stationary boundary value problem is given by:

$$|\nabla T| F(x,y) = 1 \quad s.t. \quad \Gamma = \{(x,y) | T(x,y) = 0\} \tag{3.9}$$

where Γ is the starting position of the interface. The first order finite difference discretization form of the Eikonal equation (Sethian, 1999b) at the grid point (i,j) is given by:

$$[max(D_{ij}^{-x}T,0)^2 + min(D_{ij}^{+x}T,0)^2 + max(D_{ij}^{-y}T,0)^2 + min(D_{ij}^{+y}T,0)^2]^{1/2} = \frac{1}{F_{ij}}$$

or,

$$\begin{aligned}[max(max(D_{ij}^{-x}T,0), -min(D_{ij}^{+x}T,0))^2 + \\ max(max(D_{ij}^{-y}T,0), -min(D_{ij}^{+y}T,0))^2] = \frac{1}{F_{ij}^2}\end{aligned} \tag{3.10}$$

Equation 3.10 is essentially a quadratic equation for the value at each grid point (assuming that values at the neighboring nodes are known). An iterative algorithm for computing the solution to Equation 3.10 was introduced by Ruoy and Tourin (1992). FMM is based on the observation that the upwind difference structure of Equation 3.10 means that the information propagates "one way", i.e. from the smaller values of T to the larger values. Therefore, FMM rests on solving Equation 3.10 by building the solution outward from the smallest time value T. The front is swept ahead in an upwind manner by considering a set of points in a *narrow band* around the existing front and bringing new points into the *narrow band* structure. The fast marching algorithm is:

1. Initialize

   (a) *Alive* points: Let A be the set of all grid points (i,j) on the starting position of the interface Γ; set $\mathrm{T_{ij}} = 0$ for all points in A.

   (b) *Narrow Band* points: Let the *Narrow Band* be the set of all grid points (i,j) in the immediate neighborhood of A; set $T_{ij} = \frac{d}{F_{ij}}$ for all points in the *Narrow Band* where, d is the grid separation distance.

   (c) *Far Away* points: Let the *Far Away* region be the set of all remaining grid points (i,j); set $T_{ij} = \infty$ for all points in the *Far Away* region.

2. Marching Forward

   (a) Begin Loop: Let (i_{min},j_{min}) be the point in the *Narrow Band* with the smallest value for T.

   (b) Add the point (i_{min},j_{min}) to A; remove it from the *Narrow Band*.

   (c) Tag as neighbors any points ($i_{min}-1$,j_{min}), ($i_{min}+1$,j_{min}), (i_{min},$j_{min}-1$), (i_{min},$j_{min}+1$) that are either in the *Narrow Band* or the *Far Away* region. If the neighbor is in the *Far Away* region, remove it from that list and add it to the *Narrow Band*.

   (d) Recompute values of T at all neighbors in accordance with Equation 3.10. Select the largest possible solution to the quadratic equation.

   (e) Return to the top.

Here are some properties of the fast marching algorithm. The smallest value in the *Narrow Band* is always correct. Other *Narrow Band* or *Far Away* points with larger values of T cannot affect the smallest value. Also, the process of recomputing T values at the neighboring points cannot give a value smaller than any of the accepted value at *Alive points*, since the correct solution is obtained by selecting the largest possible solution to the quadratic equation (Equation 3.10). Thus the algorithm marches forward by selecting the minimal T value in the *Narrow Band* and recomputing the values of T at all neighbors in accordance with Equation 3.10.

The key to an efficient version of the algorithm lies in finding a fast way to locate the grid point in the *Narrow Band* with the minimum value for T. To do so, the heapsort algorithm (Williams, 1964, Sedgewick, 1988) with backpointers is often implemented and it is the algorithm we used here. This sorting algorithm generates a "complete binary tree" with the property that the value at any given parent node is less than or equal to the value at its child node. Heap is represented sequentially by storing a parent node at the location k and its child at locations $2k$ and $2k+1$. The member having the smallest value is stored at the location $k=1$.

All *Narrow Band* points are initially sorted in a heapsort. The fast marching algorithm works by first finding, and then removing, the member corresponding to the

smallest T value from the *Narrow Band* which is followed by one sweep of DownHeap to ensure that the remaining elements satisfy the heap property. The DownHeap operation moves the element downwards in the heap till the new heap satisfies the heap properties. *Far Away* neighbors are added to the heap using the Insert operation which increases the heap size by one and brings the new element to its correct heap location using the UpHeap operation. The UpHeap operation moves the element upwards in the heap till the new heap satisfies the heap properties. The updated values at the neighbor points obtained from Equation 3.10 are also brought to the correct heap location by performing the UpHeap operation.

Numerics and operation count for the FMM: MATLAB code has been developed for Objective Analysis using the Fast Marching Method. Once again, for estimating the optimal distance, the scalar speed function F is set to 0 for the grid points on land and 1 for the grid points on the water. FMM has a significantly lower operation count of $O(N^2 \text{ Log } N)$ for N^2 grid points (Sethian, 1999b). Thus, it is a computationally inexpensive technique as compared to the Level Set Method.

The Fast Marching Method, as discussed above, is an efficient way to obtain the correlation between two locations by selecting the optimal path. The length of the optimal path computed using FMM or LSM can then be used for setting up the covariance matrix using the analytical correlation function (Equation 2.4).

3.2 Objective Analysis based on using Stochastically Forced Differential Equations (SDE's)

The use of Euclidean distance in the field covariance computed from the isotropic correlation function is not applicable in coastal regions since the complex coastline constraints, e.g. there should be no direct relationship across landforms (islands, peninsulas etc.), need to be accounted for. The approach discussed in this section represents the field and its coastline constraints by a partial differential equation subject to stochastic forcing. The central idea of this approach, which is based on

using stochastically forced differential equations (SDE), is the numerical construction of a field covariance such that it accounts for the coastal constraints. The underlying field variability is represented as an outcome of a stochastic process using a SDE and the stochasticity represents the uncertainty in this differential equation. For example, the stochastically forced Helmholtz equations in 1-D and 2-D in space for the field ψ in an unbounded domain (Balgovind et al., 1983) are associated with the following covariance functions respectively:

$$\begin{aligned} \frac{\partial^2\psi}{\partial x^2} - k^2\psi = \epsilon(x) \quad &\Leftrightarrow \quad C_{\psi\psi}(r) = (1+kr)e^{(-kr)} \\ \nabla^2\psi - k^2\psi = \epsilon(x,y) \quad &\Leftrightarrow \quad C_{\psi\psi}(r) = krK_1(kr) \simeq \left(\frac{\pi}{2}kr\right)^{1/2}\left(1+\frac{3}{8kr}\right)e^{-kr}, kr \to \infty \end{aligned} \tag{3.11}$$

where, K_1 is the Bessel function of the second kind. The process noise ϵ is a random disturbance with mean 0, standard deviation 1 and has no spatial correlation. Also, the length scale corresponds to the inverse of the SDE parameter (k). By the way, Denman and Freeland (1985) have proposed other correlation functions which can also be linked to the appropriate SDE's.

A major advantage of this SDE approach is that the field-to-field covariance Cor(**x**,**x**) can be computed numerically from the discretized SDE along with appropriate boundary conditions (i.e. no flux boundary condition across islands) to directly account for the coastline constraints (Lynch and McGillicuddy, 2001). The discretization of SDE equations (Equation 3.11) or any other differential operator on a finite element grid leads to the matrix form:

$$[A]\{\psi\} = \{e\} \tag{3.12}$$

All coastline constraints are then incorporated automatically in the discretization Equation (3.12). Since $[C_{ee}] = [I]$, the covariance matrices for field-to-field points

and field-to-data points are directly obtained from Equation 3.12 and given by:

$$Cor(\mathbf{x},\mathbf{x}) = [A]^{-1}[C_{ee}][A]^{-T} = ([A]^T[A])^{-1}$$
$$Cor(\mathbf{x},\mathbf{X}) = [A]^{-1}[C_{ee}][A]^{-T}[H]^T = ([A]^T[A])^{-1}[H]^T \tag{3.13}$$

The covariance matrix (3.13) obtained using the SDE approach can be used along with Gauss-Markov Estimation theory to perform Objective Analyses in coastal regions. A limitation of this approach is that the resulting fields can be affected by the discretization error associated with the discretized form of the SDE. In fact, we found that we often need to postprocess (smooth out) the SDE-gridded fields to remove spurious field gradients. Such gradients, even when small, can lead to spurious velocities by aggregate integration in the vertical for the estimation of absolute velocity under geostrophic balance. It has also been verified that that the SDE approach is computationally expensive when compared to our new FMM-based methodology.

A similar variant of the above methodology represents the covariance ($C_{\psi\psi}$), instead of the field (ψ), by a SDE like Helmholtz equation (Logoutov, personal communication). Spatial variation in the resulting OA field are found to be more prominent with this new scheme. An heuristic reason is that this new representation corresponds to carrying out "smoothing" using the Helmholtz equation only once as compared to twice in the original representation. Both of these methods, the SDE specified for the field (ψ) and the SDE specified for the covariance ($C_{\psi\psi}$) were implemented in MATLAB, using guidance from Logoutov (personal communication).

Even though many different SDE's could be utilized for mapping a field, in the example that follows, we selected the stochastically forced Helmholtz equation. First, the dynamics of the atmosphere can be approximately governed on the time scale of a few days by a Helmholtz-like equation, which is the equation for the conservation of potential vorticity under the assumptions of a quasi-geostrophic, frictionless, shallow water model without topography (Balgovind et al., 1983, Pedlosky, 1987). Second, the Helmholtz equation can also be reduced from the diffusion or wave equations. In these linear PDE's, if the solution is assumed separable in time and space, one

obtains for the time variation an ordinary differential equation of the first order. For the spatial variations, one always obtains the Helmholtz equation (Selvadurai, 2000), which is the equation that would be used for spatial mapping. Thirdly, the Helmholtz equation is also equivalent to the steady state diffusion-reaction equation. The Helmholtz equation can also be obtained by discretizing the diffusion equation in a single time step.

In our examples in Equation 3.11, the SDE parameter (k) is chosen such that the correlation function corresponding to the stochastically forced Helmholtz equation best fits the analytical correlation function used by the standard OA scheme and the LSM or FMM-based schemes (Section 3.1). These methods are compared to each other and to the FMM and LSM schemes in Chapter 4 using the World Ocean Atlas, 2005 data in the sub-domain of Philippines Archipelago.

3.3 Estimation of the absolute velocity under geostrophic balance by minimizing the inter-island transport using FMM

For ocean flows, which evolve over long spatial-time scales and away from the immediate vicinity of the sea-surface, the dominant terms in the horizontal momentum equations are the terms corresponding to the Coriolis force and the pressure gradient. Such a flow field, where a balance is struck between the Coriolis and the pressure forces, is called geostrophic. The thermal wind equations, which have also been central to physical oceanography for over 100 years, are obtained for geostrophic flow by assuming that the vertical momentum equation is approximately given by hydrostatic balance. The thermal wind equations are:

$$-f\frac{\partial(\rho v)}{\partial z} = g\frac{\partial \rho}{\partial x} \quad and \quad f\frac{\partial(\rho u)}{\partial z} = g\frac{\partial \rho}{\partial y} \tag{3.14}$$

where, ρ is the density, u and v are the horizontal fluid velocity in the zonal (x) and meridional (y) directions respectively, and $f = 2\Omega\ sin\phi$ is the Coriolis parameter for the spherical earth rotating at a rate of Ω at latitude ϕ. The thermal wind equations (Equation 3.14) when integrated in the vertical give:

$$\rho v(x,y,z,t) = \frac{-g}{f}\int_{z_0}^{z}\frac{\partial\rho}{\partial x}dz + \rho v_0 \quad and \quad \rho u(x,y,z,t) = \frac{g}{f}\int_{z_0}^{z}\frac{\partial\rho}{\partial y}dz + \rho u_0 \tag{3.15}$$

where, z_0 or the level of no motion for $v_0, u_0 = 0$ or a level of reference for $v_0, u_0 \neq 0$.

Flow estimation based on thermal wind balance (Equation 3.15), is a classical problem in physical oceanography (Wunsch, 1996). Historically, the only significant routine measurements possible were the temperature, T, and salinity, S, of the water at various depths. The equation of state for seawater then permits the estimation of density at a given pressure from the temperature and salinity measurements. Thus the geostrophic flow can be computed using the above method (Equation 3.15) from the shipboard measurements of T and S alone. The formulation has been well defined for the open oceans without any landforms. For complex coastal regions having landforms such as islands and peninsulas, estimation of the inter-island transport is first required before proceeding with the geostrophic formulation discussed above.

The optimization methodology for estimating the inter-island transport, proposed by Haley and Lermusiaux (2009) is utilized and discussed below. The objective of this methodology is to find a set of constant values for the transport streamfunction (Ψ) along the island coastlines that produce a suitably smooth initialization velocity field, e.g. with the fewest large velocity hot-spots, i.e. minimize the maximum absolute velocity in the initialized geostrophic flow field. The working assumptions for Haley's methodology are listed below:

1. Coastlines in the given domain can be divided into two distinct subsets:

   (a). Set A: N coastlines along which the transport streamfunction is unknown, $N \neq 0$.

   (b). Set B: M coastlines along which the transport streamfunction is known.

2. The solution for the transport streamfunction Ψ_0 exists for the case which includes

coasts in set B, but coasts in set A, along with the corresponding interiors, are replaced by open ocean (e.g. island sunk to 10m depth).

3. The difference between the initial solution Ψ_0 and the final solution Ψ is not extremely large. Otherwise, the information from Ψ_0 would not be accurate enough.

Ψ_0 contains useful information like the relative position of major currents to various coastlines and the effects of topography on the flow. Thus, the information in Ψ_0 can be utilized to estimate the constant value of the transport streamfunction along the island coastlines by constructing an optimization functional for minimizing the inter-island transport subject to weak constraints. Haley's methodology for constructing the optimization functional is now discussed.

The problem is divided into three parts to construct the optimization functional. The optimization functional (E) in the general form, which is a summation of three terms, is given by:

$$E = E_1 + E_2 + E_3 \tag{3.16}$$

where, E_1 is the minimizing target for the transport between all pairs of the unknown (Set A) coasts, E_2 is the minimizing target for the transport between all pairs of unknown (Set A) and known (Set B) coasts and E_3 is the minimizing target for the transport between all pairs of the unknown (Set A) coasts and the open boundaries of the domain. These three terms in Equation 3.16 are:

1. Constructing the optimization functional for minimizing the transport between all pairs of island coastlines with unknown (Set A) transport streamfunction: Let C_n and C_m be two of the coasts (coast n and coast m) in Set A. Ψ_0 is not constrained to be a constant along these coasts. Find the grid point i^0 on the coastline n and the grid point j^0 on the coastline m such that $[i^0, j^0] = \arg\max_{[i,j]} |\Psi_{0n}(i) - \Psi_{0m}(j)|$ and $\delta\Psi_{n,m} = \Psi_{0n}(i^0) - \Psi_{0m}(j^0)$. Here, we denote Ψ_0 at point b on coastline a by $\Psi_{0a}(b)$.

The optimization functional for minimizing the inter-island transport between islands n and m is given by $(\Psi_{C_n} - \Psi_{C_m} - \delta\Psi_{n,m})^2$, where, Ψ_{C_a} is the unknown optimized, constant value of the transport streamfunction along the coast a. Haley

proposes to weight this optimization function by $w_{nm} = 1/d_{nm}^2$ where, d_{nm} is the minimum distance between C_n and C_m. However, since the objective is to smooth the resulting initialization velocity flow field, the above weighting will be appropriate if the ocean depth is uniform in between all pairs of islands. An alternative weighting along with its computational methodology for non-uniform ocean depths will be proposed later in this section.

2. Constructing the optimization functional for minimizing the transport between all pairs of island coastlines with known (Set B) and unknown (Set A) transport streamfunction: Let C'_k be one of the coasts along which the transport streamfunction $\Psi_{C'_k}$ is known (Set B) and C_n be the coast in Set A. Ψ_0 is not constrained to be a constant along C_n. Find the grid point i' on the coastline n such that $[i'] = \arg\max_{[i]} |\Psi_{0n}(i) - \Psi_{C'_k}|$ and $\delta\Psi'_{n,k} = \Psi_{0n}(i') - \Psi_{C'_k}$.

The optimization functional for minimizing the inter-island transport between islands n and m is given by $(\Psi_{C_n} - \Psi_{C'_k} - \delta\Psi'_{n,k})^2 = (\Psi_{C_n} - \Psi_{0n}(i'))^2$. As before, Haley proposes to weight these optimization function by $w'_{nk} = 1/d'^2_{nk}$ where, d'^2_{nk} is the minimum distance between C_n and C'_k.

3. Constructing the optimization functional for minimizing the transport between all pairs of island coastlines with unknown (Set A) transport streamfunction and the open boundaries of the domain: Let (C''_b) be the open boundary, $\{b\}$ be the set of open boundary points and C_n be the coast in Set A. Ψ_0 is not constrained to be a constant along C_n. Find the grid point i'' on the coastline n and the grid point b'' on the open boundary such that $[i'', b''] = \arg\max_{[i,b]} |\Psi_{0n}(i) - \Psi_{C''_b}(b)|$ and $\delta\Psi''_{n,b} = \Psi_{0n}(i'') - \Psi_{C''_b}(b'')$. Here, we denote Ψ_0 at the point b on the open boundary by $\Psi_{C''_b}(b)$.

The optimization functional for minimizing the inter-island transport between the island n and the open boundary is given by $(\Psi_{C_n} - \Psi_{C''_b}(b'') - \delta\Psi''_{n,b})^2 = (\Psi_{C_n} - \Psi_{0n}(i''))^2$. As before, Haley proposes to weight this optimization function by $w''_{nb} = 1/d''^2_{nb}$ where, d''^2_{nb} is the minimum distance between C_n and the open boundary C''_b.

The weighted average of the optimization functionals constructed from the above

three parts is given by:

$$E = \frac{1}{2}\sum_{n=1}^{N}[\sum_{m=1,m\neq n}^{N} w_{nm}(\Psi_{C_n} - \Psi_{C_m} - \delta\Psi_{n,m})^2 + \sum_{k=1}^{M} w'_{nk}(\Psi_{C_n} - \Psi_{0n}(i'))^2 + w''_{nb}(\Psi_{C_n} - \Psi_{0n}(i''))^2] \tag{3.17}$$

The minimum of E is computed by solving the standard least square problem i.e by setting gradients with respect to Ψ_{C_j}'s equal to zero. Therefore, the solution to the optimization problem in Equation 3.17 is given by:

$$\Psi_{C_j}[\sum_{m=1,m\neq j}^{N} 2w_{jm} + \sum_{k=1}^{M} w'_{jk} + w''_{jb}] - \sum_{m=1,m\neq j}^{N} 2w_{jm}\Psi_{C_m} = \sum_{m=1,m\neq j}^{N} 2w_{jm}\delta\Psi_{j,m} + \sum_{k=1}^{M} w'_{jk}\Psi_{0j}(i') + w''_{jb}\Psi_{0j}(i'') \tag{3.18}$$

Equation 3.18 represents a system of N equations which can be solved to obtain the transport streamfunctions (Ψ_{C_j}) along coastlines in set A. These streamfunction values, which smooth the velocity field, will be used as Dirichlet boundary conditions while solving the geostrophic flow equations using the Temperature and Salinity OA maps. The illustration of this methodology in the complex domain of Philippines Archipelago is discussed in Section 4.3.

Here, we discuss an extension of Equation 3.18 to involve new more suitable weights. Consider the stream function (Ψ) for a two-dimensional horizontal flow. It is defined such that the flow velocity can be expressed as:

$$\vec{u} = (u, v) = \frac{1}{H}\nabla \times \Psi\hat{k} \Rightarrow u = \frac{1}{H}\frac{\partial\Psi}{\partial y}, v = -\frac{1}{H}\frac{\partial\Psi}{\partial x} \tag{3.19}$$

Here, H is the ocean depth. The transport between a pair of islands having streamfunction ψ_1 and ψ_2 is given by:

$$\psi_2 - \psi_1 = \int_A \vec{u}.\hat{n}dA \tag{3.20}$$

where, A is the vertical area between the two islands and $\hat{n}$ is the unit vector normal

to the vertical area. Equation 3.19 and 3.20 suggests that the appropriate weight function to smooth the velocity field should be $w_{nm} = 1/A_{nm}^2$, where, A_{nm} is the minimum vertical area along any path between the two islands. The weight function proposed by Haley ($w_{nm} = 1/d_{nm}^2$) will be appropriate when the ocean depth is uniform in between all pairs of islands. Since the ocean depth is not uniform, a new methodology is required to compute the minimum area along any path between a pair of islands. Using the Fast Marching Method (FMM), which was described in Section 3.1.2, is a very convenient and efficient way to compute A_{nm}. Simulations have been performed with several other weight functions to confirm that the proposed weight function based on the minimum vertical area (A_{nm}) is the most appropriate for smoothing the velocity flow field (see Chapter 4 for illustration).

Computational details for obtaining the transport streamfunction: Fortran-90 code from MSEAS (Haley, personal communication) has been modified to utilize the weight function based on the minimum vertical area between islands, which was computed using the FMM, instead of the weight function based on the minimum distance between islands. For obtaining the minimum vertical area, the scalar speed function in the Eikonal Equation (Equation 3.7) is chosen to be F(x,y) = 1/H(x,y). The cost of computing the minimum distance is equal to the cost of computing the minimum vertical area using the FMM. Thus, the computational cost is independent of the choice of the weight function.

New methodologies for Objective Analysis in the multiply-connected coastal regions were proposed in this Chapter. The applications of these methodologies are discussed in Chapter 4. The Level Set Method and the Fast Marching Method have been used for OA in the complex domains of the Philippines Archipelago and Dabob Bay. These methodologies have been compared with the approach proposed by Lynch and McGillicuddy (2001) and the standard OA. Estimation of absolute velocity under geostrophic balance in Philippines Archipelago is also illustrated in Chapter 4. This is followed by a computational study of properties of the new mapping schemes in Chapter 5.

Chapter 4

Applications illustrating the novel OA methodologies

New methodologies for Objective Analysis in complex multiply-connected coastal regions were described in Chapter 3. These new methodologies are based on computing the optimal path lengths using the Level Set Method and the Fast Marching Method. These methods efficiently incorporate coastline constraints (e.g. there is no direct relationship across landforms). The above methodologies are utilized to map the temperature, salinity and biological (chlorophyll) fields using a 2-staged mapping scheme in subsets of the following regions: Dabob Bay and Philippines Archipelago.

Section 4.1 evaluates the use of our new OA methodology in Dabob Bay and shows that it is more effective over other classic distance optimizing algorithms like Bresenham's line algorithm (Bresenham, 1965). Section 4.2 shows a comparison of the different methodologies introduced in Chapter 3 for Objective Analysis in a subdomain of Philippines Archipelago. The estimation of absolute velocity under geostrophic balance by minimizing the inter-island transport is illustrated in Section 4.3. Section 4.4 discusses approaches for including non-homogeneous dynamical effects in our new Objective Analysis schemes.

4.1 Objective Analysis in Dabob Bay

Dabob Bay data are used to illustrate the effectiveness of the Fast Marching Method over other distance optimizing algorithms like Bresenham line algorithm (Bresenham, 1965). Maps for the temperature and salinity fields in a subdomain of Dabob Bay corresponding to the spatially irregular data in Figure C-4 are obtained using the a. Bresenham line algorithm, b. Averaged Bresenham line algorithm, and c. Fast Marching Method. The limitation of Bresenham line algorithm, which is explained in Chapter 3, is that the optimal distance computed using this method is discontinuous. This results in discontinuities in the covariance and also in the resultant field maps.

Figure C-5 shows the temperature and salinity field maps in Dabob bay obtained using large length scales $(L_0 = 60,\ L_e = 30)_{\mathrm{LS}}$, most energetic length scales $(L_0 = 30,\ L_e = 15)_{\mathrm{ME}}$ and observational error $(R = 0.25I)$. Temperature and salinity have higher magnitudes in the northern part of the western arm of Dabob bay. The eastern arm of Dabob bay has relatively low temperature and salinity. Effects due to the discontinuity in distance obtained from Bresenham line algorithm is clearly evident in Figure C-5(top). Numerical fronts having high temperature and salinity gradients exist at the intersection of the two arms. Such fronts lead to numerical problems in dynamical simulations. The geostrophic velocity obtained using these field maps will be unrealistic and will have high magnitudes along these fronts. A possible remedy, which reduces the discontinuity effects, is to smooth the distance by averaging distances of neighboring points (Lermusiaux and Haley, personal communication). The above averaging technique becomes numerically very expensive as shown by Lermusiaux and Haley.

The field maps obtained using the averaged Bresenham algorithm (Figure C-5(middle)) clearly show that the intensity of the erroneous fronts are reduced, but they still exist. Finally, the Fast Marching Method is used to compute distances and the Objective Analysis field maps obtained using FMM are clearly devoid of any numerical fronts (Figure C-5(bottom)). Along with that, FMM accurately satisfies coastline constraints and it is computationally inexpensive compared to using the

averaged Bresenham line algorithm. Thus, the use of FMM is recommended over the Bresenham line algorithm.

4.2 Objective Analysis in the Philippines Archipelago

This research study is motivated by the Philippines Straits Dynamics Experiment (PhilEx) sponsored by the Office of Naval Research. Novel OA techniques for such complex coastal regions are an important requirement to map very irregular datasets and initialize simulations. A comparison of the different OA methodologies will be illustrated in this region. We compare our new methods a. Level Set Method, b. Fast Marching Method, to the existing schemes, the a. Standard OA Method which ignores islands and uses the direct Euclidean distance, b. Stochastically forced Differential Equation approach (SDE specified for the field) and c. Stochastically forced Differential Equation approach (SDE specified for the covariance).

A comparison of these methods using the World Ocean Atlas, 2005 (Locarnini et al., 2006, Antonov et al., 2006) data for the temperature and salinity field maps is discussed in Section 4.2.1. WOA-05 data are data mapped using 'Levitus climatology' scheme (see Section 2.2) and is regularly spaced. Regularly spaced WOA-05 data is used here primarily to illustrate and discuss the comparison of the different methodologies. Subsequently, synoptic in situ data is used. These real direct ocean data are the spatially irregular temperature and salinity data. Results are presented in Section 4.2.2 (using Melville exploratory cruise data, Global Temperature-Salinity Profile Program - GTSPP (Center, 2006) data and HB2 Climatology for June-July'07), section 4.2.3 (using Melville exploratory cruise, sg122 and sg126 glider data for June-July'07) and section 4.2.4 (using joint Melville cruise data for Nov'07-Jan'08). Results of the new OA methodology based on FMM is illustrated in section 4.2.5 for the biological field (chlorophyll) using the exploratory cruise data. These biological OA field maps obtained using our FMM scheme can be utilized in the initialization for coupled

physics-biology modeling in MSEAS (Burton, 2009).

4.2.1 Objective Analysis using WOA-05 data: Comparison of the different OA methodologies

Two-dimensional horizontal OA maps for temperature and salinity fields in a subdomain of the Philippines Archipelago corresponding to the data in Figure C-6 computed using methodologies proposed in Chapter 3 are shown in Figures C-7 - C-16. Figures C-7 (LSM), C-8 (FMM), C-9 (Standard), C-10 (SDE specified for the covariance) and C-11 (SDE specified for the field) show the temperature field maps, while Figures C-12 (LSM), C-13 (FMM), C-14 (Standard), C-15 (SDE specified for the covariance) and C-16 (SDE specified for the field) show the salinity field maps. Depths shown are 0m, 40m, 200m, 450m, 1000m and 3000m. Large length scales $(L_0 = 540,\ L_e = 180)_{\mathrm{LS}}$ and most energetic length scales $(L_0 = 180,\ L_e = 60)_{\mathrm{ME}}$ are used with an observational error covariance $R = 0.25I$. For the SDE approach, the SDE parameter $k = 1/200$ and the observational error $(R = 0.25I)$ are used.

The OA field maps from all methods indicate that the Philippines Sea and the region near Palawan island is warmer than the rest of the region at the surface (0m). The region south of the Sulu sea around the Sulu Archipelago has relatively lower temperature. At levels below 500m, there is a significant difference in the temperature of the Sulu sea (warm) as compared to the rest of the region (cold) (Gamo et al., 2007, Gordon, 2009). These temperature fields clearly show that direct correlation across landforms are weak. Similar observations can be made for Salinity. Salinity in the Sulu Sea and South China Sea is lower than the salinity in the rest of the region at the surface (0m). At levels below 500m, the salinity in the Sulu sea is significantly lower as compared to the rest of the region. These salinity fields further support the hypothesis that direct correlation across landforms are weak.

The comparison of the temperature field maps and the salinity field maps obtained using different methods at level 1000m is shown in Figures C-17 and C-18, respectively. The methods based on LSM, FMM and SDE clearly satisfy coastline

constraints. The data in the Sulu Sea, which has high temperature and low salinity compared to the remaining region, does not have any influence on the field outside the Sulu Sea since the two regions are not connected by water. On the other hand, the standard OA does not satisfy coastline constraints. Thus the data outside the Sulu Sea, where the temperature is low and salinity is high, is correlated to the field inside the Sulu Sea. This is undesirable since the direct relationship across landforms is at best very weak. This leads to spurious high temperature and salinity gradients in the Sulu Sea, which will lead to problems for the estimation of geostrophic flow. Differences between temperature field maps and salinity field maps obtained using the Fast Marching Method and using other OA methods at level 1000m are shown in Figures C-19 and C-20, respectively. These plots show that there is a very small difference in field maps obtained using the FMM and LSM. The difference is larger between field maps obtained using the FMM and SDE approach. This is because the analytical correlation function corresponding to the stochastically forced Helmholtz equation, which is used in the SDE approach, is different from the analytical correlation function in the FMM. The difference between field maps obtained using the FMM and standard OA are significantly large because standard OA does not incorporate coastline constraints.

The field maps obtained by LSM (Figures C-7, C-12) and FMM (Figures C-8, C-13) are almost identical, but the FMM has a significantly lower computational cost. While LSM constructs the solution by iterating towards the solution, FMM is based on the direct construction of the stationary solution as described in Section 3.1. There is a very small difference in the field obtained using LSM and FMM because FMM exactly constructs the solution of the discretized Eikonal equation whereas LSM computes the solution within a desired tolerance limit. So, FMM is more accurate and less expensive compared to LSM. Thus, our OA methodology based on FMM should clearly be preferred over our methodology based on LSM.

The SDE approach satisfies coastline constraints, but the discretization errors in SDE are significant and this results in prominent spatial variations in the temperature and salinity fields. The impact of such huge spatial variations on the

geostrophic flow velocity is not good, and often additional smoothing has to be employed (post-processing) after obtaining the OA fields using the SDE approach. Such post-processing is not required for our FMM-based scheme. The SDE approach can be implemented by specifying the SDE for the field or by specifying it for the covariance (Logoutov, Lermusiaux, personal communication). If the SDE is specified for the field (Figure C-11, C-16) as opposed to the covariance (Figure C-10, C-15), spatial variation in the field will be less prominent. Specifying SDE (say Helmholtz equation) for the field is equivalent to carrying out the smoothing twice by using the Helmholtz equation. Thus, specifying the SDE for the field will be more expensive than specifying the SDE for the covariance, but this will make the spatial variation in the field less prominent and it will reduce the need for post-processing. Finally, we confirmed that the computational time required by the SDE approach is higher than that of FMM. Thus, FMM appears to be the best among all the methodologies discussed in Chapter 3 for Objective Analysis in coastal regions. Therefore, in Sections 4.2.2, 4.2.3, 4.2.4 and 4.2.5, we show and discuss results of our FMM-based Objective Analysis scheme for mapping spatially irregular data.

4.2.2 Objective Analysis for Summer 2007: Melville exploratory cruise, GTSPP and HB2 Climatology data

The coarse WOA-05 data used in Section 4.2.1 is regularly spaced and is already mapped using the 'Levitus Climatology' mapping scheme. The data used now is sampled in situ and is irregularly spaced. They were collected from the Melville Exploratory cruise, the Global Temperature-Salinity Profile Program - GTSPP (Center, 2006) and the HB2 Climatology for the June-July'07 period. The data location plot is shown in Figure C-21. Large length scales $(L_0 = 1080,\ L_e = 360)_{\mathrm{LS}}$, most energetic length scales $(L_0 = 270,\ L_e = 90)_{\mathrm{ME}}$ and observational error $(R = 0.2I)$ are used.

The temperature and salinity field maps obtained using the FMM-based OA scheme at the surface (0m) in Figure C-22 clearly show that coastline constraints are appropriately incorporated, since the warm region in the west of Luzon island is

uncorrelated with the region on the east of Luzon island. The same holds true for salinity, since the data in the low salinity region i.e. west of Luzon island does not have a significant impact on the field in the east of Luzon island. It is also observed that local effects and wind patterns lead to higher temperature and salinity in the Visayan Sea while the temperature and salinity in the Bohol Sea remain low.

Again, it should be noted that the data from the HB2 climatology is mapped data. Section 4.2.3 and 4.2.4 will discuss the examples of Objective Analysis using the exploratory cruise data alone.

4.2.3 Objective Analysis for Summer 2007: Melville exploratory cruise, sg122 and sg126 glider data

The data used in this example is collected from the Melville exploratory cruise, sg122 and sg126 gliders for the June-July'07 period. The data location plot is shown in Figure C-23. Since the data is available only in a small region of the Philippines Archipelago near islands, Objective Analysis maps are computed in a portion of the regular Philex domain. Large length scales $(L_0 = 1080,\ L_e = 360)_{\mathrm{LS}}$, most energetic length scales $(L_0 = 270,\ L_e = 90)_{\mathrm{ME}}$ and observational error $(R = 0.2I)$ are used. The temperature and salinity field maps obtained using the methodology based on the Fast Marching Method are shown in Figures C-24 and C-25, respectively at depths of 0m, 40m, 200m, 450m, 1000m and 3000m. Once again, these maps clearly indicate that coastline constraints are appropriately satisfied. At depths of 0m and 40m, the warm region in the west of Luzon island is uncorrelated with the region on the east of Luzon island. The warm Sibuyan and Visayan Seas can be distinguished from the relatively cold Bohol Sea. At depths of 450m and 1000m, the data in the warm Sulu sea and Bohol Sea does not have any impact on the remaining regions, clearly suggesting that there is no direct relationship across landforms. Similar observations are made for the salinity. At depths of 0m and 40m, the low salinity region in the west of Luzon island is uncorrelated with the region on the east of Luzon island.

We now compare fields in Summer 2007 from Melville exploratory cruise, sg122

and sg126 glider data (Figures C-24 and C-25) with fields from from Melville exploratory cruise, GTSPP and HB2 Climatology data (Figure C-22) (Section 4.2.3). This comparison illustrates differences in fields obtained using different datasets for Summer 2007. There is a good comparison between the two fields near islands. While the exploratory cruise and glider data is available in a small region around islands, the GTSPP and HB2 Climatology data is also available away from islands. Thus away from the island, fields from Melville exploratory cruise, GTSPP and HB2 Climatology data (Figure C-22) will be more accurate.

Section 4.2.4 will now discuss the example of Objective Analysis using the joint Melville cruise data in the winter season (Nov'07-Jan'08).

4.2.4 Objective Analysis for Winter 2008: Melville joint cruise data

The data used in this example is obtained from the joint Melville cruise for the Nov'07-Jan'08 period. The data location plot is shown in Figure C-26. Once again, since data are available in a small region of the Philippines Archipelago near islands, maps are obtained in a smaller subsection of the regular Philippines region. Large length scales $(L_0 = 1080,\ L_e = 360)_{\mathrm{LS}}$, most energetic length scales $(L_0 = 270,\ L_e = 90)_{\mathrm{ME}}$ and observational error $(R = 0.2I)$ are used for the OA field maps. The temperature and salinity field maps obtained using the FMM-based scheme are shown in Figures C-27 and C-28, respectively. Depths shown are 0m, 40m, 200m, 450m, 1000m and 3000m. Once again, at depths of 0m and 40m, the warm region in the west of Luzon island is uncorrelated with the region on the east of Luzon island. At depths of 450m and 1000m, the data in the warm Bohol Sea does not have any impact on the remaining regions, clearly suggesting that there is no direct relationship across landforms. Similar observations are made for salinity. At depths of 0m and 40m, the low salinity region in the west of Luzon island is uncorrelated with the region in the east of Luzon island.

We now compare fields in Winter 2008 from Melville joint cruise data with fields in

Summer 20007 from Melville exploratory cruise, sg122 and sg126 glider data (Section 4.2.3). It is clearly evident that the difference in temperature during Winter 2008 and Summer 2007 is more near the ocean surface. Beyond the depth of 200m, the difference is significantly less and the same inference is valid for salinity as well. At surface (0m), the temperature in the Sulu sea is nearly the same for both Summer 2007 and Winter 2008. But the temperature near Luzon island is significantly lower during Winter 2007 than the temperature during Summer 2007.

Section 4.2.5 illustrates the application of our FMM-based scheme for biological field (chlorophyll).

4.2.5 Objective Analysis for biological field (chlorophyll)

Application of our new FMM-based scheme for the biological field (chlorophyll) is illustrated here using Exploratory cruise Summer 2007 data. The biological OA field map obtained using FMM can be utilized in the initialization for coupled physics-biology modeling studies (Burton, 2009). The data location plot is shown in Figure C-29. Large length scales $(L_0 = 1080,\ L_e = 360)_{\mathrm{LS}}$, most energetic length scales $(L_0 = 270,\ L_e = 90)_{\mathrm{ME}}$ and observational error $(R = 0.2I)$ are used for the OA field maps at depths of 0m, 40m, 200m, 450m, 1000m, 3000m. The chlorophyll maps computed using our FMM-based scheme are shown in Figure C-30 at depths of 0m, 10m, 50m, 100m, 150m, 200m. The concentration of biological fields like chlorophyll, phytoplankton and zooplankton is substantial only near the surface due to the presence of sunlight. Therefore, the coupled physics-biology modeling studies are usually carried up to the depth of 200m.

The chlorophyll concentration is maximum near islands. Away from islands, it approaches the mean data value. At depth of 0m and 10m, the maximum chlorophyll concentration is observed in the south of the Visayan sea and in the Bohol Sea. At a depth of 50m, the chlorophyll concentration in the south of the Visayan sea and in the Bohol Sea remains significant. The maximum chlorophyll concentration is observed in the north of Palawan island.

4.3 Estimation of the absolute velocity under geostrophic balance in Philippines Archipelago

Estimation of absolute velocity under geostrophic balance in the Philippines Archipelago is illustrated in this section. The algorithm for minimizing the inter-island transport (Chapter 3) is utilized for computing a smooth geostrophic velocity flow field.

We proposed to utilize weight functions based on the minimum vertical area along each pair of islands in the algorithm for minimizing the inter-island transport. The estimation of the minimum vertical area has been carried out using the FMM by specifying the scalar speed function in the Eikonal equation (Equation 3.7) as F(x,y) = 1/H(x,y), where H is the ocean depth. The temperature and salinity data are from the World Ocean Atlas 2005 (Figure C-6). They are mapped using our FMM-based OA scheme (Figures C-8 and C-13) and the SDE approach (Figures C-11 and C-16), with the stochastically forced Helmholtz equation employed for the field. The streamfunction and velocity fields (at depths 0m, 100m, 1000m) using the maps from our FMM-based scheme are shown in Figure C-31. These plots show a very good comparison with the streamfunction and velocity obtained using the temperature and salinity field maps based on the stochastically forced Helmholtz equation, which are shown in Figure C-32. These maps suggest that the velocity is maximum in the Mindoro strait, near the Mindanao island and in the Balabac strait. At lower depths, the velocity remain high in the Mindoro strait and near the Mindanao island. There is a large inter-island transport across the Mindoro strait since the vertical area between the Mindoro and Palawan island is very large.

Haley's methodology utilizes weight functions based on the minimum inter-island distance which can be obtained using the FMM by specifying the scalar speed function in the Eikonal equation (Equation 3.7) as 1 for the sea points and 0 for the land points. The streamfunction and velocity fields (at depths 0m, 100m, 1000m) are obtained using the weight functions based on the minimum inter-island distance. The streamfunction and velocity fields using field maps from our FMM-based scheme are

shown in Figure C-33. Once again, these plots show a very good comparison with the streamfunction and velocity obtained using the temperature and salinity field maps based on the stochastically forced Helmholtz equation, which are shown in Figure C-34. These maps also suggest that the velocity is maximum in the Mindoro strait, near the Mindanao island and in the Balabac strait. But the velocity estimated in Balabac strait is very high and is clearly not acceptable. Such high velocity is obtained due to the inaccurate computation of inter-island transport.

These results clearly show that the weight functions based on the minimum vertical area will produce smooth geostrophic flow field with the least velocity hot spots.

4.4 Non-homogeneous dynamical effects in Objective Analysis

We satisfied coastline constraints using the FMM/LSM-based schemes, which solve the Eikonal equation (Equation 3.7) to obtain the length of the optimal path. By appropriately specifying the scalar speed function F in the Eikonal equation, which simply says that the gradient of the arrival time function is inversely proportional to the speed, the optimal path length can be obtained. The scalar speed function is specified as 1 for the sea points and 0 for the land points in the illustrations in Section 4.1 and 4.2. Additional effects due to the ocean bathymetry and the dynamics can also be incorporated in the Objective Analysis by appropriately modifying the scalar speed function (F) or the choice of the length scales.

Such dynamical effects can be explained in the context of continental a shelf. The scales in a continental shelf are not uniform. The correlation between any two points in the ocean will depend on the optimal path between the points and the non-uniform length scales on the optimal path. While the optimal path can be obtained using the FMM or LSM, the utilization of all the length scales on the optimal path has to be appropriately done. It can be argued that the dynamics will be governed by the smallest length scale on the optimal path, since the smallest length scale will govern

the correlation between the two points. Consider the example of a continental shelf shown in Figure C-35. In this figure, the scales in y-direction are large in both the regions: region A and region B. These regions are separated by a front having small length scales. Therefore, the correlation between any two points in the same region will be governed by the large length scale and the correlation between the points in different regions will be governed by the small length scale. Thus, the effect of non-homogeneous length scales can be incorporated by choosing the smallest scale on the optimal path.

Effects due to the bathymetry can be incorporated by specifying the scalar speed function at a given depth as the ratio of the bathymetry at the grid point and the depth at which the OA is carried out. This will ensure that even if the two points in the domain are separated by land at a certain depth, the correlation between those points at that depth is not necessarily zero. Since the land may not extend to a significant height above the depth at which the OA is carried out, it will be inappropriate to specify the scalar speed function as zero for such a pair of points. This is illustrated in Figure C-36 for the Philippines Archipelago at a depth of 450m. This figure shows the scalar speed functions for the general case and for the case in which effects due to the bathymetry are incorporated. The temperature and salinity fields obtained for these different cases are also compared. The difference is clearly visible in the Bohol Sea. In the general case, the data in the Sulu Sea is uncorrelated with the field in the Bohol Sea. But the use of modified scalar speed function shows that the data in the Sulu Sea has an affect on the field in the Bohol Sea. The scalar speed function can also be modified using other non-linear functions which depend on the bathymetry at the grid point and the depth at which the OA is carried out.

This discussion of the modification of the length scales or the scalar speed function can similarly be altered in different situations to include the dynamical effects (for example, conservation of the potential vorticity) in the Objective Analysis. This concludes the demonstration of the new OA methodologies and the methodology for obtaining the geostrophic flow velocities in complex coastal regions. The computational details of the OA methodologies will be discussed in Chapter 5.

Chapter 5

Computational Analysis and Derivations

Computational studies of properties of the new mapping schemes are carried out in this Chapter. Section 5.1 introduces the sequential processing of observations for mapping irregular data using our new OA schemes. Sequential processing reduces computational costs and it also allows to estimate the impact of the individual data. We introduce definitions of convex, simply-connected and multiply-connected domains here. A domain is said to be convex if for every pair of points within the domain, every point on the straight line segment that joins them is also within the domain. A domain is said to be simply-connected if any closed curve within it can be continuously shrunk to a point without leaving the domain. A domain which is not simply-connected is called multiply-connected. Section 5.2 introduces the Wiener-Khinchin and Bochner theorems for positive definite correlation functions. Positive definite correlation functions can generate a positive definite covariance matrix for a simply-connected convex domain using the Euclidean distance. Our mapping of observations is linked to the Kalman Filter's state update. It is known that the Kalman Filter encounters divergence problems if the covariance matrix becomes negative due to numerical issues (Brown and Hwang, 1997). Some useful techniques to counter these divergence problems are discussed in Section 5.3. The comparison of computational costs for different schemes is made in Section 5.4.

The Wiener-Khinchin and Bochner theorems are valid for the background error covariance matrix, Cor($\mathbf{x}$,$\mathbf{x}$) computed using the Euclidean distance for simply-connected convex domains. For complex coastal regions, Cor($\mathbf{x}$,$\mathbf{x}$) may not necessarily be positive definite due to: a. numerical error in the computation of the optimal path length using FMM/LSM b. the presence of landforms. This may lead to divergence problems for the field mapping based on the FMM/LSM scheme in complex coastal regions. Such divergence problems are illustrated using the WOA-05 data (Spliced February and Winter Climatology) shown in Figure C-37. The field maps obtained using our FMM-based scheme (one-scale) with length scales ($L_0 = 540$, $L_e = 180$) and length scales ($L_0 = 1080$, $L_e = 360$) are shown in Figure C-38. Fields obtained using the larger scales clearly show divergence problems near the Palawan island. Such problems are not encountered when the smaller length scales are used. Specifically, questions which motivate our research in Section 5.5 and 5.6 are: a. What are the computational errors in optimal path lengths computed using the FMM/LSM and how can they be reduced? b. What are the computational issues including non-positive definite covariances that arise in a multiply-connected coastal domain and how can they be remedied? A higher-order Fast Marching Method than the first-order one (see Section 3.1.2) is discussed in Section 5.5. Higher-order FMM results in a significant reduction of errors in distance estimates, i.e. the difference between numerically computed and true optimal distances. Thus, the higher-order FMM helps in dealing with divergence problems to some extent. In Section 5.6, methods to deal with negative covariances arising due to the presence of islands and due to the numerical error in computing the optimal path length are discussed. These methods, which can remove divergence problems, are discarding the problematic data, introducing the process noise and the dominant singular value decomposition of a-priori covariance.

5.1 Sequential Processing of Observations

A block-diagonal structure of the observation error covariance matrix (R) can be very advantageous for improving the computational efficiency and also for understand-

ing the impact of the individual data during the update step of the Kalman filter. Many pairs of observations, such as the observations from different instruments, can have uncorrelated errors resulting in a block-diagonal error covariance matrix ($\mathbf{R}$). In fact, Chapter 2 states that in most situations, the observation matrix for each data type is chosen diagonal with a uniform non-dimensional error variance ϵ^2, i.e. $R = \epsilon^2 I$. A Cholesky factorization can also be applied to diagonalize the $\mathbf{R}$ matrix prior to using sequential processing of observations. The modified algorithm, which takes the advantage of uncorrelated observations and the block-diagonal structure of $\mathbf{R}$ is now discussed (see Parrish and Cohn (1985), Cho et al. (1996)). One step (one scale) of the MSEAS OA equations (Equations 2.1, 2.2, 2.3) can be rewritten as:

$$
\begin{aligned}
K &= Cor(\mathbf{x},\mathbf{x})H^T[HCor(\mathbf{x},\mathbf{x})H^T + R]^{-1} && (5.1)\\
P^{OA} &= (I - KH)Cor(\mathbf{x},\mathbf{x}) && (5.2)\\
\psi^{\mathbf{OA}} &= \bar{\psi} + K[\mathbf{d} - H\bar{\psi}] && (5.3)
\end{aligned}
$$

where $\mathbf{H}$ is the observation matrix, $\bar{\psi}$ is the background field and P^{OA} is the error covariance of the estimated field. The block-diagonal matrix $\mathbf{R}$ can be written as:

$$
R = \begin{pmatrix} R_1 & & & \\ & R_2 & & \\ & & . & \\ & & & R_J \end{pmatrix} \qquad (5.4)
$$

where each block R_j, $j = 1, 2, ...J$ is a $p_j \times p_j$ matrix, such that $p_1 + p_2 + ... + p_j = p$ is the total number of observations. Similarly the observation vector d and the observation matrix H can be written as:

$$
d = \begin{pmatrix} d_1 \\ d_2 \\ . \\ d_J \end{pmatrix} \quad and \quad H = \begin{pmatrix} H_1 \\ H_2 \\ . \\ H_J \end{pmatrix} \qquad (5.5)
$$

Here, d_j is a vector of size p_j and H_j is the $p_j \times n$ observation matrix corresponding to the data in batch j. The scalar n is the length of the grid point position vector x. Thus, there are J batches of observations such that the observation error in the same batch may be correlated but the observations in different batches are uncorrelated. In order to sequentially process the observations by batch, lets begin by defining:

$$Cor(x,x)_0 = Cor(x,x) \quad and \quad \Psi_0 = \bar{\Psi}. \tag{5.6}$$

Then the modified equations for the sequential processing algorithm with j = 1,2,...N are:

$$\begin{aligned} K_j &= Cor(\mathbf{x},\mathbf{x})_{j-1} H_j^T [H_j Cor(\mathbf{x},\mathbf{x})_{j-1} H_j^T + R_j]^{-1} && (5.7)\\ Cor(\mathbf{x},\mathbf{x})_j &= (I - K_j H_j) Cor(\mathbf{x},\mathbf{x})_{j-1} && (5.8)\\ \psi_{\mathbf{j}} &= \psi_{\mathbf{j-1}} + K_j[\mathbf{d}_j - H_j \psi_{\mathbf{j-1}}] && (5.9) \end{aligned}$$

This gives $\psi^{OA} = \psi_{\mathbf{J}}$ and $P^{OA} = Cor(\mathbf{x},\mathbf{x})_J$ for each scale (step) of the OA scheme. The equivalence of Equations 5.1 - 5.3 and Equations 5.7 - 5.9 as proven by Parrish and Cohn (1985) is shown in Appendix A. Due to the smaller sizes of the matrices to invert, Equations 5.7 - 5.9 with the relevant matrix dimensions p_j are significantly less expensive than Equations 5.1 - 5.3 with dimension p.

The detailed implementation of the sequential processing Equations (5.7 - 5.9) is now discussed. Consider the case when all observations are uncorrelated i.e $p_j = 1$, j=1,2,...J. Then, the scalar R_j, row vector H_j of length n and the column vector K_j of length n are written as:

$$\sigma_j^2 = R_j, \quad h_j = H_j^T, \quad k_j = K_j \tag{5.10}$$

The final sequential processing algorithm is:

$$\begin{aligned} v_j &= Cor(x,x)_{j-1} h_j \\ \alpha_j &= h_j^T v_j + \sigma_j^2 \end{aligned}$$

$$
\begin{aligned}
k_j &= \frac{v_j}{\alpha_j} \\
\beta_j &= d_j - h_j^T \psi_{j-1} \\
\psi_j &= \psi_{j-1} + \beta_j k_j \\
Cor(x,x)_j &= Cor(x,x)_{j-1} - k_j v_j^T
\end{aligned} \tag{5.11}
$$

The computational efficiency can be further improved by taking the sparsity of h_j into account. For example, when an observation falls at a grid point, h_j will consist of a single one and the rest zeros. In this case, the v_j will be a column of $Cor(x,x)_{j-1}$. Apart from increasing the computational efficiency, the above algorithm also allows to estimate the impact of the individual observation on the OA field.

5.2 Positive definite correlation functions: Weiner-Khinchin and Bochner theorems

It was discussed in Chapter 2 that the covariance matrix is generated using analytical correlation functions. Such analytical correlation functions are termed "positive definite correlation functions" if they generate positive definite covariance matrix using the Euclidean distance for a simply-connected convex domain. It has been well established using the Wiener-Khinchin relationships that if a Fourier transform (or the spectral density of a correlation function) is non-negative for all frequencies then the correlation function is positive definite (Yaglom, 1987, Papoulis, 1991, Yaglom, 2004, Dolloff et al., 2006). The spectral density (or power spectrum) $S(\omega)$ is defined as the Fourier transform of the correlation function, i.e., $R(\tau) \leftrightarrow S(\omega)$, where:

$$
\begin{aligned}
S(\omega) &= \int_{-\infty}^{\infty} R(\tau) e^{-j\omega\tau} d\tau \\
R(\tau) &= \frac{1}{2\pi} \int_{-\infty}^{\infty} S(\omega) e^{j\omega\tau} d\omega
\end{aligned} \tag{5.12}
$$

The above equations are known as Wiener-Khinchin relationships. The sufficient condition for the validity of the above equation (to guarantee the existence of a

Fourier transform pair) is:

$$\int_{-\infty}^{\infty} |R(\tau)| d\tau < \infty. \tag{5.13}$$

The Wiener-Khinchin relationships are a part of the Wiener-Khinchin theorem, which states that $R(\tau)$ is a positive definite correlation function if $S(\omega) \geq 0 \ \forall \ \omega$. This is also known as the Bochner theorem (Yaglom, 1987, 2004, Dolloff et al., 2006).

The proof for the Weiner-Khinchin relationships or Bochner theorem (see Papoulis (1991), Yaglom (2004), Dolloff et al. (2006)) is described next. Let Γ be the matrix obtained from the correlation function $R(\tau)$. The proof of the statement, which says that Γ will be a semi-definite matrix if the spectral density $S(\omega)$ is non-negative ($S(\omega) \geq 0$), is as follows:
Let z be an arbitrary vector. Since ($S(\omega) \geq 0$) therefore,

$$\begin{aligned}
z^T \Gamma \bar{z} &= \sum_{i,k} z_i \bar{z_k} R(t_i - t_k) \\
&= \sum_{i,k} z_i \bar{z_k} \frac{1}{2\pi} \int_{-\infty}^{\infty} S(\omega) e^{j\omega(t_i - t_k)} d\omega \\
&= \frac{1}{2\pi} \int_{-\infty}^{\infty} S(\omega) [\sum_{i,k} z_i \bar{z_k} e^{j\omega(t_i - t_k)}] d\omega \\
&= \frac{1}{2\pi} \int_{-\infty}^{\infty} S(\omega) [\sum_{i} z_i e^{j\omega t_i}] [\sum_{i} \bar{z_i} e^{-j\omega t_i}] d\omega \\
&= \frac{1}{2\pi} \int_{-\infty}^{\infty} S(\omega) |\sum_{i} z_i e^{j\omega t_i}|^2 d\omega \geq 0
\end{aligned} \tag{5.14}$$

Note that the above proof assumes that the correlation function depends on the difference $t_i - t_k$ only, which is the case for the Euclidean distance in a simply-connected convex domain. But, this is not necessarily the case for the optimal path length computed on *multiply-connected domains* (e.g. using the Fast Marching or the Level Set Method). So, some computational problems may be observed with our new OA schemes for complex multiply-connected coastal regions and archipelagos since the covariance matrix may not be positive definite. Some numerical approaches to deal with such divergence problems will be discussed in this Chapter.

Using the above theorem, the necessary condition for the correlation function defined in Equation 2.4 to be positive definite, can be obtained. The conditions are derived next. The following Fourier transform relations (Dolloff et al., 2006) are used:

$$e^{-\alpha r^2} \quad \leftrightarrow \quad \left(\frac{\pi}{\alpha}\right)^{\frac{1}{2}} e^{\frac{-\omega^2}{4\alpha}} \tag{5.15}$$

$$r^n f(r) \quad \leftrightarrow \quad (i)^n \frac{d^n F}{d\omega^n} \tag{5.16}$$

Here, F is the Fourier transform of f(r). Using Equation 5.15, the following Fourier transform pairs are obtained:

$$e^{-\frac{x^2}{2L_e^2}} \quad \leftrightarrow \quad (2\pi L_e^2)^{\frac{1}{2}} e^{\frac{-\omega_1^2 L_e^2}{2}} \tag{5.17}$$

$$e^{-\frac{y^2}{2L_e^2}} \quad \leftrightarrow \quad (2\pi L_e^2)^{\frac{1}{2}} e^{\frac{-\omega_2^2 L_e^2}{2}}. \tag{5.18}$$

Multiplying Equations 5.17 and 5.18 gives:

$$e^{-\frac{x^2+y^2}{2L_e^2}} \quad \leftrightarrow \quad (2\pi L_e^2) e^{\frac{-(\omega_1^2+\omega_2^2)L_e^2}{2}}. \tag{5.19}$$

Using Equations 5.16 and 5.17, the Fourier transform of $(x^2+y^2)e^{-\frac{x^2}{2L_e^2}}$ w.r.t. the variable x is given by:

$$(x^2+y^2)e^{-\frac{x^2}{2L_e^2}} \quad \leftrightarrow \quad (2\pi L_e^2)^{\frac{1}{2}} e^{\frac{-\omega_1^2 L_e^2}{2}} [L_e^2 - \omega_1^2 L_e^4] + y^2 (2\pi L_e^2)^{\frac{1}{2}} e^{\frac{-\omega_1^2 L_e^2}{2}}. \tag{5.20}$$

Using Equations 5.20, 5.18 and 5.16, the Fourier transform of $(x^2+y^2)e^{-\frac{x^2+y^2}{2L_e^2}}$ w.r.t. the variable y is given by:

$$(x^2+y^2)e^{-\frac{x^2+y^2}{2L_e^2}} \quad \leftrightarrow \quad (2\pi L_e^2) e^{\frac{-(\omega_1^2+\omega_2^2)L_e^2}{2}} [L_e^2 - \omega_1^2 L_e^4] + (2\pi L_e^2) e^{\frac{-(\omega_1^2+\omega_2^2)L_e^2}{2}} [L_e^2 - \omega_2^2 L_e^4]. \tag{5.21}$$

Finally, Equations 5.21 and 5.19 are combined to obtain the Fourier transform of the

correlation function in equation 2.4. Thus:

$$\left(1-\frac{x^2+y^2}{L_0^2}\right)e^{-\frac{x^2+y^2}{2L_e^2}} \quad \leftrightarrow \quad (2\pi L_e^2)e^{\frac{-(\omega_1^2+\omega_2^2)L_e^2}{2}}\left[1-2\frac{L_e^2}{L_0^2}+(\omega_1^2+\omega_2^2)\frac{L_e^4}{L_0^2}\right] \quad (5.22)$$

Thus, Equation 5.22 shows that the correlation (Equation 2.4) will be positive definite when $\left[1-2\frac{L_e^2}{L_0^2}+(\omega_1^2+\omega_2^2)\frac{L_e^4}{L_0^2}\right] \geq 0$, i.e. when $L_0 \geq \sqrt{2}L_e$, as the power spectrum will then be non-negative for all ω. It is important to note that the above derivation holds only when the Euclidean distance is used along with the correlation function in a simply-connected convex domain.

5.3 Divergence issues with the Kalman filter

Our mapping schemes can encounter divergence problems associated with the Kalman Filter state and covariance update equations (Brown and Hwang, 1997). If the number of observations is large, divergence problems can arise under certain conditions due to truncation errors even if the background covariance is positive definite. Like any numerical procedure, the round off errors can lead to problems as the number of steps increase. This can also occur in the sequential processing of observations (recursive algorithm). If the covariance matrix loses the property of positive definiteness, then the solution of the Gauss Markov Estimation (equivalent here to the Kalman Filter update) will not necessarily be stable. Of course, such problems due to truncation errors can be minimized by using a high-precision arithmetic.

Some of the useful techniques described by Brown and Hwang (1997) to counter the divergence problems are:

a. Introduce Process Noise: As the number of steps increases, the covariance matrix approaches a semidefinite condition. A small numerical error can thus make the covariance matrix non-positive definite, which may lead to divergence problems. A solution is to add a small process noise (model wise or in the OA case background noise) to the diagonal elements of the covariance matrix. This will lead to a degree of sub-optimality but will prevent the divergence problems from arising.

b. Symmetrize covariance matrix: The covariance matrix may become asymmetric due to roundoff errors and this asymmetry can grow if it is left unchecked, leading to divergence problems. The remedy is to symmetrize the covariance matrix after each recursive step. One approach will be to assume the symmetry and to use only the upper (or lower) triangular part of the covariance matrix for all matrix operations.

c. Use Joseph's form: If a large initial uncertainty (covariance matrix with large eigen values) is followed by a very precise measurement (small observational error, R), the covariance matrix has to transition from a large value to a small value in a single step and this situation can numerically be very sensitive. The Kalman Filter update equation for the covariance (P) is given by (see also Table 2.1):

$$P_t = (I - K_t H_t) P_{t|t-1}. \tag{5.23}$$

It is recommended to use other covariance update formulas like the Joseph form (Grewal and Andrews, 1993) which has a natural symmetry. The Joseph form is given by:

$$P_t = (I - K_t H_t) P_{t|t-1} (I - K_t H_t)^T + K_t R_t K_t^T. \tag{5.24}$$

The Joseph form (Equation 5.24) has a better numerical behavior (Grewal and Andrews, 1993) for unusual numerical situations than the form in Equation 5.23.

d. U-D factorization: The U-D factorization algorithm (Bierman, 1977), which is mathematically equivalent to the regular Kalman Filter algorithm and belongs to the class of Kalman Filter algorithms known as square-root filtering (Battin, 1964, Bierman, 1977, Maybeck, 1979), has much better numerical behavior for a large number of steps (equivalent to the number of observations). This algorithm, which will preserve the symmetry and positive definiteness, is based on propagating the factors of covariance (P) rather than the full covariance (P). This algorithm is favored over the regular Kalman Filter when numerical stability is a concern. The U-D factorization algorithm is now described. Note that it has some similarity to the Error Subspace

Statistical Estimation (ESSE) update scheme (see Lermusiaux and Robinson (1999), Lermusiaux (1999a,b)).

A symmetric, positive definite covariance matrix can be decomposed into the form:

$$P = UDU^T. \tag{5.25}$$

where U is a upper triangular matrix (having ones along the major diagonal) and D is diagonal ($D \geq 0$). The a-priori covariance matrix ($P_{1|0}$) at $t = 0$ is factored using the U-D decomposition:

$$P_{1|0} = U_{1|0} D_{1|0} U_{1|0}^T. \tag{5.26}$$

The Kalman gain (K) and the state update are carried out using the usual Kalman Filter equations by replacing the a-priori covariance using Equation 5.26. The covariance update form is:

$$\begin{aligned} P_t &= P_{t|t-1} - P_{t|t-1} H(t)^T (H(t) P_{t|t-1} H(t)^T + R(t))^{-1} H(t) P_{t|t-1} \\ &= P_{t|t-1} - \frac{P_{t|t-1} H(t)^T H(t) P_{t|t-1}}{\alpha} \end{aligned} \tag{5.27}$$

where the scalar α is given by:

$$\alpha = H(t) P_{t|t-1} H(t)^T + R(t) \tag{5.28}$$

Note that in the sequential processing of observations, a single observation is taken in each step of processing since the observational error matrix (R) is diagonal. Therefore, α is a scalar. In the general case, when R is a block diagonal matrix, the covariance update form is:

$$P_t = P_{t|t-1} - P_{t|t-1} H(t)^T \alpha^{-1} H(t) P_{t|t-1} \tag{5.29}$$

The covariances P_t and $P_{t|t-1}$ can be replaced by their U-D factors. This gives:

$$\begin{aligned} U_t D_t U_t^T &= U_{t|t-1} D_{t|t-1} U_{t|t-1}^T - \frac{U_{t|t-1} D_{t|t-1} U_{t|t-1}^T H(t)^T H(t) U_{t|t-1} D_{t|t-1} U_{t|t-1}^T}{\alpha} \\ &= U_{t|t-1} \left[D_{t|t-1} - \frac{(D_{t|t-1} U_{t|t-1}^T H(t)^T)(D_{t|t-1} U_{t|t-1}^T H(t)^T)^T}{\alpha} \right] U_{t|t-1}^T \end{aligned} \tag{5.30}$$

The bracketed term in Equation 5.30 is symmetric, so it can be factored using U-D factorization.Thus:

$$\left[D_{t|t-1} - \frac{(D_{t|t-1} U_{t|t-1}^T H(t)^T)(D_{t|t-1} U_{t|t-1}^T H(t)^T)^T}{\alpha} \right] = \bar{U}_t \bar{D}_t \bar{U}_t{}^T. \tag{5.31}$$

This gives:

$$\begin{aligned} U_t D_t U_t^T &= U_{t|t-1} \bar{U}_t \bar{D}_t \bar{U}_t{}^T U_{t|t-1}^T \\ &= (U_{t|t-1} \bar{U}_t) \bar{D}_t (U_{t|t-1} \bar{U}_t)^T \end{aligned} \tag{5.32}$$

Since $(U_{t|t-1}\bar{U}_t)$ is an upper triangular and $\bar{D}_t$ is diagonal, therefore:

$$\begin{aligned} U_t &= U_{t|t-1} \bar{U}_t \\ D_t &= \bar{D}_t. \end{aligned} \tag{5.33}$$

These equations are the same as the ESSE update equations (see Lermusiaux and Robinson (1999), Lermusiaux (1999a,b)).

For Objective Analysis, using the sequential processing of observations, the covariance update in terms of U-D factors U_j and D_j (j=1,2,...J, J is the number of observations) is:

$$U_{j+1} = U_j \bar{U}_j \tag{5.34}$$

$$D_{j+1} = D_j. \tag{5.35}$$

where, U_0 and D_0 can be expressed in terms of the background covariance (Cor($\mathbf{x}$,$\mathbf{x}$)):

$$U_0 D_0 U_0^T = Cor(\mathbf{x}, \mathbf{x}) \tag{5.36}$$

As mentioned, the U-D factorization helps in dealing with divergence issues by ensuring that the covariance matrix always remains positive definite. In situations where there are adequate process noise entering the system states, the usual Kalman Filter update equation (Equation 5.23) is also capable of handling all the divergence issues and the algorithm based on U-D factorization may not be necessary.

5.4 Comparison of Computational Costs

For a 2-dimensional domain with N points in each direction, a comparison of the operation count for computing the optimal distance from a data location to all other grid points in the domain using different Methods is given in Table 5.1.

Method	Operation Count
Level Set Method	O(N^3)
Fast Marching Method	O($N^2 logN$)
Dijkstra's Method	O(N^3)

Table 5.1: Comparison of the operation count for the optimal distance obtained using LSM, FMM and Dijkstra's Method.

There are a total of N^2 grid points at each level and the operation count for LSM is obtained from an optimistic guess that LSM will take roughly N steps to converge. In reality, the iterations can take much longer to converge, and therefore LSM is not a very efficient method for computing the optimal distance to perform OA. On the other hand, FMM is an efficient technique which requires a fast method to locate the smallest value grid point in the *narrow band*. The Min-Heap data structure with backpointers (Sedgewick, 1988) is employed to efficiently locate the grid point with the minimum value. The total work done in the DownHeap and UpHeap operations, which ensure that the updated quantities do not violate the heap properties, is O(log

N). Thus 2-dimensional FMM with N grid points in each direction has an operation count of $N^2 logN$, which is a significant improvement over LSM. It has also been observed that FMM requires less computational time (approximately 15 %) than the SDE approach proposed by Lynch and McGillicuddy (2001). Thus, the OA based on FMM is computationally the most efficient technique for mapping in multiply-connected domains.

5.5 Higher order Fast Marching Method

In a domain with no islands or landforms, the optimal path length obtained using the FMM/LSM should ideally be equal to the Euclidean distance. But the numerical estimation of the optimal path length using the FMM/LSM has discretization errors and this leads to an inaccurate estimation of the optimal path length. We have discussed that the Weiner Khinchin and Bochner theorems are valid for covariances computed using the Euclidean distance in a simply-connected convex domain. The covariance matrix may no longer be positive definite due to the inaccurate computation of the optimal path length by FMM/LSM or due to the presence of islands. This may lead to divergence problems in the resultant field maps based on the FMM/LSM scheme as shown in Figure C-38. Specifically, the question which motivates this Section is: What are the computational errors in optimal path lengths computed using the FMM/LSM and how can they be reduced? In this section, we introduce the higher order Fast Marching Method which will reduce errors in the estimation of the optimal path length.

The Fast Marching Method presented in Section 3.2 is a first order scheme, since the first order discretization form (Equation 3.10) of the Eikonal equation (Equation 3.7) was used. A different implementation of FMM with higher accuracy (Sethian, 1999a,b) is discussed here. Note that the second order backward approximation to the first derivative T_x is given by:

$$T_x \approx \frac{3T_i - 4T_{i-1} + T_{i-2}}{2\Delta x} \Leftrightarrow T_x \approx D^{-x}T + \frac{\Delta x}{2} D^{-x-x}T \tag{5.37}$$

Similarly, the second order forward approximation to the first derivative T_x is given by:

$$T_x \approx \frac{3T_i - 4T_{i+1} + T_{i+2}}{2\Delta x} \Leftrightarrow T_x \approx D^{+x}T - \frac{\Delta x}{2} D^{+x+x}T \tag{5.38}$$

Here D^{-x} and D^{+x} are the first order forward and backward approximations for the first derivative, respectively (Equation 3.6), $D^{-x-x} \equiv D^{-x}D^{-x}$and $D^{+x+x} \equiv D^{+x}D^{+x}$.

Consider the switch functions defined by:

$$switch_{ij}^{-x} = \begin{pmatrix} 1 & \text{if } T_{i-2,j} \text{ and } T_{i-1,j} \text{ are known ('Alive') and } T_{i-2,j} \leq T_{i-1,j} \\ 0 & \text{otherwise} \end{pmatrix}$$
$$switch_{ij}^{+x} = \begin{pmatrix} 1 & \text{if } T_{i+2,j} \text{ and } T_{i+1,j} \text{ are known ('Alive') and } T_{i+2,j} \leq T_{i+1,j} \\ 0 & \text{otherwise} \end{pmatrix} \tag{5.39}$$

Similar functions are defined in the y direction. The higher accuracy scheme attempts to use a second order approximation for the derivative whenever the points are tagged as 'alive' (the points inside the band where the value of the arrival time function is frozen: see Section 3.2) but reverts to the first order scheme otherwise.

The modified discretization equation for the higher accuracy FMM is given by:

$$\begin{pmatrix} max([D_{ij}^{-x}T + switch_{ij}^{-x}\frac{\Delta x}{2}D_{ij}^{-x-x}T], -[D_{ij}^{+x}T - switch_{ij}^{+x}\frac{\Delta x}{2}D_{ij}^{+x+x}T], 0)^2 \\ + \\ max([D_{ij}^{-y}T + switch_{ij}^{-y}\frac{\Delta y}{2}D_{ij}^{-y-y}T], -[D_{ij}^{+y}T - switch_{ij}^{+y}\frac{\Delta y}{2}D_{ij}^{+y+y}T], 0)^2 \end{pmatrix} = \frac{1}{F_{ij}^2} \tag{5.40}$$

It should be noted that the above scheme is not necessarily a second order scheme. The accuracy of the above scheme depends on how often the switches evaluate to zero and how the number of points where the first order method is applied changes as the mesh is refined. When the number of points where the first order method is applied is relatively small (occurs only near the coastlines), the error is reduced considerably by using the higher accuracy FMM. This is clearly evident from Figures

C-39 and C-40, which show a comparison of the distances and correlation (difference and normalized difference from Euclidean distance) obtained using the first order and higher accuracy FMM schemes in the trivial case when a scalar speed function F is equal to one everywhere in the domain. It should also be noted that a third or higher-order approximations for the derivative T_x can similarly be used to construct more accurate FMM schemes, but this will increase the computational cost. Figures C-39 and C-40 also show that the relative error in the optimal distance computed using FMM is higher near the data point and it reduces as the distance increases. To keep the computational cost low and a uniform relative error, one can use higher accuracy FMM near the data point and then progressively shift to the lower order schemes as the distance increases.

The higher order Fast Marching Method has been used to minimize errors in the estimation of the optimal path length in Philippines Archipelago. Figure C-41 clearly shows that the use of higher order Fast Marching Method has attenuated the divergence problems compared to the first order FMM. The divergence problems do not vanish completely because of the presence of landforms and due to discretization errors associated with higher order FMM. We introduce other methods to deal with such divergence problems for multiply-connected coastal domains in Section 5.6.

5.6 Positive Definite covariance matrix for complex multiply-connected coastal regions

We discussed in Section 5.2 that the Weiner-Khinchin and Bochner theorems are valid for the background error covariance matrix computed using the Euclidean distance for simply-connected convex domains. The matrix may become negative due to the discretization error in the optimal path length computed using FMM/LSM. The use of higher order FMM was therefore recommended in Section 5.5. The covariance matrix may also become negative due to the presence of islands and coastlines.

Specifically, the question which motivates this Section is: What are the compu-

tational issues including non-positive definite covariances that arise in a multiply-connected coastal domain and how can they be remedied? The presence of islands and archipelagos results in stretching of the Euclidean path in the physical domain which can potentially make the covariance matrix negative. A negative covariance matrix results in divergence problems associated with the Kalman Filter (which is linked to the algorithm for sequential processing of observations). Examples of this will be shown next. Possible remedies are then discussed starting with curvilinear coordinates (Section 5.6.1). Then, other methods to deal with the negative covariance matrix due to the presence of islands and due to the inaccurate estimation of the optimal path length using the FMM or LSM are discussed (Section 5.6.2).

Consider the idealized multiply-connected domain having an island, shown in Figure C-42. This domain has 12 grid points which are marked as ocean points and 4 grid points which are marked as land points. The length of the optimal path is computed exactly to form the covariance matrix to keep it untouched from effects due to discretization errors in the FMM/LSM. The positive-definite correlation function $Cor(r) = exp\left[-\frac{r^2}{2L^2}\right]$ with L=2 is used to form the covariance matrix. We find that the covariance matrix is not positive definite. The maximum eigen value for the covariance matrix is 6.3345 while the minimum is -0.0504. This idealized example clearly shows that the covariance matrix based on the optimal path length for a complex multiply-connected region may not necessarily be positive definite.

5.6.1 Curvilinear grids

If a very high accuracy FMM is used, the optimal distance computed using this high accuracy FMM is equivalent to the Euclidean distance only for simply-connected convex domain. Thus, to ensure that the Weiner-Khinchin relationship or Bochner theorem hold, a mapping technique based on using curvilinear coordinates can be used (Cebeci et al., 2005). However, this will stretch the correlation scales as we will describe now. First, an irregular region having islands in the physical plane in the Cartesian (x,y) or the polar (r,θ) coordinates is mapped on the curvilinear (ζ, η) coordinates such that the mapped region is a simply-connected convex domain.

A simple example of such a mapping in a domain having a circular island (which is mapped to a rectangular domain and islands are absent in the mapped region) is illustrated in Figure C-43. The domain having a circular island in the polar (r,θ) coordinates is mapped on the curvilinear (ζ, η) coordinates. The optimal distance in this transformed coordinate system will be the Euclidean distance for which the Weiner-Khinchin and Bochner theorems hold. These optimal distances also satisfy coastline constraints i.e. there is no direct relationship across landforms. For example, the distance between the locations (ζ0,η3) and (ζ0,η7) (which are separated by the island in the polar coordinates) in the curvilinear coordinates (Figure C-43) will be equal to the length of the optimal path in the polar coordinates which is different from the across-land Euclidean distance between the locations (r0,θ3) and (r0,θ7) in the polar coordinates. It should also be noted that the distance between the locations (ζ0,η3) and (ζ0,η7) is equal to the distance between the location (ζ3,η3) and (ζ3,η7) in the curvilinear coordinates. This is not the case in the polar coordinates where the length of the optimal path between (r0,θ3) and (r0,θ7) is smaller than the length of the optimal path between (r3,θ3) and (r3,θ7). This corresponds to decreasing the grid resolution away from the island. Thus, the mapping in transformed coordinates will lead to deformations of the length scales specified for the Objective Analysis in the physical region. Also, the mapping becomes complicated when the domain has multiple islands of distorted shapes. Therefore, alternative methods are required to remove problems arising due to the presence of islands.

5.6.2 Other methods

Other methods which are very useful in removing the divergence problems (Figure C-44 (Top-Left)) due to the negative covariance matrix are:

a. Discarding the problematic data: One method to deal with the problem of a negative covariance matrix is to discard the data corresponding to the negative values of $H_j Cor(\mathbf{x}, \mathbf{x})_{j-1} H_j^T$. Even though, this will ensure that there are no divergence issues in the resultant OA, this method is a not the most acceptable one since the information in the data is discarded entirely. The field map obtained by discarding

the problematic data is shown in Figure C-44 (Top-Right). Clearly, the divergence problems are removed but loosing all the information in the data is not acceptable.

b. Introducing process noise: As discussed in Section 5.3, adding a small process noise to the diagonal elements of the covariance matrix helps in dealing with the divergence problems associated with a negative covariance matrix. The disadvantage is that the process noise introduced will lead to a degree of sub-optimality. It is often a more acceptable method compared to discarding the data. Once again, the field map obtained by introducing the process noise is free from divergence problems and the plot is shown in Figure C-44 (Bottom-Left).

c. Dominant Singular Value Decomposition (SVD) of a-priori covariance: To construct the field maps using the OA techniques, the full covariance matrix is not required. The computation of the full covariance matrix (Cor($\mathbf{x}$,$\mathbf{x}$)) is expensive and it is therefore rarely done for the OA in complex coastal regions. The necessary requirement to obtain the field maps is the matrix corresponding to the grid and the data point covariance (Cor($\mathbf{x}$,$\mathbf{X}$)). The divergence problems in the Kalman update or in the sequential processing of observations can be removed by first obtaining the singular value decomposition (SVD) of Cor($\mathbf{x}$,$\mathbf{X}$) and then reconstructing the new covariance matrix by retaining only the dominant singular values and setting the smaller singular values (less than 1 percent of the maximum singular value) to zero. The above procedure will make the covariance positive definite. It has been verified that the magnitude of the negative eigen values in the covariance matrix is very small compared to the magnitude of the maximum eigen value. This verification establishes that the use of the dominant singular value decomposition method is the most acceptable method to remove the divergence problems in the update because it looses the least information contained in the data. Once again, the field map obtained by dominant singular value decomposition (SVD) of a-priori covariance is free from divergence problems and the plot is shown in Figure C-44 (Bottom-Right). It has also been verified that fields obtained by introducing the process noise and fields obtained by dominant singular value decomposition of the a-priori covariance are very similar.

Another important and challenging problem in oceanography is estimating the

scales from the data. New methodologies for scale estimation based on the structure function method, short term Fourier transform (STFT) and second generation wavelet (SGW) analysis are discussed in the next Chapter.

Chapter 6

Adaptive Scale Estimation

A major but apparently simple challenge in geophysical fluid dynamics at sea is the estimation of the dominant spatial-time scales in field measurements. This may seem basic for scientists and engineers not used to ocean data, but due to the multi-scale, turbulent and/or intermittent ocean dynamics and due to the irregular properties of the data, it is a very common question in ocean meetings. In this chapter, we investigate new methods for adaptive spatial-time scale estimation from irregular ocean field measurements. Solving this question would significantly help in better understanding and sampling of ocean processes.

New adaptive schemes to learn the largest and the most energetic scales based on structure functions (Denman and Freeland, 1985) and on non-linear least square fitting methods (Appendix B) are first outlined in Section 6.1. An example of an adaptive scheme based on short term Fourier transforms (STFT), which can be used for non-stationary signals, is illustrated in Section 6.2. It is applied to an idealized dataset generated using a chirp signal, in which the frequency and the wave number varies with time. In Section 6.3, we illustrate another new adaptive scale-estimation scheme based on second generation wavelets (Sweldens, 1998, Jansen and Oonincx, 2005). Second generation wavelets are applicable to both irregularly sampled and non-dyadic data sets. This is important since we would like to estimate scales in the data without mapping the data. To map the data, one needs scale estimates, as described in previous chapters. Ultimately, the goal of all new methods investigated

below would be to create a map of time and space scales that evolves as ocean data are collected or are fed to the scale estimation scheme, all without requiring to map the data.

6.1 A new adaptive scale estimation method using structure functions

The new adaptive algorithm derived in this section can be employed to estimate the spatial-time scales from the available oceanic data field. The approach proposed by Denman and Freeland (1985) is utilized to obtain the isotropic structure function ($B(r)$) from the data field (θ). The structure function ($B(r)$) is defined by:

$$\begin{aligned} B_i(r) &= E[(\theta(x_i + r) - \theta(x_i))^2] + 2N \\ &= E[\theta(x_i + r)\theta(x_i + r)] + E[\theta(x_i)\theta(x_i)] - 2E[\theta(x_i + r)\theta(x_i)] + 2N \\ &= 2[F(0) - F(r) + N] \\ &= 2N + 2F(0)[1 - Cor(r)] \end{aligned} \tag{6.1}$$

where $F(r) = E[\theta(x_i + r)\theta(x_i)]$, $Cor(r) = F(r)/F(0)$ and N is the noise variance. We have assumed that errors in measurements $\theta(x_i + r)$ and $\theta(x_i)$ are independent. So the variance of the error in $(\theta(x_i + r) - \theta(x_i))$ is given by $2N$. The noise-free correlation function with properties $Cor(0) = 1$ and $Cor(r) \to 0$ as $r \to \infty$ has been given in Equation 2.4.

Our new adaptive learning algorithm utilizes the structure function $B(r)$ obtained from the available data to learn the unknown scale parameters by using the non-linear least squares fitting method (Appendix B). An adaptive learning algorithm for estimating the length scale (L) and the time scale (τ) is as follows:

1. Assume an initial approximation for the scales. Consider the data in the time window $\Delta t = \tau_s/4$.

2. Obtain the structure function from the data available in the time interval Δt

and the spatial window $|x - x_i| \leq L_l$ for all the grid points.

3. Length scales (L_s^S and L_l^S) are obtained by the non-linear least square fit of the structure function from the data to the analytical structure function.

4. The following learning equation is used to obtain the new length scales.

$$L_l^{(k+1)} = L_l^k + lr(L_l^S - L_l^k)$$
$$L_s^{(k+1)} = L_s^k + lr(L_s^S - L_s^k) \tag{6.2}$$

   Here, lr is the learning rate.

5. A similar analysis is repeated for obtaining the time scales.

It should be noted that more than one spatial or time scales can be estimated by appropriately selecting the spatial and temporal window. The data in the corresponding spatial-temporal window can be used for estimating the large and small scales.

Scales estimated from the adaptive learning algorithm based on the structure function in the complex domain of Philippines Archipelago using the Melville (Summer 2007) exploratory cruise data (Figure C-23) are shown in Figure C-45. Small scale estimates on 26^{th} June, 2007 are obtained from the exploratory cruise data collected on and before 26^{th} June, 2007. Scale estimates are available in the Bohol Sea and near the Panay island. As more data gets collected, the new scale estimate plot on 15^{th} July, 2007 shows that estimates are also available in the Mindoro strait. It can also be observed that scales in the Bohol Sea are slightly smaller due to the change in wind circulation during the period between 26^{th} June, 2007 and 15^{th} July, 2007.

6.2 A new adaptive scale estimation method using short term Fourier transforms (STFT)

Another adaptive learning scheme based on short term Fourier transforms (STFT) is proposed in this section to estimate the spatial-time scales, but assuming a regularly

spaced and idealized dataset. This allows us to evaluate capabilities of the STFT method.

Idealized data corresponding to the chirp signals (swept sinusoids) has been generated and the adaptive algorithm is employed to learn the instantaneous frequency of the chirp signal. The data has been generated at N ($N = 40000$) time instances for the spatial domain ($0 \leq x \leq X = 50$) and the time domain ($0 \leq t \leq T = 50$). The data function is given by:

$$u(x_i, t_i) = 3sin\{k_1(x_i)x_i + \omega_1(t_i)t_i\} + sin\{k_2(x_i)x_i + \omega_2(t_i)t_i\}$$

where,

$$\begin{aligned}
t_i = T\frac{i-1}{N} \quad &; \quad x_i = X\frac{mod(i-1, \sqrt{N})}{\sqrt{N}-1}; \\
k_1(x_i) = \frac{2\pi}{1.5} + \frac{x_i}{2X}(\frac{2\pi}{2.5} - \frac{2\pi}{1.5}) \quad &; \quad k_2(x_i) = \frac{2\pi}{6} + \frac{x_i}{2X}(\frac{2\pi}{12} - \frac{2\pi}{6}); \\
\omega_1(t_i) = \frac{2\pi}{2.5} + \frac{t_i}{2T}(\frac{2\pi}{1.5} - \frac{2\pi}{2.5}) \quad &; \quad \omega_2(t_i) = \frac{2\pi}{12} + \frac{t_i}{2T}(\frac{2\pi}{6} - \frac{2\pi}{12}).
\end{aligned} \tag{6.3}$$

The instantaneous wave numbers (k_{1inst}, k_{2inst}), frequencies (ω_{1inst}, ω_{2inst}), length scales (L_{1inst}, L_{2inst}) and time scales (T_{1inst}, T_{2inst}) corresponding to this chirp signal are given by:

$$\begin{aligned}
k_{1inst}(x_i) = \frac{2\pi}{1.5} + \frac{x_i}{X}(\frac{2\pi}{2.5} - \frac{2\pi}{1.5}) \quad &; \quad k_{2inst}(x_i) = \frac{2\pi}{6} + \frac{x_i}{X}(\frac{2\pi}{12} - \frac{2\pi}{6}); \\
\omega_{1inst}(t_i) = \frac{2\pi}{2.5} + \frac{t_i}{T}(\frac{2\pi}{1.5} - \frac{2\pi}{2.5}) \quad &; \quad \omega_{2inst}(t_i) = \frac{2\pi}{12} + \frac{t_i}{2T}(\frac{2\pi}{6} - \frac{2\pi}{12}); \\
L_{1inst}(x_i) = \frac{2\pi}{k_{1inst}(x_i)} \quad &; \quad L_{2inst}(x_i) = \frac{2\pi}{k_{2inst}(x_i)} \\
T_{1inst}(x_i) = \frac{2\pi}{\omega_{1inst}(x_i)} \quad &; \quad T_{2inst}(x_i) = \frac{2\pi}{\omega_{2inst}(x_i)}
\end{aligned} \tag{6.4}$$

The stepwise algorithm based on STFT, which has been implemented to adaptively learn the length and time scales, is as follows:

1. Assume an initial approximation for the small and large spatial scales (L_s, L_l) and the small and large time scales (T_s, T_l) at all the grid points.

2. Consider the data in a time interval which is significantly smaller than the smallest time scale ($T_s/8 \geq \Delta t$). Apply the short term Fourier transform (STFT) in the spatial window ($|x - x_i| \leq L_l$) and analyze the corresponding wave number spectrum. The two wave numbers corresponding to the peak amplitudes of the wave number spectrum will give an estimate of the small (L_s^F) and the large (L_l^F) spatial scales in the signal. The new length scales are obtained using the learning equations:

$$L_l^{(k+1)} = L_l^k + lr(L_l^S - L_l^k)$$
$$L_s^{(k+1)} = L_s^k + lr(L_s^S - L_s^k) \tag{6.5}$$

   Here, lr is the learning rate.

3. A similar analysis is repeated for obtaining the time scales. STFT is applied in the time window ($|t - t_i| \leq T_l$) to analyze the data frequency. The two frequencies corresponding to the peak amplitudes of the frequency spectrum will give an estimate of the small (T_s^F) and the large (T_l^F) time scales in the signal. The new time scales can be obtained by using the learning equations (similar to Equation 6.5). The process is repeated to adaptively learn the new length and time scales as the new data is received for the next time interval Δt ($T_s/8 \geq \Delta t$).

Plots for the small and the large length scales for chirp signal data (Equation 6.3) computed using the adaptive learning algorithm described above, are shown in Figure C-46. A comparison has been made between the analytical instantaneous length scales (Equation 6.4) and the scales adaptively learned from the data with a learning rate, $lr = 0.1$. The accuracy of scales depends on the resolution of Fourier spectrum. The analytical small scales and the small scales obtained using the adaptive learning algorithm compare well, since the STFT wave number resolution is good (see Figure C-46 (Top-Left)). Jumps observed in the small scales are due to the finite resolution of wave numbers. However, for the large scales, the STFT wave number resolution is not as good as the small scales, and the scale estimate obtained using the adaptive

learning algorithm does not match well with the analytical instantaneous scales (see Figure C-46 (Top-Right)). Similar trends are observed from plots for time scales shown in Figure C-46. There is a good comparison between plots for small time-scales obtained using the learning algorithm with a learning rate 0.1 and the instantaneous small time scales corresponding to the chirp signal data (see Figure C-46 (Bottom-Left)). But, the large time scales do not compare well since the frequency resolution is not good (see Figure C-46 (Bottom-Right)).

Results obtained above are encouraging and a possible approach to improve the scale estimates is by adaptively learning scales using the wavelet analysis (since the signal is not stationary and the frequency changes with time). To understand effects of varying the learning rate (lr), spatial-time scales have been obtained for the same chirp signal data with a learning rate $lr = 0.2$. With an enhanced learning rate, the scales are now more sensitive to the incoming data. The plots for the large spatial scales and the large time scales (see Figure C-47 (Right panel)) obtained using the adaptive learning algorithm with learning rate $lr = 0.2$ show that the oscillations in the estimated length and time scales are severe compared to the adaptive learning with learning rate $lr = 0.1$. The advantage of having a larger learning rate is that scales will converge to the true scales in a small number of steps, but at the cost of higher sensitivity to the incoming data.

Another data set has been generated at N ($N = 40000$) time instances for the spatial domain ($0 \leq x \leq X = 50$) and the time domain ($0 \leq t \leq T = 50$) to validate the adaptive algorithm based on STFT for learning the spatial-time scales. The wavenumber and frequency for the data function (Data Set 2) are given by:

$$\begin{pmatrix} k_1(x_i,t_i) \\ k_2(x_i,t_i) \\ \omega_1(x_i,t_i) \\ \omega_2(x_i,t_i) \end{pmatrix} = \begin{pmatrix} \frac{2\pi}{1.5} \\ \frac{2\pi}{12} \\ \frac{2\pi}{1.5} \\ \frac{2\pi}{12} \end{pmatrix}_{\substack{0\leq x_i\leq X/2, \\ 0\leq t_i\leq T/2}} ; \begin{pmatrix} X/2\leq x_i\leq X \\ T/2\leq t_i\leq T \end{pmatrix} \begin{pmatrix} \frac{2\pi}{2.5} \\ \frac{2\pi}{6} \\ \frac{2\pi}{2.5} \\ \frac{2\pi}{6} \end{pmatrix}_{\substack{X/2\leq x_i\leq X, \\ 0\leq t_i\leq T/2}} \begin{pmatrix} 0\leq x_i\leq X/2 \\ T/2\leq t_i\leq T \end{pmatrix}$$

$$t_i = T\frac{i-1}{N}; x_i = X\frac{mod(i-1,\sqrt{N})}{\sqrt{N}-1}; \tag{6.6}$$

The true spatial-time scales are given by:

$$\begin{aligned} L_{1true}(x_i,t_i) &= \frac{2\pi}{k_1(x_i,t_i)} \quad ; \quad L_{2true}(x_i,t_i) = \frac{2\pi}{k_2(x_i,t_i)} \\ T_{1true}(x_i,t_i) &= \frac{2\pi}{\omega_1(x_i,t_i)} \quad ; \quad T_{2true}(x_i,t_i) = \frac{2\pi}{\omega_2(x_i,t_i)} \end{aligned} \tag{6.7}$$

Our new STFT-based adaptive algorithm for learning the spatial-time scales is employed, and the estimated scales are compared with the true scales. Plots comparing the spatial-time scales obtained using the learning algorithm and the true spatial-time scales are shown in Figure C-48. The estimated small spatial-temporal scales compare well with the true small spatial-temporal scales (see Figure C-48 (Left panel)) but oscillations are observed in the large spatial-temporal scale estimates (see Figure C-48 (Right panel)) due to limited resolution by STFT. These results indicate that the learning algorithm suggested in this section is a reasonable approach to estimate the spatial-temporal scales. Further improvement in accuracy of the estimated scales can be expected by using wavelet analysis.

Note that STFT can only be used on data signals which are regularly spaced. But the oceanic data is collected by platforms whose positions vary irregularly with time. Therefore, the learning algorithm based on the structure function (Section 6.1) and the algorithm based on second generation wavelets (Section 6.3) will be more relevant to the ocean data. The above work was mainly carried out to quantify capabilities of the STFT method.

6.3 A new adaptive scale estimation method using second generation wavelets

Scales in the ocean vary with time. The scale estimation is thus a non-stationary problem, which makes the use of Fourier Transform less adequate. Short term Fourier

transforms (STFT) and first generation wavelets are applicable to non-stationary signals and are proven to be very useful in engineering and computer science, but they require regularly spaced dyadic data which is not the case with ocean data. The ocean data is irregular and non-dyadic. The use of a regular field obtained by mapping the data should also be avoided if possible, since the mapping procedure introduces artificial scales and therefore scales estimated from mapped fields will be different from scales estimated using the ocean data.

Wavelets are mathematical functions that divide the data into different frequency components and each component is then studied with a resolution that matches its scale. Two well-known admissible wavelets (Figure C-49) which have been used in several applications are:

a. Haar Wavelet: The Haar wavelet is defined by:

$$\psi(x) = \begin{cases} 1, & x\epsilon[0, 1/2), \\ -1, & x\epsilon[1/2, 1), \\ 0, & otherwise. \end{cases} \tag{6.8}$$

a. Mexican Hat Wavelet: Mexican hat wavelet is the second derivative of the Gaussian function. It is given by:

$$\psi(x) = \frac{-d^2}{dx^2} e^{-x^2/2} = (1 - x^2) e^{-x^2/2} \tag{6.9}$$

Second generation wavelet (SGW) decomposition (Sweldens, 1998, Jansen and Oonincx, 2005), which is evaluated directly on irregular locations and does not need dyadic data, is now discussed. The approach can also automatically adapt to the data on finite intervals, without requiring artificial techniques like extension of data near the boundaries. SGW is based on using the so called *lifting* scheme. Lifting can be viewed as a method to construct a wavelet transform, which has the ability to enhance the first generation wavelet transform, by adding desirable properties. A description of the lifted version of the Haar wavelet transform (Sweldens, 1998, Jansen and Oonincx, 2005) is now provided.

A Haar decomposition takes the fine scale scaling coefficients as inputs. It can be assumed that these fine scale coefficients are observations. The resolution level corresponding to observations is the finest. Second generation wavelet analysis proceeds in successive steps by extracting the coarser scale trends in each successive step. A *lifting* scheme consists of three operations: a split, followed by a sequence of *dual* and *primal lifting* operations. As shown in Figure C-50, the splitting step divides the input signal f into two disjoint sets: observations with odd indices (γ_1) and even indices(λ_1). Each step of the Haar decomposition computes averages and differences of the adjacent input values. Let $s_{j+1,k}$ be the input at scale $j+1$. One step of Haar decomposition transforms the input into averages $s_{j,k}$ and details (differences) $d_{j,k}$ at the scale j. The corresponding equations are:

$$d_{j,k} = s_{j+1,2k+1} - s_{j+1,2k} \tag{6.10}$$

$$\begin{aligned} s_{j,k} &= \frac{s_{j+1,2k} + s_{j+1,2k+1}}{2} \\ &= s_{j+1,2k} + \frac{d_{j,k}}{2} \end{aligned} \tag{6.11}$$

Thus the *dual lifting* step of the second generation Haar wavelet decomposition replaces the odd indexed input values by the difference between the odd and the even indexed input value. Similarly, the *primal lifting* step of the second generation Haar wavelet decomposition replaces the even indexed input values by the mean of the odd and the even indexed input value. The rectangular boxes linking the odd and the even branches in Figure C-50 stand for the convolution operations. In the *dual lifting* step (Predict), the even indexed coefficients are convolved with some sequence (P) and the result is subtracted from the odd indexed coefficients. The *primal lifting* step (Update) convolves the resulting difference with another sequence (U) and add the result to the even indexed coefficients. The convolution operators P and U for the Haar transform are 1 and 1/2 respectively.

The second generation wavelet transformation based on the Haar decomposition is utilized to obtain scales in the chirp signal. A Data set was generated at N ($N = 1025$)

time instances for the time domain ($0 \leq t \leq T = 256$) using the function:

$$3sin(\omega(t)t)$$

where,

$$\omega(t) = \frac{2\pi}{32} + \frac{.5t}{T}\left[2\pi - \frac{2\pi}{32}\right] \tag{6.12}$$

The instantaneous time scale corresponding to the above data is given by:

$$T_{inst}(t) = \frac{1}{\frac{1}{32} + \frac{t}{T}\left[1 - \frac{1}{32}\right]} \tag{6.13}$$

Figure C-51 shows the contour plot of the scale coefficients varying with time. The scale coefficients are obtained by the SGW transformation based on the Haar decomposition of the chirp signal given by Equation 6.12. The true instantaneous scales (Equation 6.13) are plotted in the same figure to study the behavior of the scale coefficients obtained using the SGW. There is a good comparison between the true instantaneous scales and the estimated scales, but a dispersion of the scale coefficients is also observed. Haar wavelets are an example of the simplest wavelet, with low resolution. However, the above illustration using chirp signals shows that SGW can potentially be a powerful tool for scale estimation in the ocean.

Adaptive scale estimation in the ocean using second generation wavelets based on other admissible wavelets like the Mexican Hat or Morkel wavelets is a subject of further research study. The *primal* and *dual lifting steps* needs to be appropriately tuned for using these wavelets. A goal will be to reduce the dispersion of scale coefficients for accurate adaptive scale estimation for oceans.

Among the three methods discussed above, the method based on the structure function and the method based on the second generation wavelets look more promising, since these methods are valid for the non-dyadic and irregularly spaced ocean dataset.

Chapter 7

Summary and Conclusions

Our research consisted of three related investigations: a. new methodologies for the mapping and dynamical inference of ocean fields from irregular data in complex multiply-connected domains, b. computational studies of properties of the new mapping schemes, and c. the adaptive estimation of spatial and temporal scales. Results, findings and future work are summarized next.

New methods for efficient field mapping, i.e. Objective Analysis, in complex coastal regions were researched, implemented and utilized. These new OA methods, which satisfy coastline constraints (e.g. there is no direct relationship across landforms), are based on estimating the length of the optimal path using either the Level Set Method (LSM) or the Fast Marching Method (FMM). These novel methods were applied and studied in complex domains of the Philippines Archipelago and Dabob Bay using realistic datasets to obtain field estimates such as temperature, salinity and biology (chlorophyll). Results were compared with those of a standard OA scheme (using across-landforms Euclidean distance in the analytical correlation function) and of OA schemes based on the use of stochastically forced differential equations (SDE), including that proposed by Lynch and McGillicuddy (2001). We have shown that our new FMM-based scheme is computationally inexpensive compared to our LSM-based scheme and the SDE approach. Our illustrations and studies show that field maps obtained using our FMM-based scheme do not require postprocessing (smoothing) of fields e.g. they are devoid of any spurious hydrographic field gradients which are un-

acceptable for flow computation. We have also shown that the use of FMM is the most appropriate method for the optimal distance estimation among the distance estimation methodologies like Dijkstra's optimization algorithm and the classic Bresenham line algorithm. The optimal distance computed using Dijkstra's algorithm is computationally expensive and inaccurate. Apart from being computationally expensive, the optimal distance computed using the Bresenham line algorithm is discontinuous. This results in the formation of fronts with high field gradients. Such high gradient fronts do not occur when our FMM-based scheme is utilized. We have also utilized our new FMM-based OA scheme for incorporating non-homogeneous dynamical effects by appropriately modifying the scalar speed function in the Eikonal equation. In particular, we have used a bathymetry-dependent scalar speed function to include bathymetric effects at lower depth levels. We also proposed the use of the smallest length scale on the optimal path to include the non-homogeneous effects due to the existence of fronts in a continental shelf. In the future, analogous modification of the scalar speed function or the length scale can be used to incorporate other dynamical effects (e.g. conservation of potential vorticity). The optimal path length obtained using our FMM/LSM-based scheme can also be used to extend the methodology proposed by Lermusiaux et al. for three-dimensional, multivariate and multi-scale spatial mapping of geophysical fields and their dominant errors (Lermusiaux et al., 1998, 2000, Lermusiaux, 2002) to complex coastal regions. Three-dimensional, multivariate and multi-scale spatial mapping using our FMM based scheme is also a subject of further research.

Computational studies of properties of the new mapping schemes were carried out. The sequential processing of observations reduces the computational cost and also helps in understanding the impact of individual data. We have used the Wiener-Khinchin and Bochner theorem to obtain the relationship among parameters of the analytical correlation function for it to be positive definite. Such analysis is valid only for the correlation functions based on the Euclidean distance for convex simply-connected domains. When the number of observations is large, the Kalman Filter or the sequential processing of observations may have divergence problems due to

numerical reasons. Methods to remove divergence problems arising from numerical issues were discussed. It was found that the covariance matrix is no longer positive definite when the optimal path length is computed using FMM. Therefore, the use of high order FMM was discussed and implemented to obtain more accurate length of shortest sea paths. However, we found that the covariance matrix also becomes negative due to the presence of islands and other non-convex landforms. Several approaches to overcome this issue were discussed. These include discarding problematic data points, introducing process noise, and reducing the covariance matrix based on the dominant singular value decomposition (SVD). Among these, we argue that introducing process noise and using the dominant SVD are the best solutions.

We have also derived and implemented new FMM based methodology for the estimation of absolute velocity under geostrophic balance in complex multiply-connected domains. FMM is used for the computation of the minimum vertical area between all pairs of islands. The minimum area is required for obtaining the transport streamfunction which minimizes the inter-island transport and produces a smooth velocity flow field. The transport streamfunction can then be utilized to estimate the geostrophic flow velocity from the temperature and salinity field maps alone. We have illustrated this method by applying it in a subdomain of the Philippines Archipelago.

The estimation of spatial-temporal scales from irregular ocean field measurements would be potentially a significant advance to the ocean community for better understanding and sampling of ocean processes. This is a challenging problem due to the multi-scale, turbulent and/or intermittent ocean dynamics and due to the irregular properties of the data. Three new methods for adaptive spatial-temporal scale estimation were proposed and implemented. These methods are based on using the structure function, short term Fourier transforms and second generation wavelet analysis. To our knowledge, this is the first time that adaptive methods for the spatial-temporal scale estimation are proposed and used in ocean studies. The application of our new scale estimation schemes based on the structure function method was illustrated using Melville (Summer 2007) exploratory cruise data. We also illustrated the application of short term Fourier transforms and second generation wavelet analysis using chirp

signal data. Second generation wavelet analysis for adaptive spatial-time scale estimation from the irregularly spaced ocean data is shown to be a promising technique and will be a subject of further research.

Appendix A

Proof of Algorithm for Sequential Processing of Observations

The equivalence of Equations 5.1 − 5.3 and Equations 5.7 − 5.9, as proven by Parrish and Cohn (1985), is given here. The proof will follow from an inductive argument after establishing the equivalence for J=2. Here we denote the background field and covariance by $\bar{\psi}$ and Cor(x,x), respectively and the estimated field and its error covariance by $\bar{\psi}^{OA}$ and P^{OA}, respectively. Equation 5.1 can be rearranged to the form:

$$K = (I - KH)Cor(x, x)H^T R^{-1}. \tag{A.1}$$

Using Equation 5.2, Equation A.1 can be written as:

$$K = P^{OA}H^T R^{-1}. \tag{A.2}$$

Using Equation A.2, Equation 5.3 becomes

$$\psi^{OA} = \bar{\psi} + P^{OA}H^T R^{-1}(d - H\bar{\psi}). \tag{A.3}$$

According to Equations 5.4 and 5.5,

$$R = \begin{pmatrix} R_1 & 0 \\ 0 & R_2 \end{pmatrix}, \quad d = \begin{pmatrix} d_1 \\ d_2 \end{pmatrix}, \quad H = \begin{pmatrix} H_1 \\ H_2 \end{pmatrix}. \tag{A.4}$$

Using A.4, Equation A.3 can be written as

$$\psi^{OA} = \bar{\psi} + P^{OA}[H_1^T R_1^{-1}(d_1 - H_1\bar{\psi}) + H_2^T R_2^{-1}(d_2 - H_2\bar{\psi})] \tag{A.5}$$

The Woodbury formula establishes the equivalence of equations in A.6 for arbitrary conformable matrices A, B, C, R, provided that the indicated inverse exists.

$$C = B - BA^T(ABA^T + R)^{-1}AB \Leftrightarrow C^{-1} = B^{-1} + A^T R^{-1} A \tag{A.6}$$

The Equations 5.1 and 5.2 lead to

$$P^{OA} = Cor(x,x) - Cor(x,x)H^T(HCor(x,x)H^T + R)^{-1}HCor(x,x) \tag{A.7}$$

Using A.6, the equivalent statement of A.7 will be:

$$(P^{OA})^{-1} = (Cor(x,x))^{-1} + H^T R^{-1} H \tag{A.8}$$

The a-posterior error covariance is obtained by substituting A.4 in Equation A.8

$$(P^{OA})^{-1} = (Cor(x,x))^{-1} + H_1^T R_1^{-1} H_1 + H_2^T R_2^{-1} H_2 \tag{A.9}$$

To show the equivalence of Equations $5.1 - 5.3$ and Equations $5.7 - 5.9$, it needs to be shown that A.5 and A.9 holds for the sequential processing of observations (Equations $5.7 - 5.9$). Apply the Woodbury formula to equations 5.7 and 5.8 and get

$$(Cor(x,x)_1)^{-1} \quad = \quad (Cor(x,x))^{-1} + H_1^T R_1^{-1} H_1 \tag{A.10}$$

$$(P^{OA})^{-1} = (Cor(x,x)_1)^{-1} + H_2^T R_2^{-1} H_2 \quad \text{(A.11)}$$

Equations A.10 and A.11 can be combined to eliminate $(Cor(x,x)_1)$. This leads to a-posterior error covariance Equation A.9. To verify that A.5 holds, Equation 5.9 is written as:

$$\psi_1 = \bar{\psi} + Cor(x,x)_1 H_1^T R_1^{-1}(d_1 - H_1\bar{\psi}). \quad \text{(A.12)}$$

$$\psi^{OA} = \psi_1 + P^{OA} H_2^T R_2^{-1}(d_2 - H_2\psi_1). \quad \text{(A.13)}$$

Eliminate ψ_1 from Equations A.12 and A.13 to obtain

$$\psi^{OA} = \bar{\psi} + (I - P^{OA} H_2^T R_2^{-1} H_2) Cor(x,x) H_1^T R_1^{-1}(d_1 - H_1\bar{\psi}) + P^{OA} H_2^T R_2^{-1}(d_2 - H_2\bar{\psi}). \quad \text{(A.14)}$$

Premultiply A.11 by P^{OA} and postmultiply it by $Cor(x,x)$ to obtain

$$P^{OA} = (I - P^{OA} H_2^T R_2^{-1} H_2) Cor(x,x). \quad \text{(A.15)}$$

Using Equation A.15 in A.14 gives Equation A.5. This proves the equivalence of Equations $5.1 - 5.3$ and Equations $5.7 - 5.9$ for J=2. The proof of the general case follows from an inductive argument.

Appendix B

Nonlinear least squares fitting method

Given a non-linear function having a known analytic form with n independent parameters i.e $f(x; \mu_1, \mu_2, \mu_3, ...\mu_n)$ and consider the over-determined set of m equations $(m > n)$:

$$\begin{aligned} y_1 &= f(x_1; \mu_1, \mu_2, \mu_3, ...\mu_n) \\ y_2 &= f(x_2; \mu_1, \mu_2, \mu_3, ...\mu_n) \\ &... \\ y_m &= f(x_m; \mu_1, \mu_2, \mu_3, ...\mu_n). \end{aligned} \tag{B.1}$$

The values μ_1,μ_2,μ_3,...μ_n, which best satisfy the above system of equations (by minimizing the sum of the squared residuals) can be obtained using the nonlinear least squares fitting method. The approach is outlined next:

1. An initial guess for μ_i is chosen. Define the error (β_i) as:

$$\beta_i = y_i - f(x_i; \mu_1, \mu_2, \mu_3, ...\mu_n) \tag{B.2}$$

2. A linearized estimate for the change in parameters $(d\mu_i)$ which reduces the error

(β_i) to zero is given by:

$$\beta = Ad\mu \tag{B.3}$$

where $m - by - n$ matrix A is given by

$$A = \begin{pmatrix} \frac{\partial f}{\partial \mu_1}\Big|_{(x_1,\mu)} & \cdots & \frac{\partial f}{\partial \mu_n}\Big|_{(x_1,\mu)} \\ \frac{\partial f}{\partial \mu_1}\Big|_{(x_2,\mu)} & \cdots & \frac{\partial f}{\partial \mu_n}\Big|_{(x_2,\mu)} \\ . & \cdots & . \\ \frac{\partial f}{\partial \mu_1}\Big|_{(x_m,\mu)} & \cdots & \frac{\partial f}{\partial \mu_n}\Big|_{(x_m,\mu)} \end{pmatrix}$$

Apply the matrix A^T to both sides of Equation B.3 to obtain

$$A^T\beta = (A^TA)d\mu \tag{B.4}$$

Equation B.4 can be solved for $d\mu$ using the standard linear algebraic equation solvers such as Gaussian elimination or LU decomposition. The offset $d\mu$ is applied to μ.

3. The process is iteratively applied till the offset $d\mu$ becomes smaller than the desired tolerance level.

This is the nonlinear least squares fitting method, which is utilized in the adaptive scale estimation using the structure function method.

Appendix C

Figures

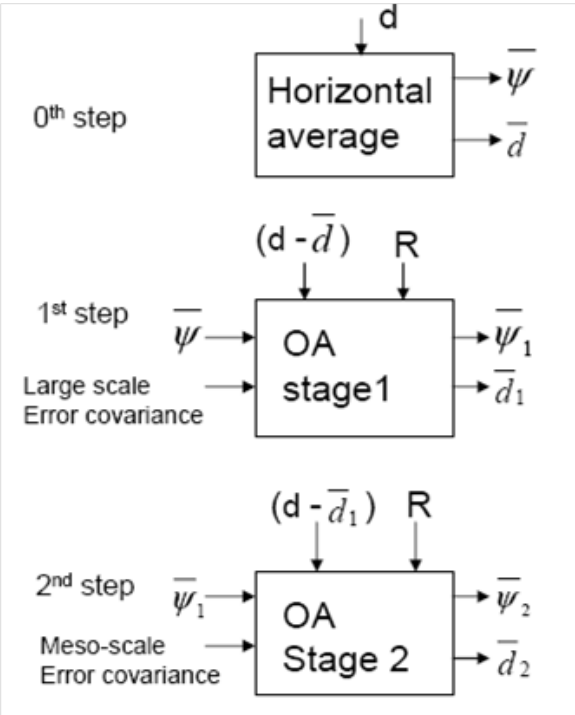

Figure C-1: MSEAS 2-stage Objective Analysis

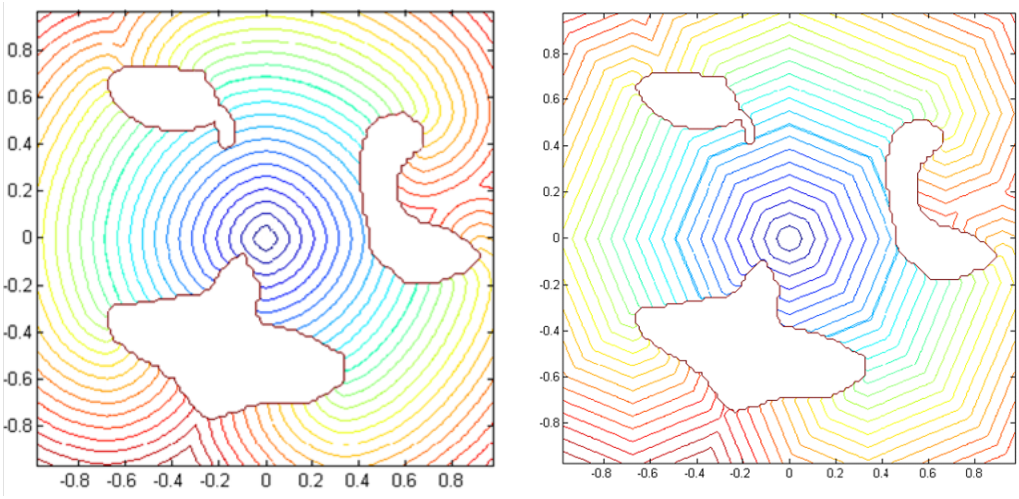

Figure C-2: Comparison between FMM (Left) and the Dijkstras (Network Flow) algorithm (order = 2) (Right) for optimal path planning (Takei, 2006)

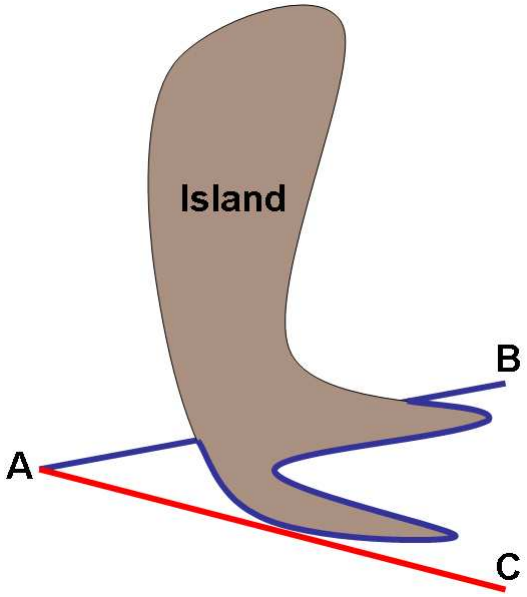

Figure C-3: Illustration of the Bresenham Line Algorithm

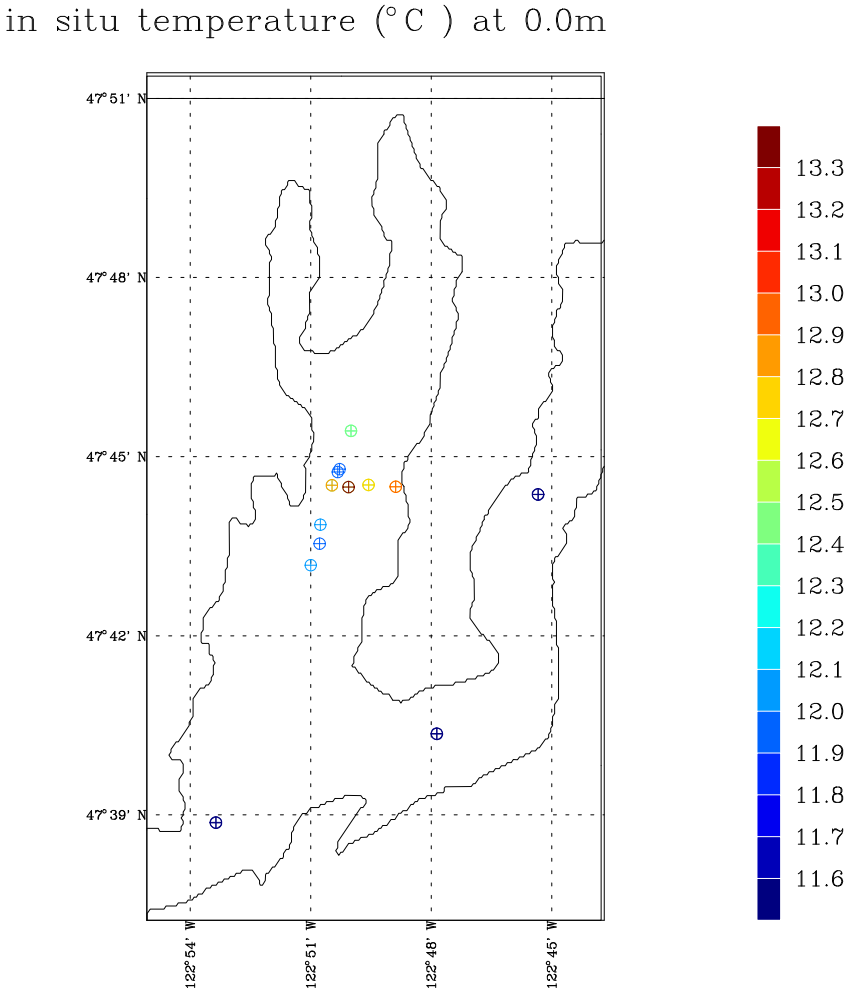

Figure C-4: Temperature data in Dabob Bay

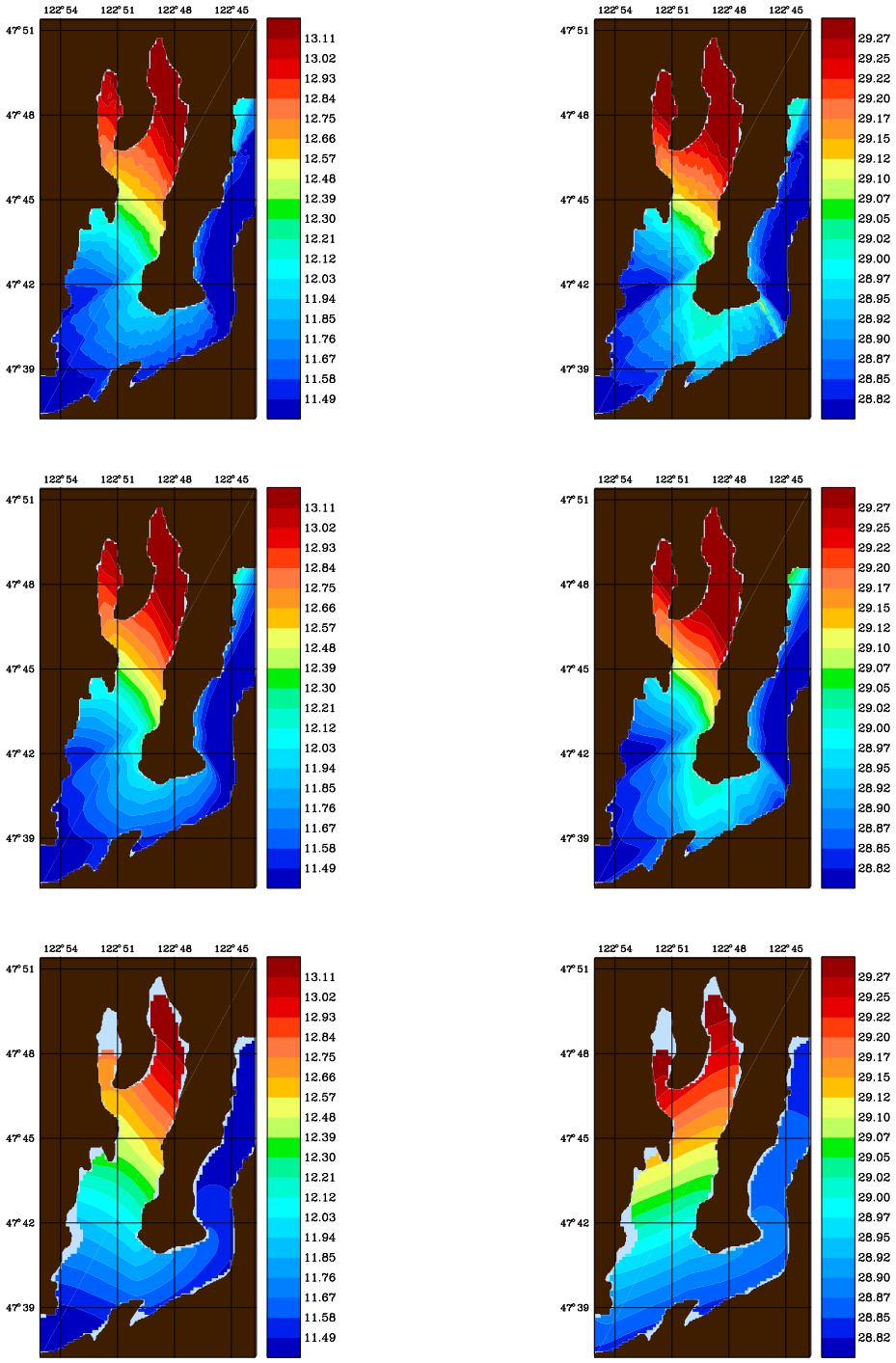

Figure C-5: Temperature (^{o}C) (Left) and Salinity (PSU) (Right) OA Fields in Dabob Bay from the optimal path length computed using: (Top) Bresenham Algorithm; (Middle) Averaged Bresenham Approach; (Bottom) Fast Marching Method

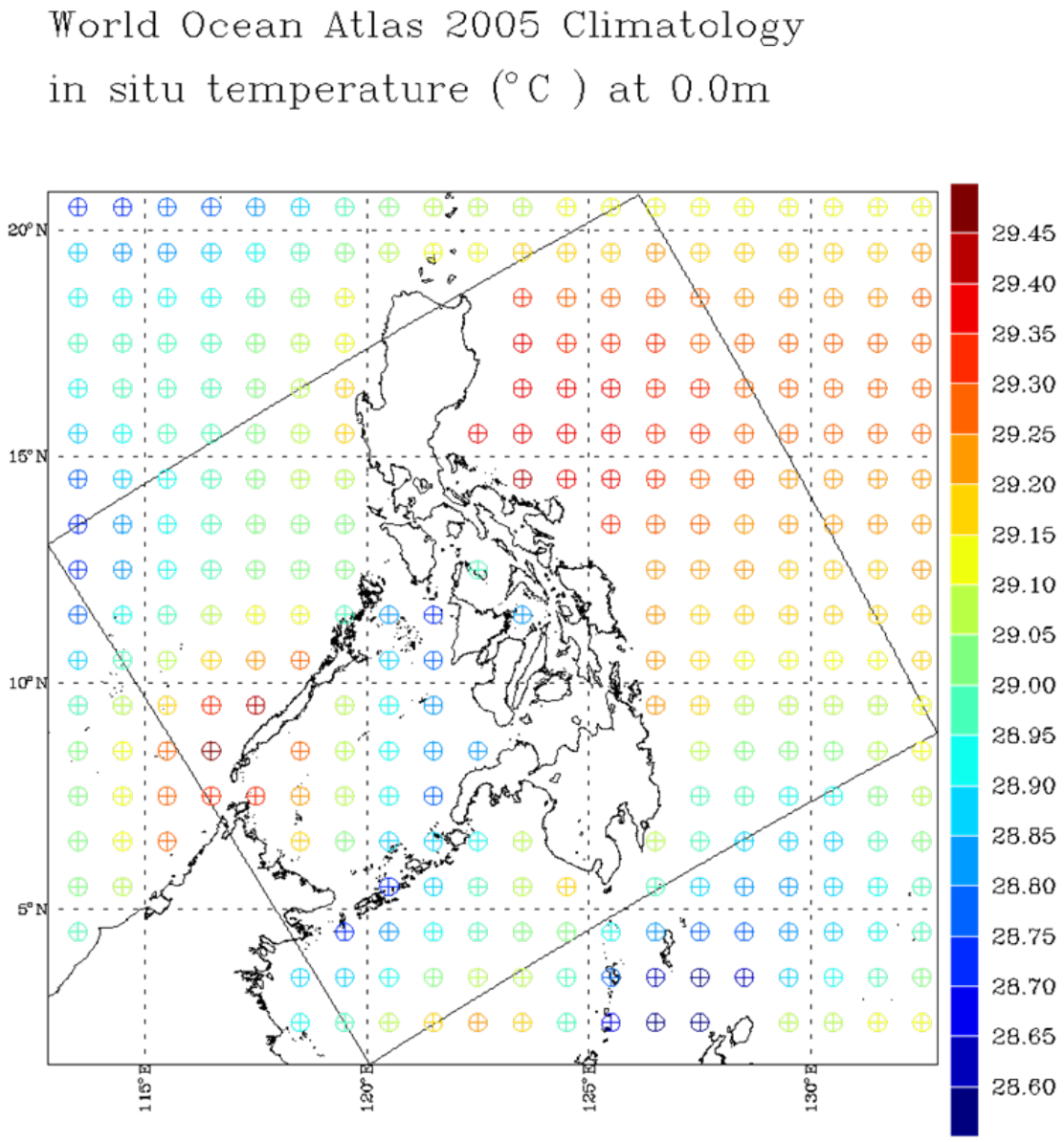

Figure C-6: World Ocean Atlas 2005 Climatology in situ temperature (°C) at 0.0m

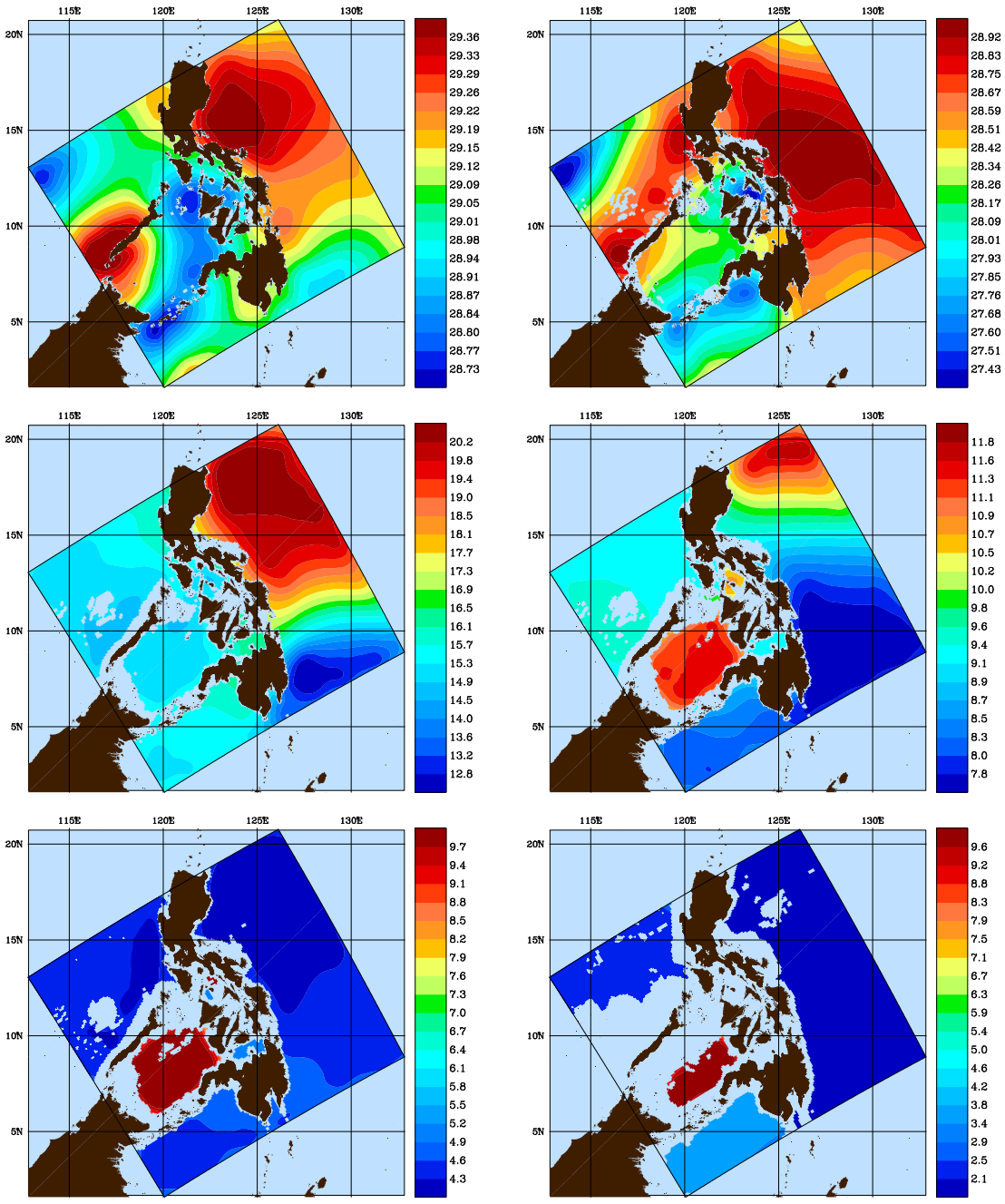

Figure C-7: Temperature (^{o}C) OA Fields obtained using the Level Set Method at Level: (Top - Left) 0m; (Top - Right) 40m; (Middle - Left) 200m; (Middle - Right) 450m; (Bottom - Left) 1000m; (Bottom - Right) 3000m

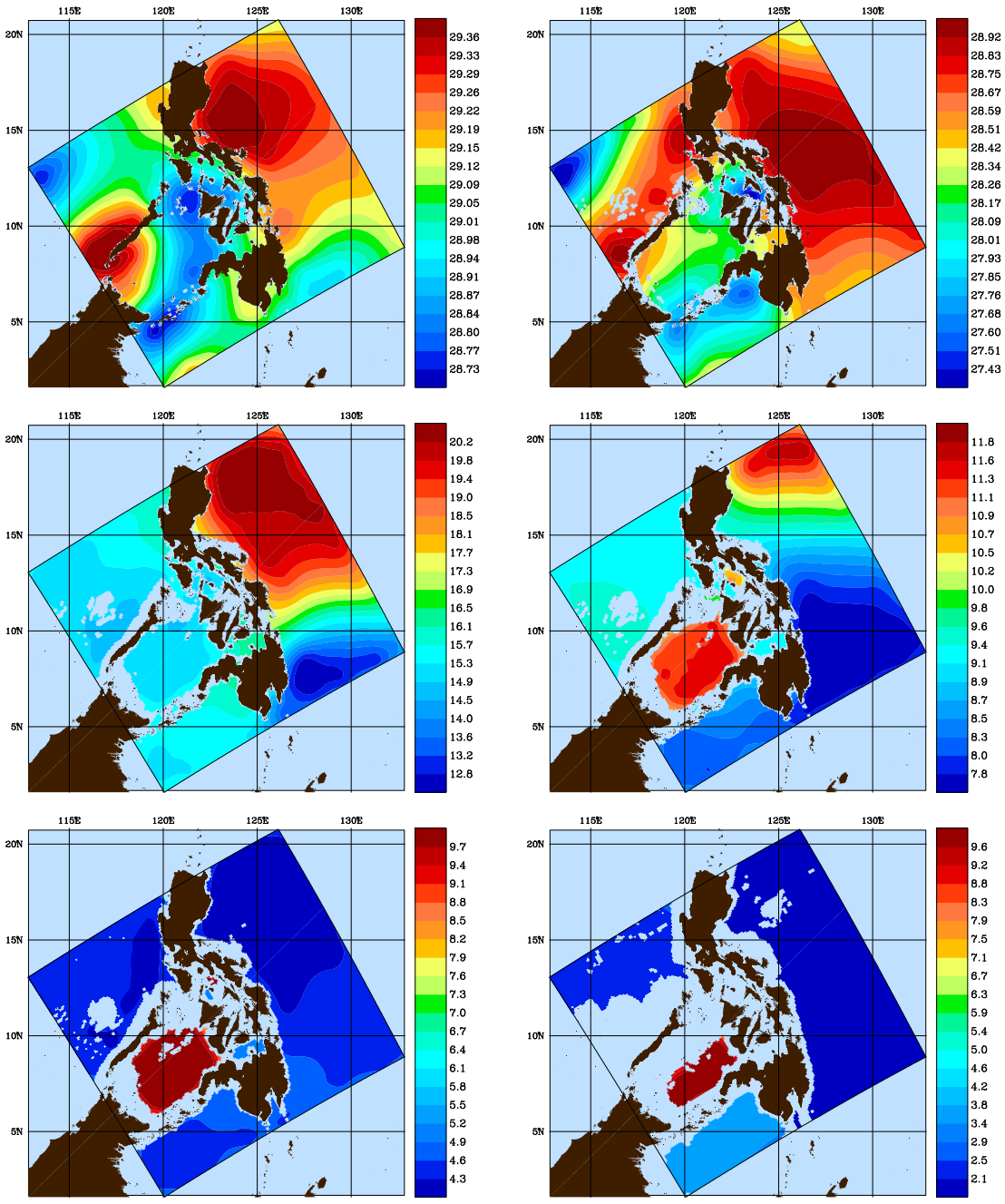

Figure C-8: Temperature (^{o}C) OA Fields obtained using the Fast Marching Method at Level: (Top - Left) 0m; (Top - Right) 40m; (Middle - Left) 200m; (Middle - Right) 450m; (Bottom - Left) 1000m; (Bottom - Right) 3000m

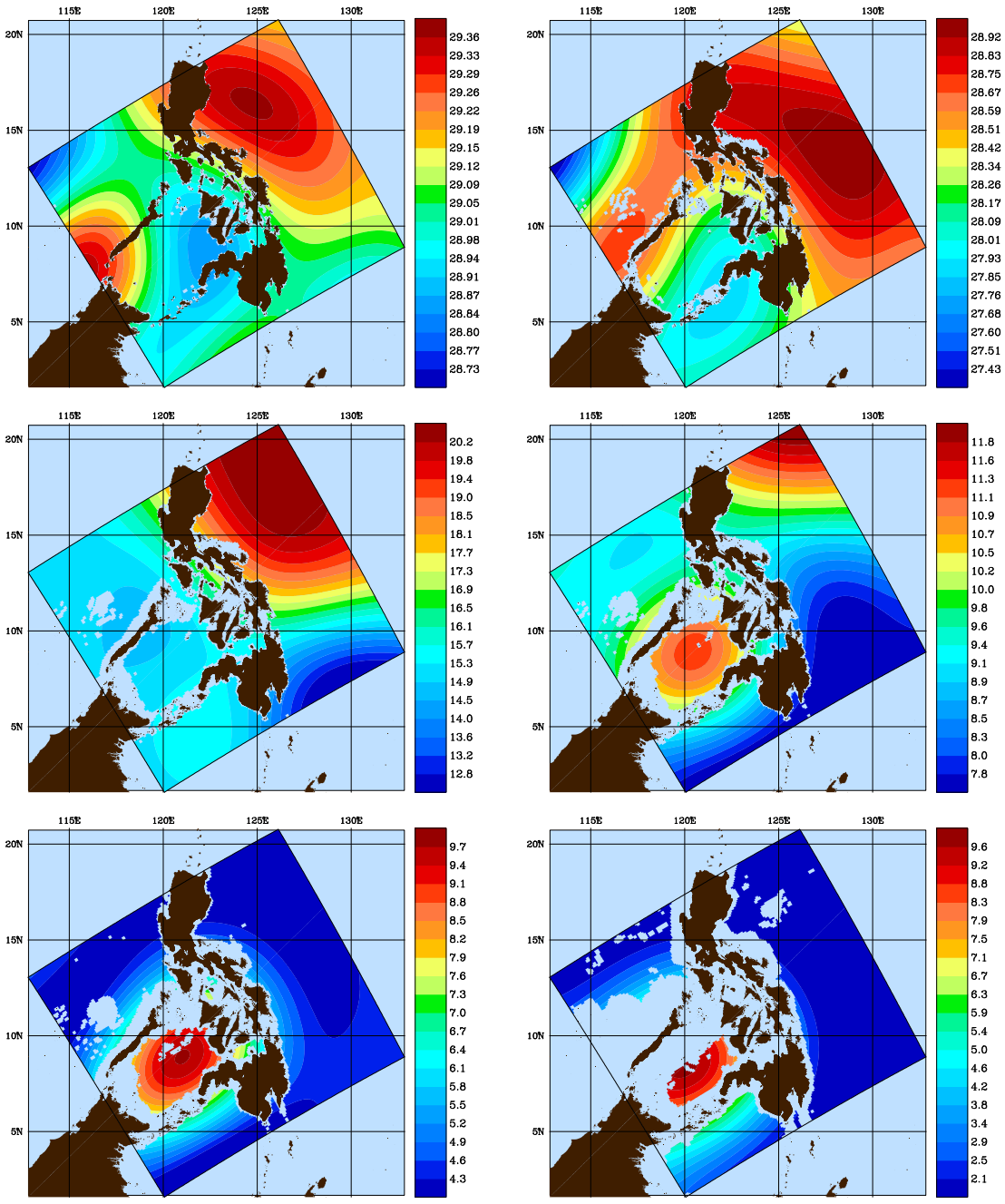

Figure C-9: Temperature (^{o}C) OA Fields (Standard OA without taking islands into account) at Level: (Top - Left) 0m; (Top - Right) 40m; (Middle - Left) 200m; (Middle - Right) 450m; (Bottom - Left) 1000m; (Bottom - Right) 3000m

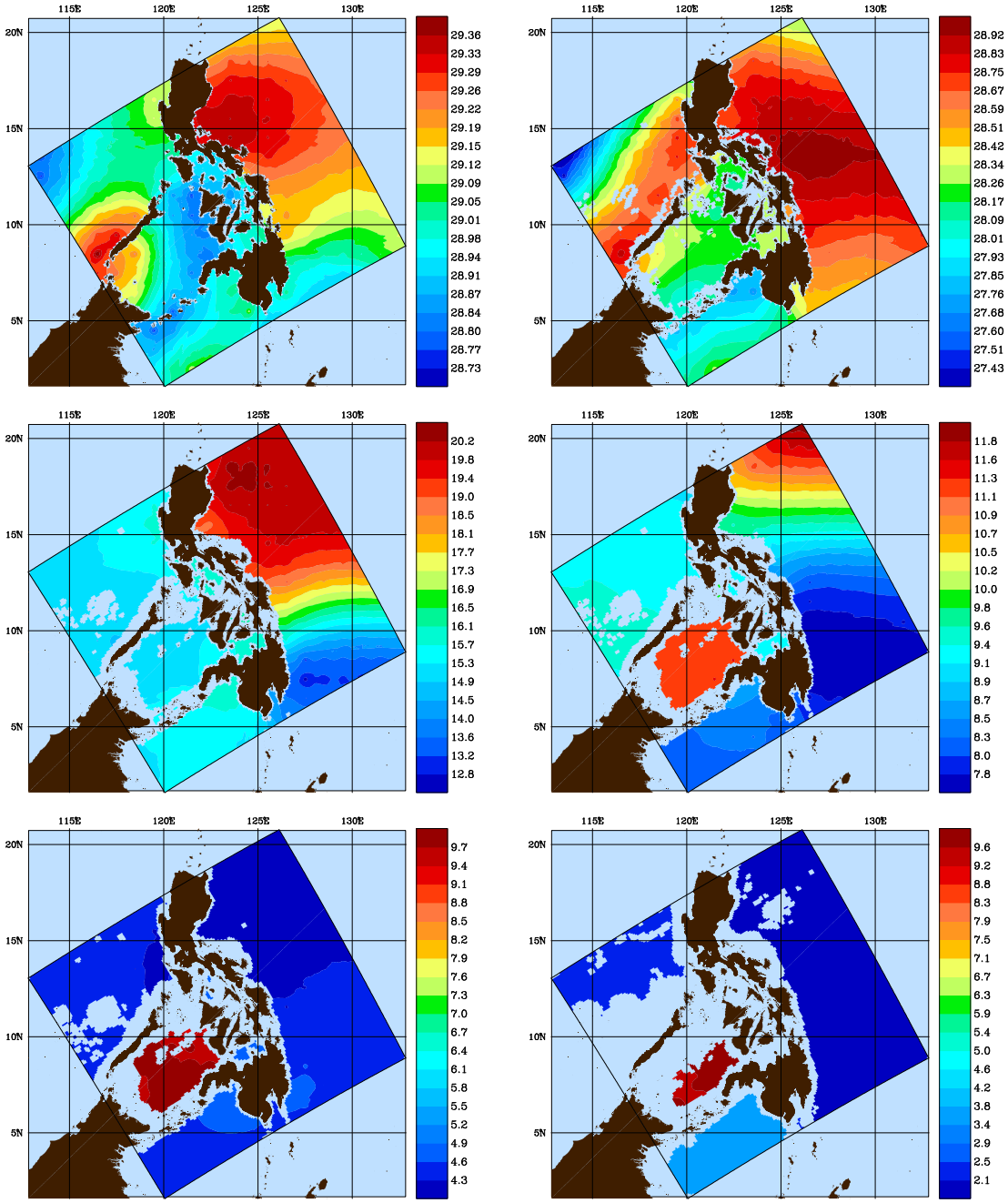

Figure C-10: Temperature (^{o}C) OA Fields using the SDE approach (representing covariance by Helmholtz equation) at Level: (Top - Left) 0m; (Top - Right) 40m; (Middle - Left) 200m; (Middle - Right) 450m; (Bottom - Left) 1000m; (Bottom - Right) 3000m

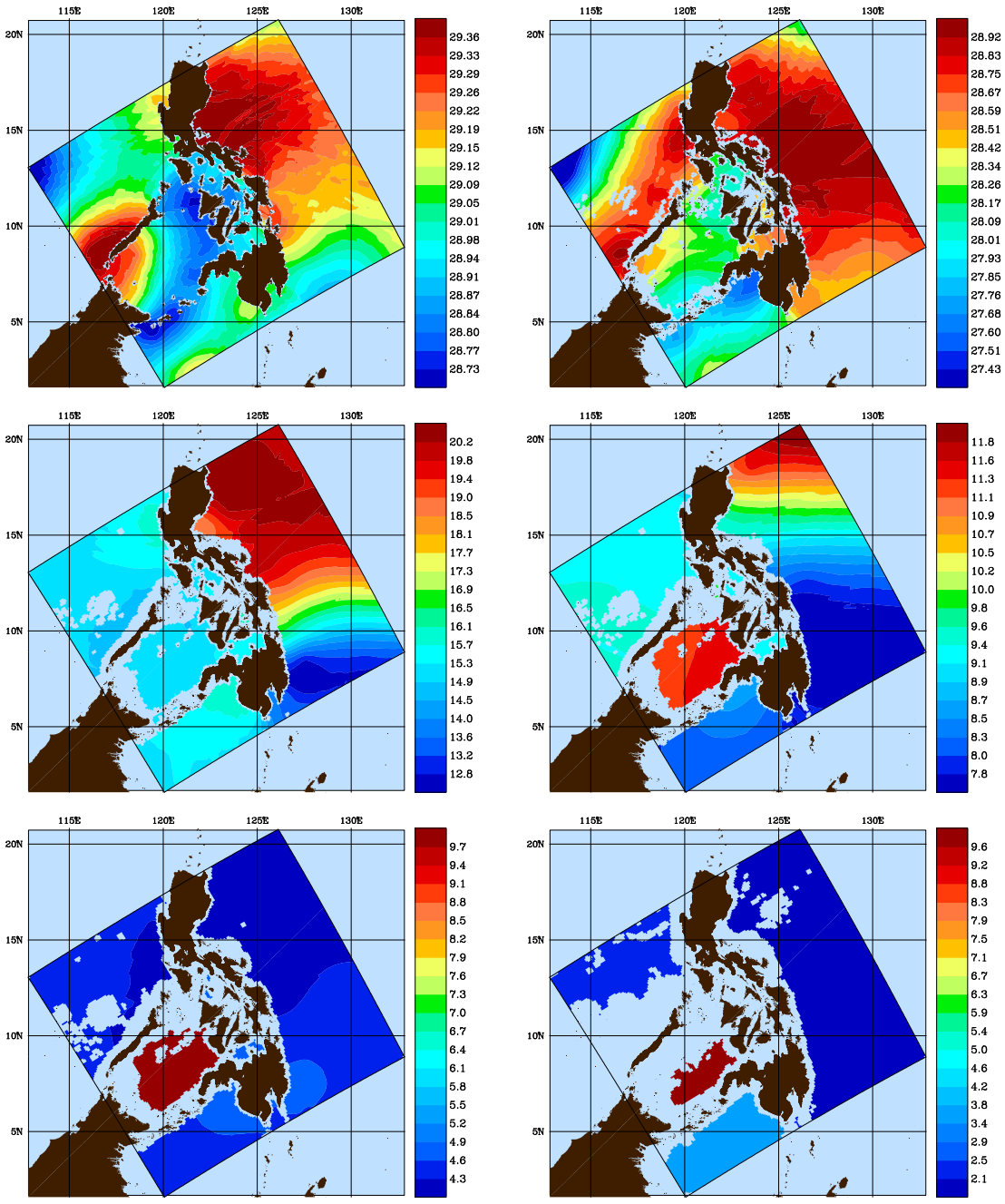

Figure C-11: Temperature (^{o}C) OA Fields using the SDE approach (representing field by Helmholtz equation) at Level: (Top - Left) 0m; (Top - Right) 40m; (Middle - Left) 200m; (Middle - Right) 450m; (Bottom - Left) 1000m; (Bottom - Right) 3000m

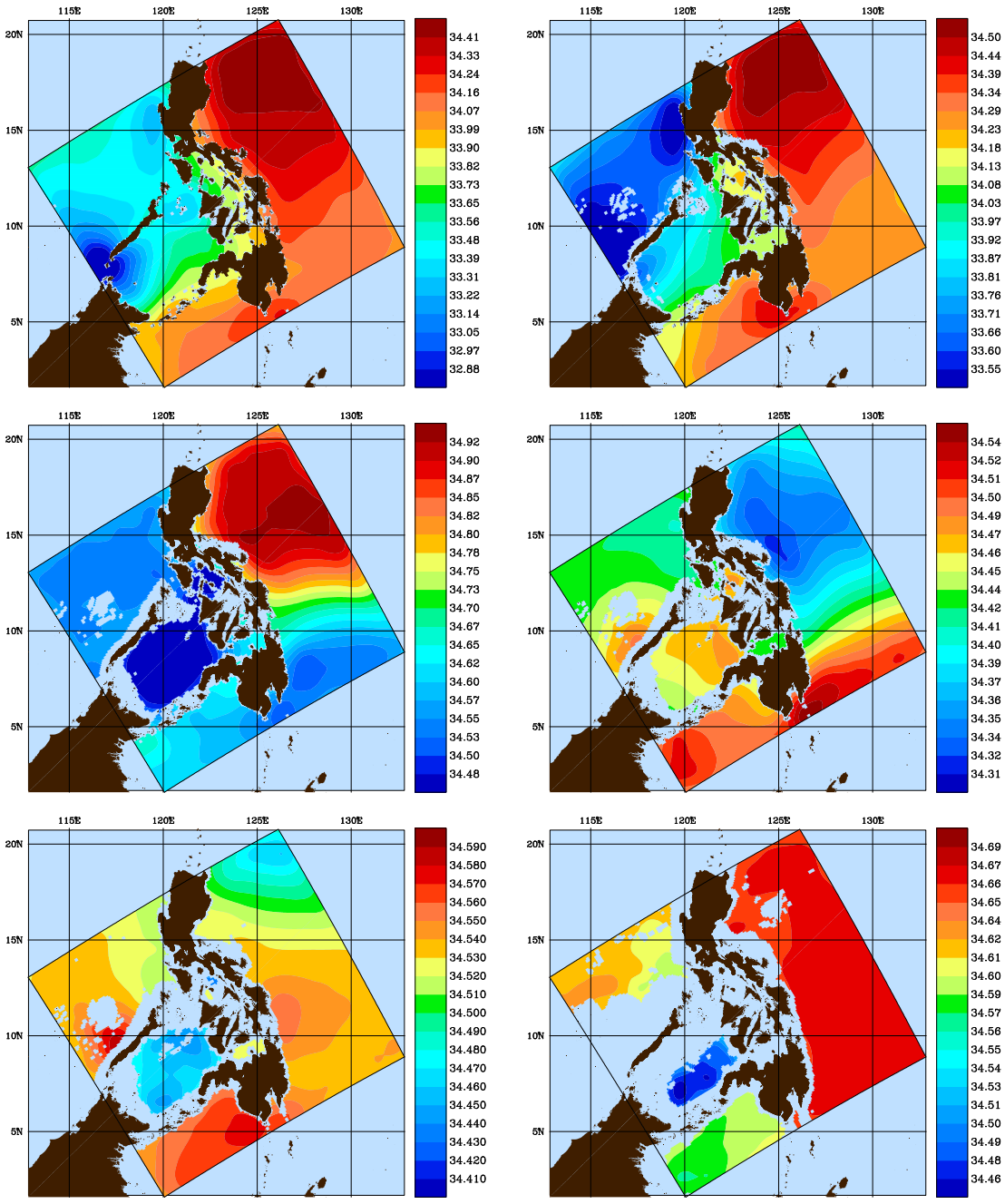

Figure C-12: Salinity (PSU) OA Fields obtained using the Level Set Method at Level: (Top - Left) 0m; (Top - Right) 40m; (Middle - Left) 200m; (Middle - Right) 450m; (Bottom - Left) 1000m; (Bottom - Right) 3000m

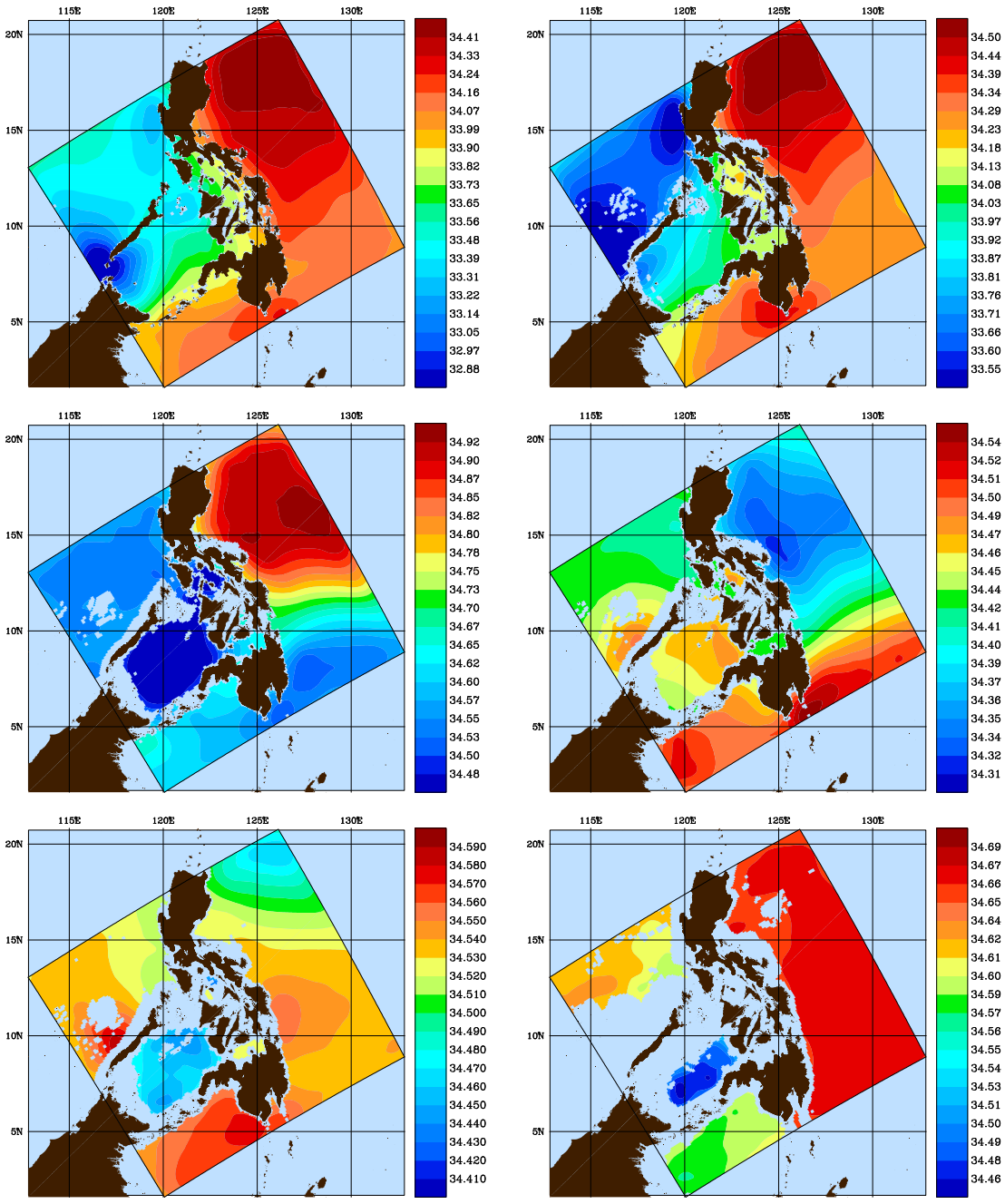

Figure C-13: Salinity (PSU) OA Fields obtained using the Fast Marching Method at Level: (Top - Left) 0m; (Top - Right) 40m; (Middle - Left) 200m; (Middle - Right) 450m; (Bottom - Left) 1000m; (Bottom - Right) 3000m

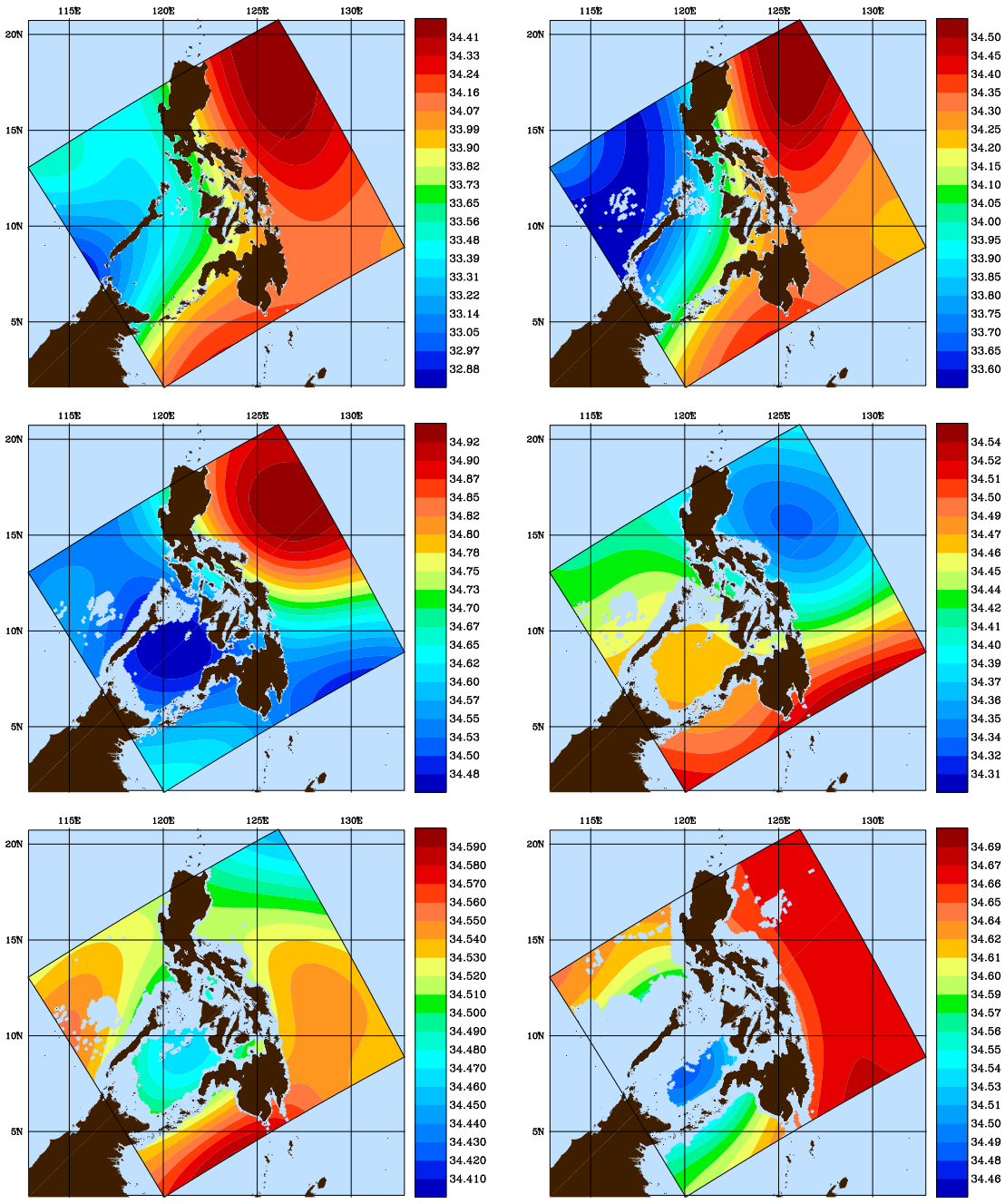

Figure C-14: Salinity (PSU) OA Fields (Standard OA without taking islands into account) at Level: (Top - Left) 0m; (Top - Right) 40m; (Middle - Left) 200m; (Middle - Right) 450m; (Bottom - Left) 1000m; (Bottom - Right) 3000m

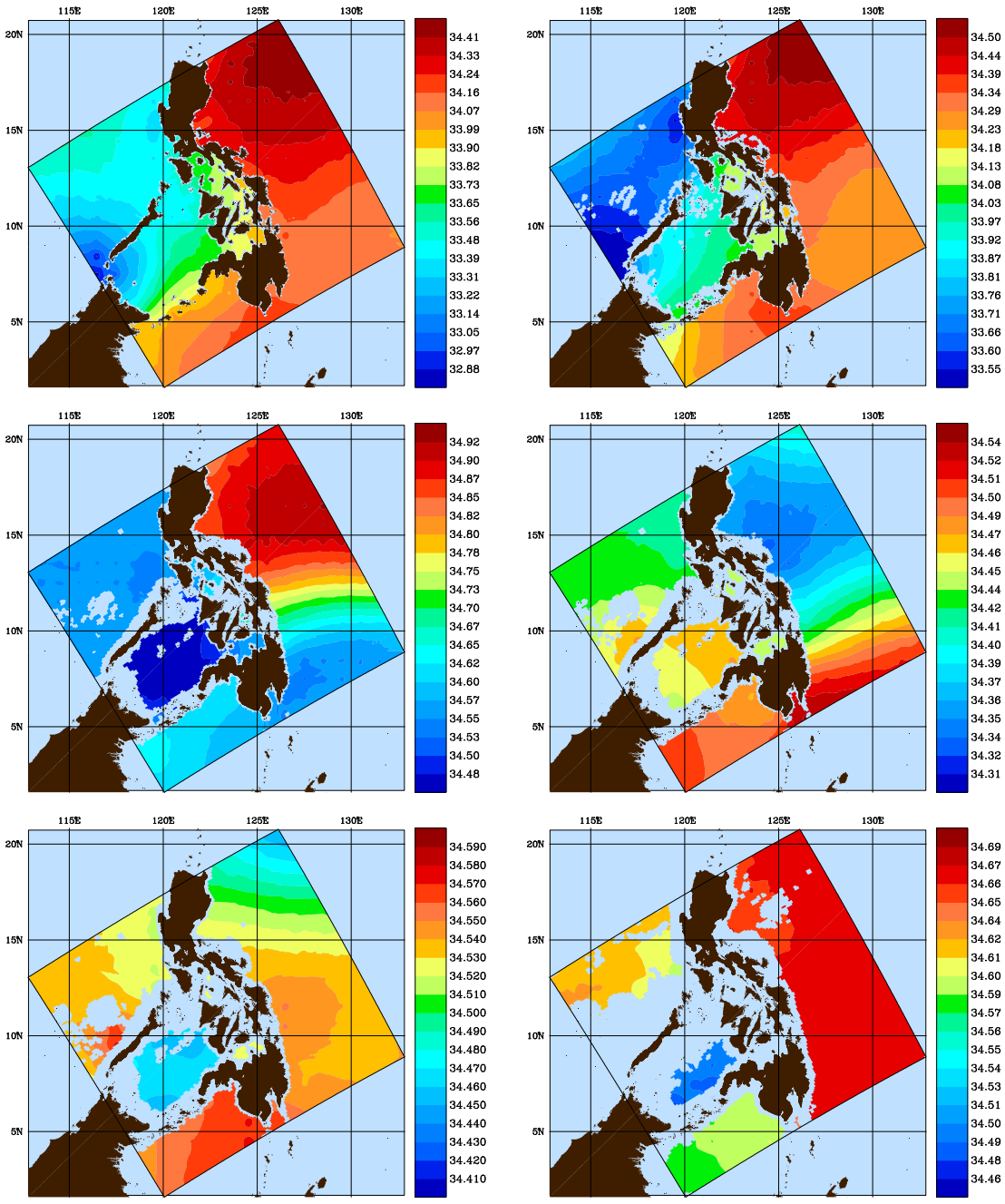

Figure C-15: Salinity (PSU) OA Fields using the SDE approach (representing covariance by Helmholtz equation) at Level: (Top - Left) 0m; (Top - Right) 40m; (Middle - Left) 200m; (Middle - Right) 450m; (Bottom - Left) 1000m; (Bottom - Right) 3000m

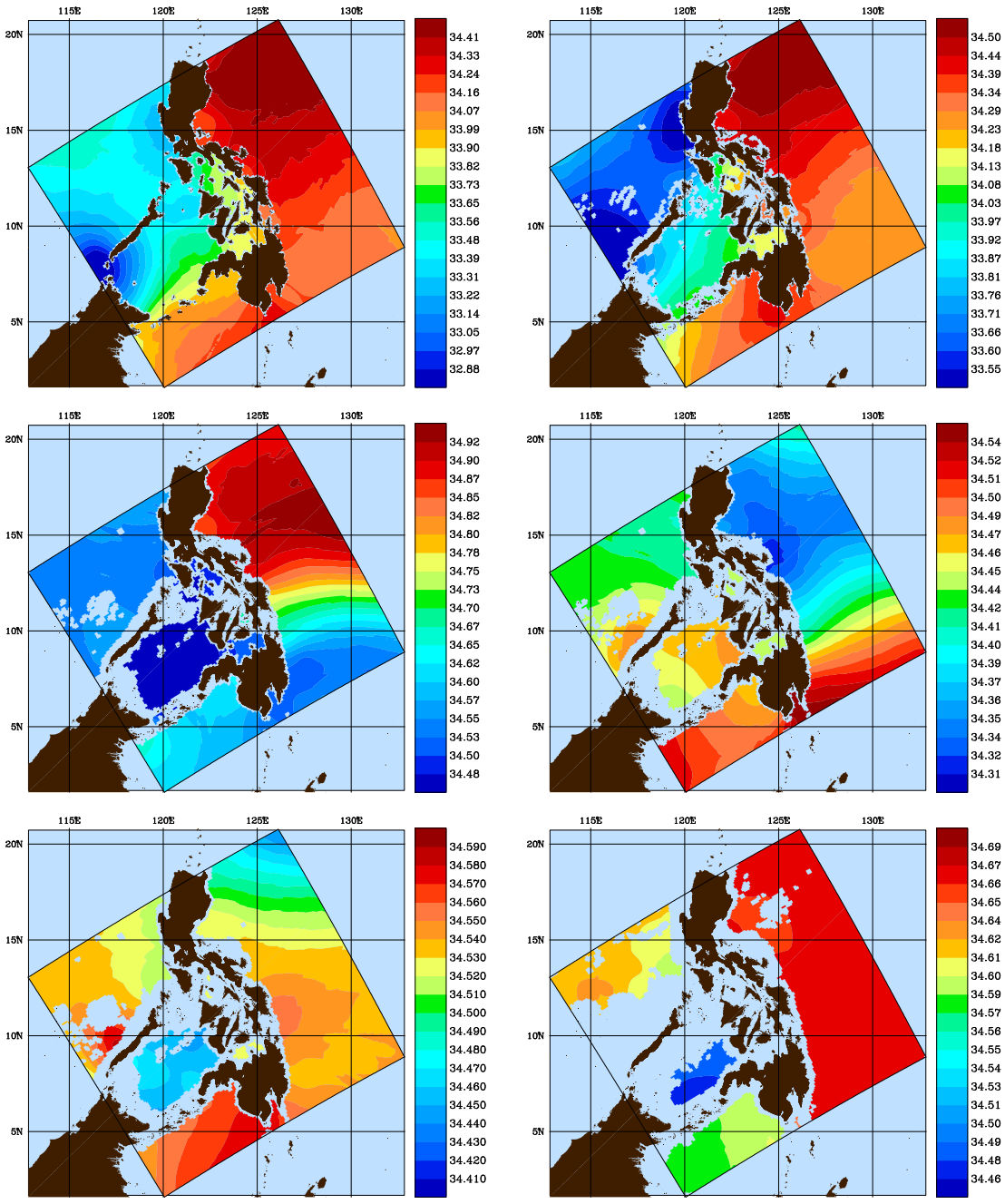

Figure C-16: Salinity (PSU) OA Fields using the SDE approach (representing field by Helmholtz equation) at Level: (Top - Left) 0m; (Top - Right) 40m; (Middle - Left) 200m; (Middle - Right) 450m; (Bottom - Left) 1000m; (Bottom - Right) 3000m

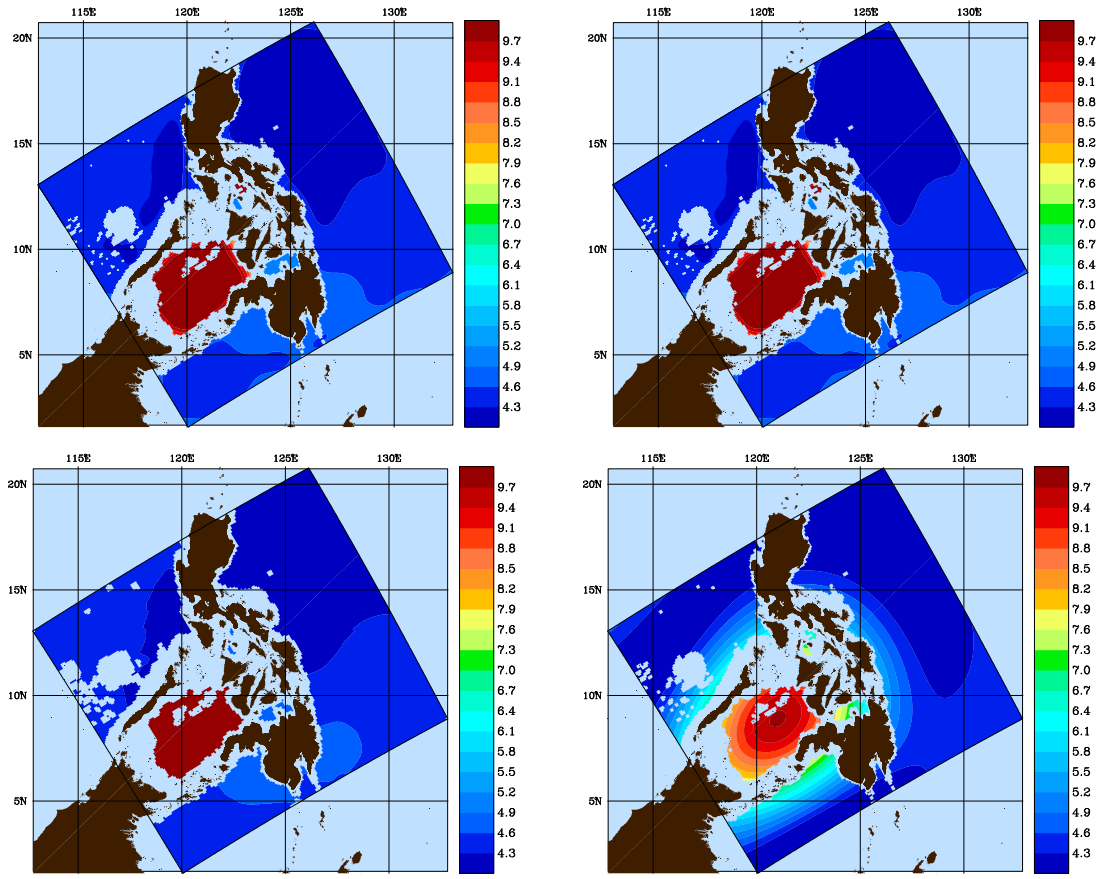

Figure C-17: Comparison of the Temperature (^{o}C) field at Level = 1000m by using: (Top - Left) Level Set Method; (Top - Right) Fast Marching Method; (Bottom - Left) SDE Approach; (Bottom - Right) Standard OA

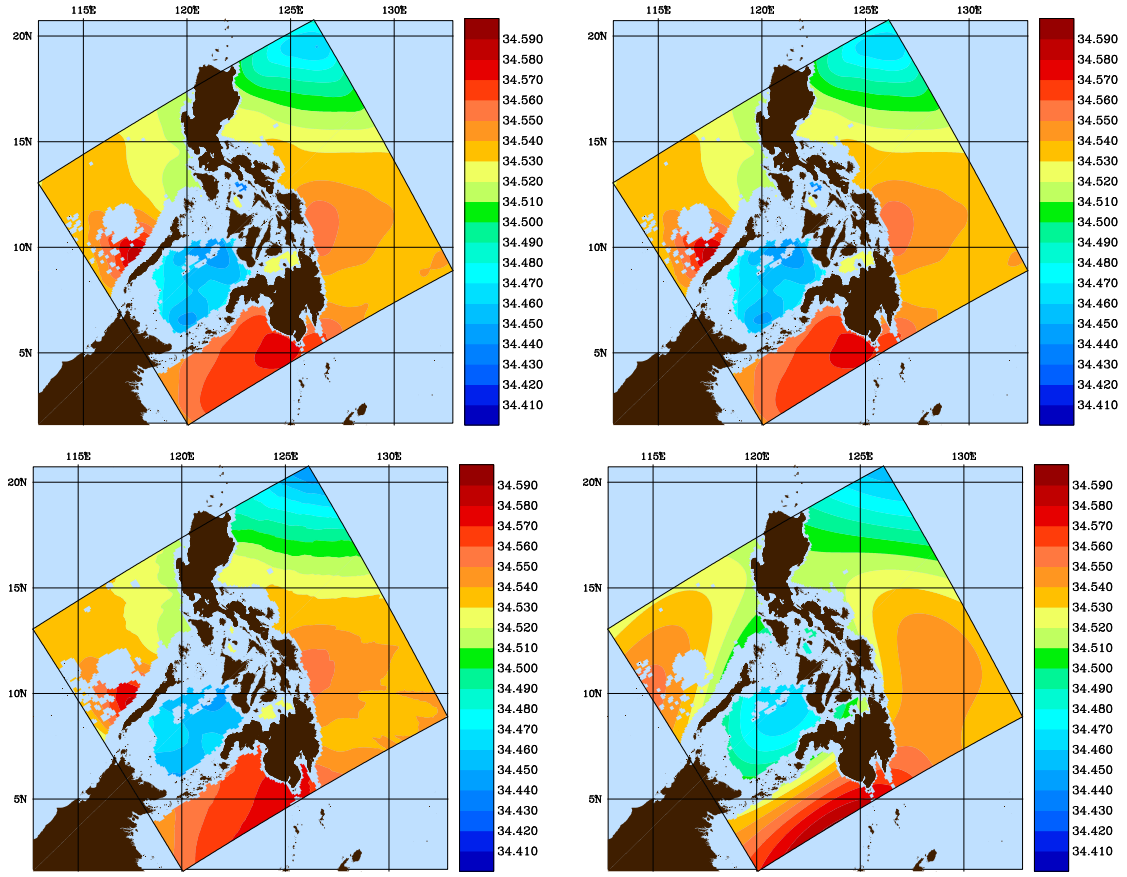

Figure C-18: Comparison of the Salinity (PSU) field at Level = 1000m by using: (Top - Left) Level Set Method; (Top - Right) Fast Marching Method; (Bottom - Left) SDE Approach; (Bottom - Right) Standard OA

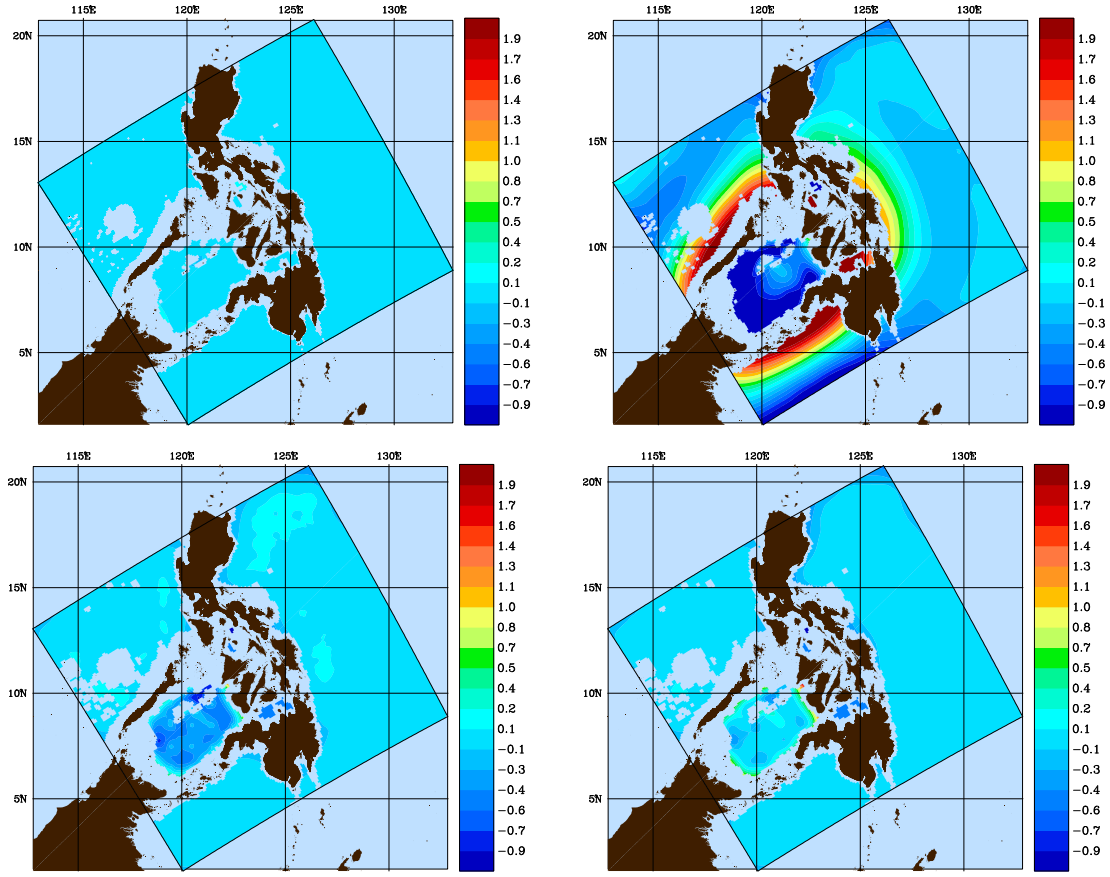

Figure C-19: Difference between Temperature (^{o}C) field at Level = 1000m obtained using Fast Marching Method and using: (Top - Left) Level Set Method; (Top - Right) Standard OA; (Bottom - Left) SDE Approach (representing covariance by Helmholtz equation); (Bottom - Right) SDE (representing field by Helmholtz equation)

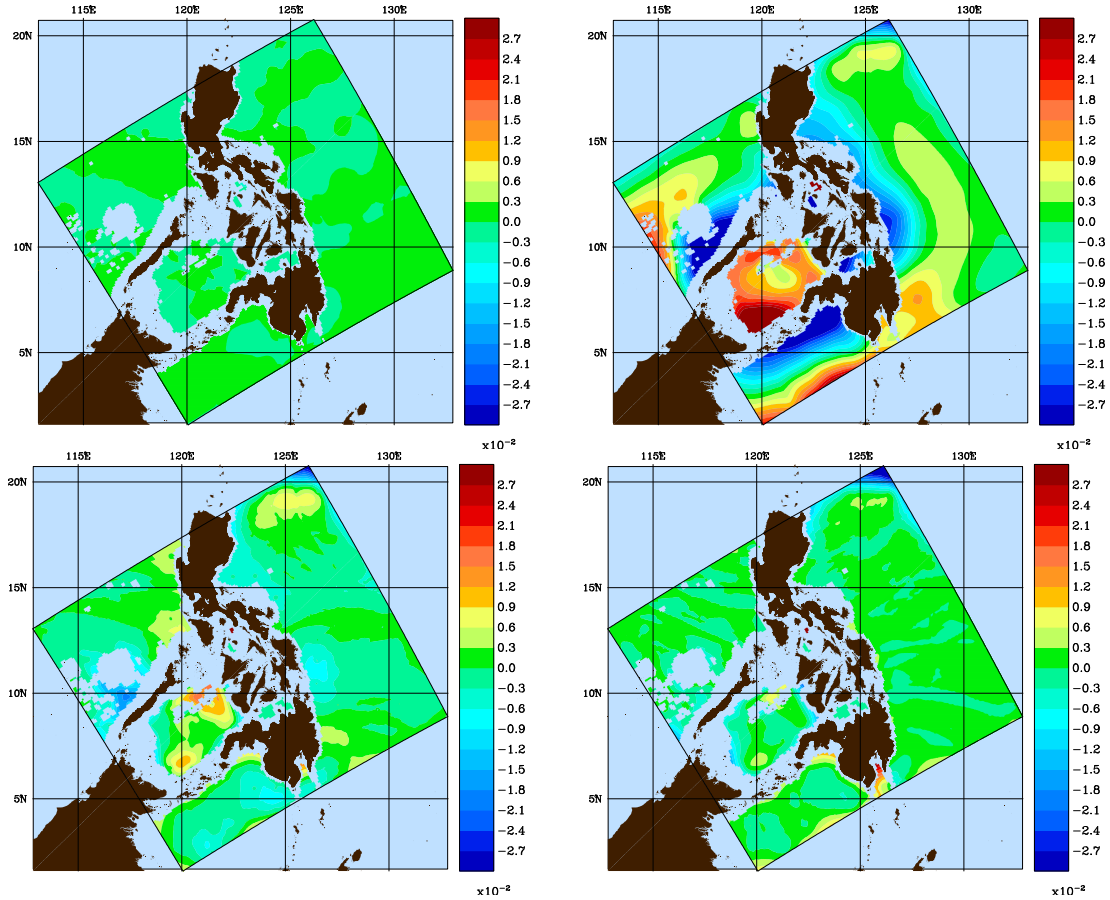

Figure C-20: Difference between Salinity (PSU) field at Level = 1000m obtained using Fast Marching Method and using: (Top - Left) Level Set Method; (Top - Right) Standard OA; (Bottom - Left) SDE Approach (representing covariance by Helmholtz equation); (Bottom - Right) SDE (representing field by Helmholtz equation)

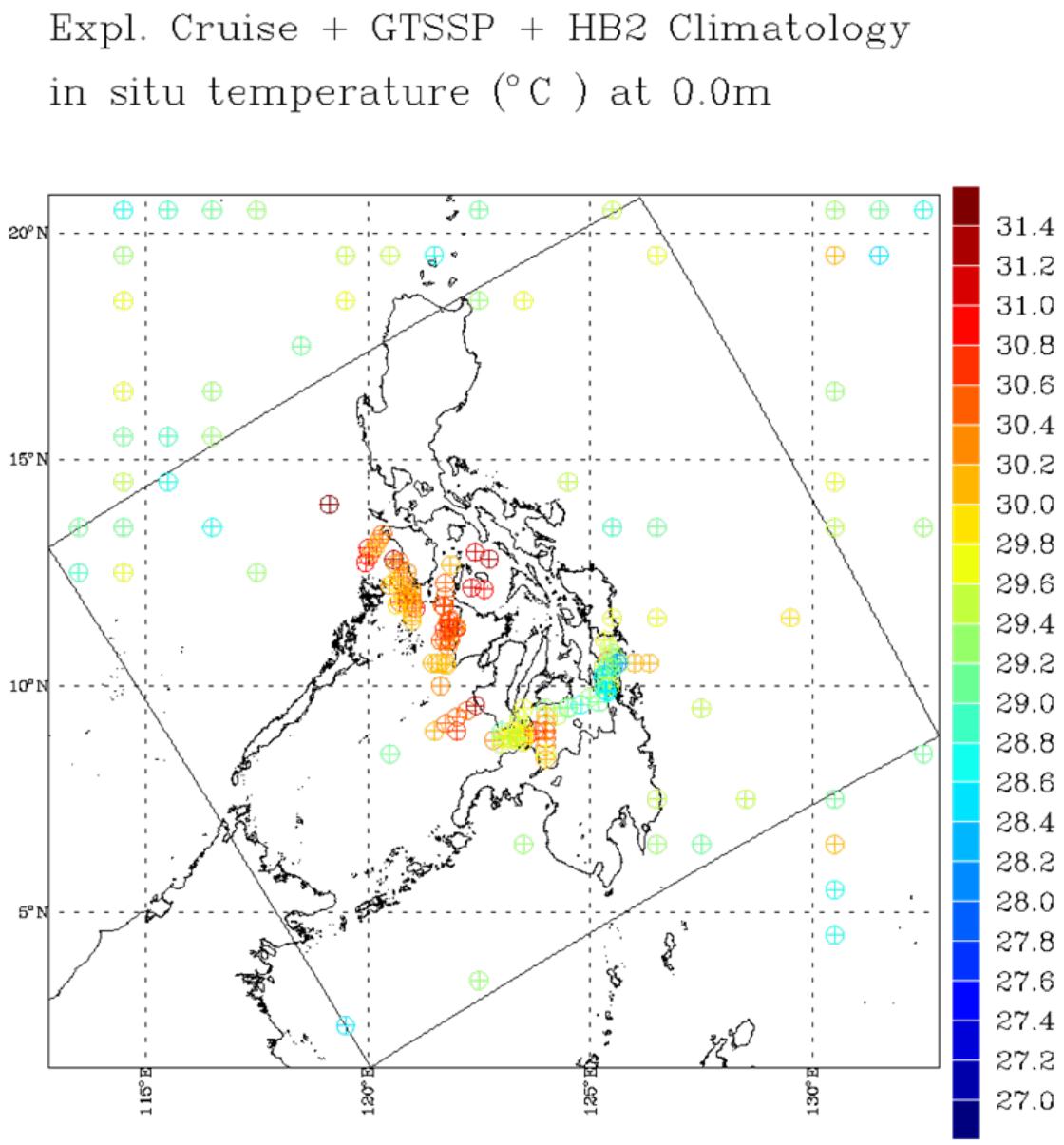

Figure C-21: Melville exploratory Cruise + GTSPP + HB2 Climatology (Summer 2007) in situ temperature (^{o}C) at 0.0m

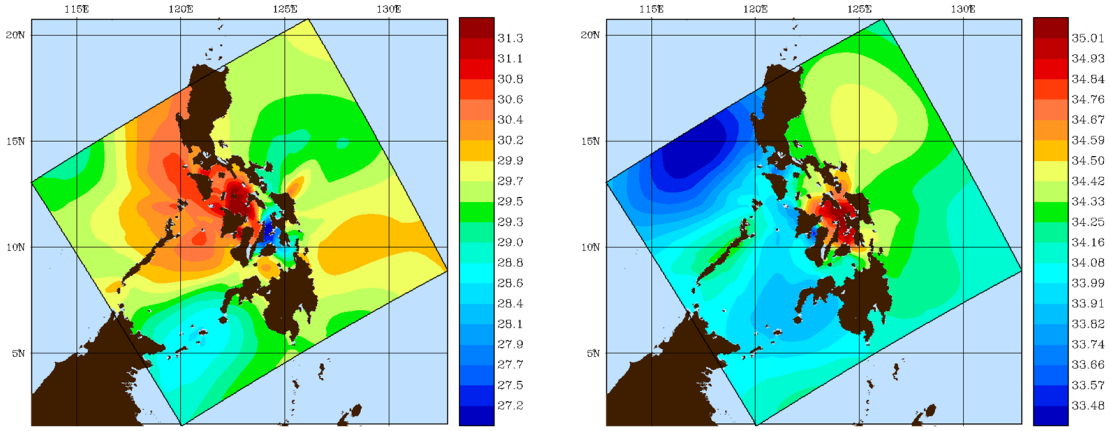

Figure C-22: Temperature (^{o}C) and Salinity (PSU) Field Maps (Melville exploratory Cruise + GTSPP + HB2 Climatology (Summer 2007) data)

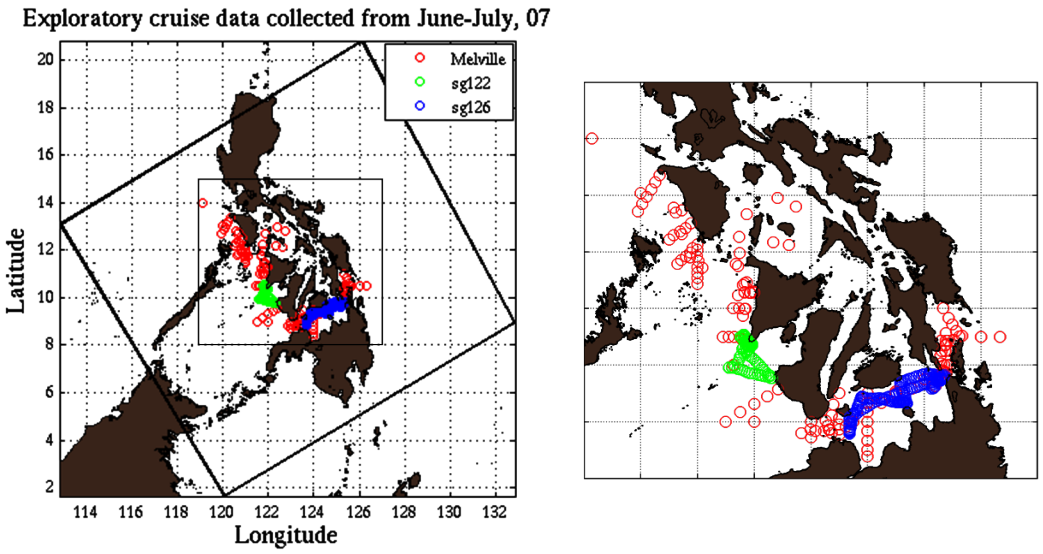

Figure C-23: Melville exploratory cruise and glider data (Summer 2007) in Philippines Archipelago

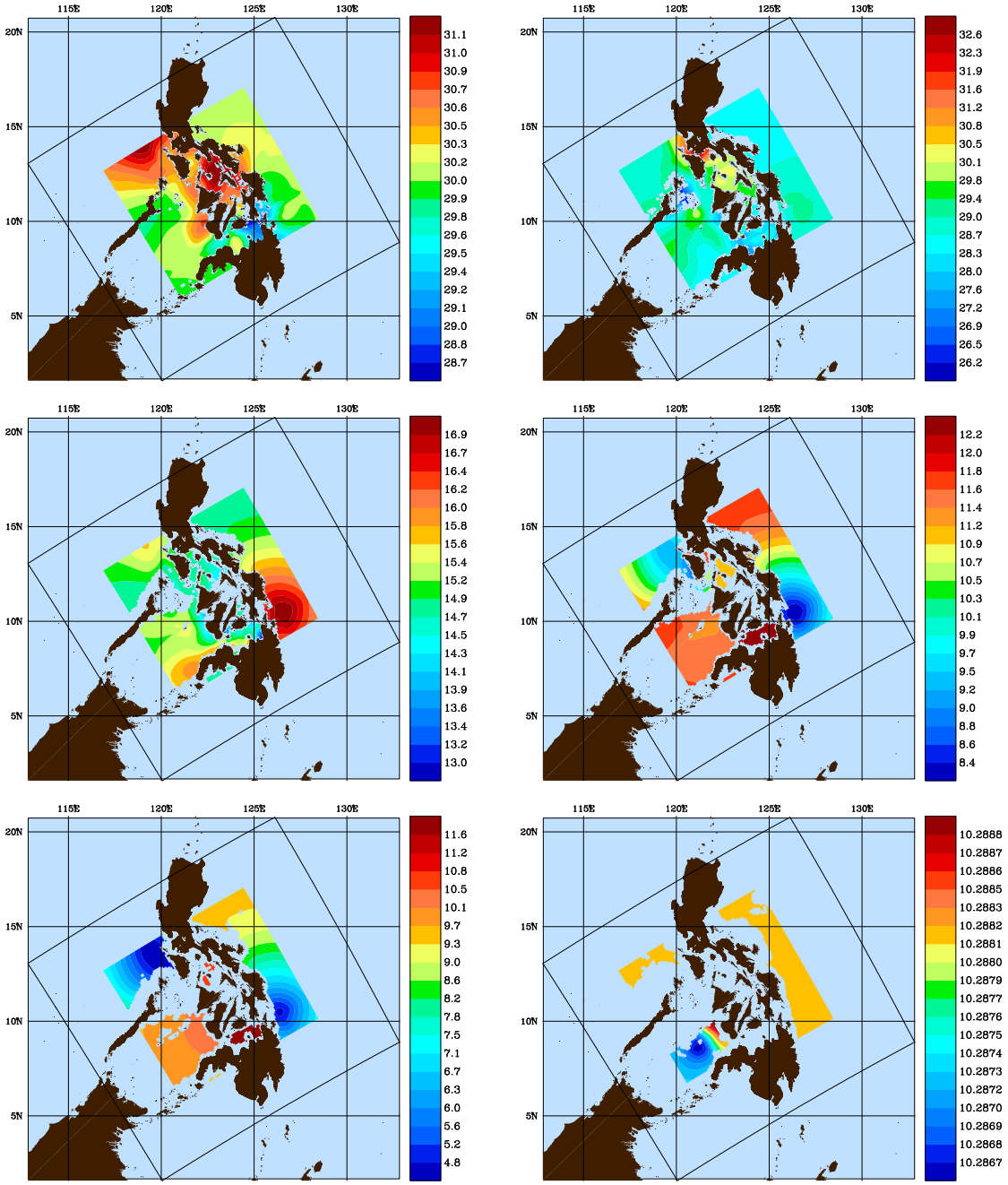

Figure C-24: Temperature (^{o}C) OA Fields using the FMM with Melville exploratory cruise and glider data (Summer 2007) at Level: (Top - Left) 0m; (Top - Right) 40m; (Middle - Left) 200m; (Middle - Right) 450m; (Bottom - Left) 1000m; (Bottom - Right) 3000m

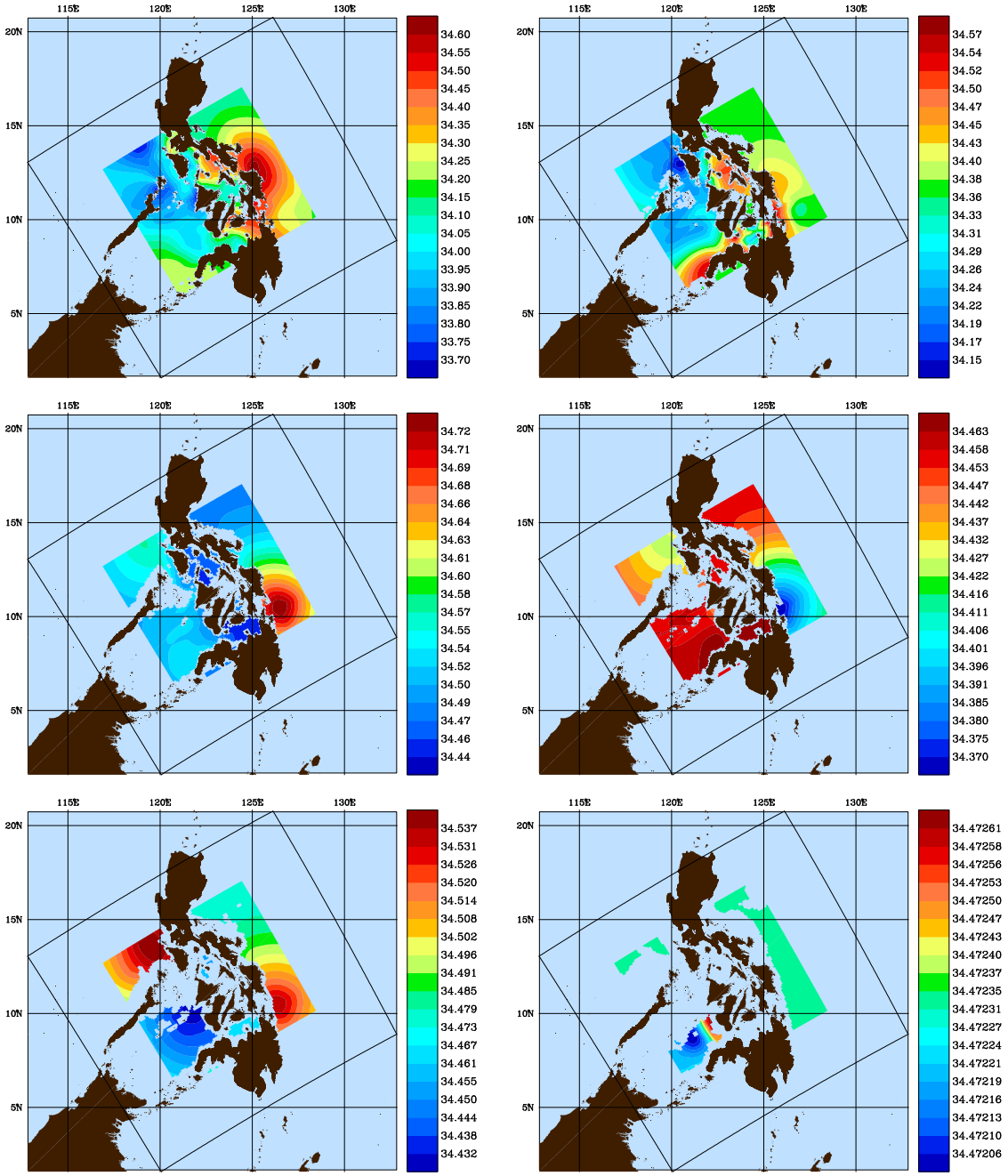

Figure C-25: Salinity (PSU) OA Fields using the FMM with Melville exploratory cruise and glider data (Summer 2007) at Level: (Top - Left) 0m; (Top - Right) 40m; (Middle - Left) 200m; (Middle - Right) 450m; (Bottom - Left) 1000m; (Bottom - Right) 3000m

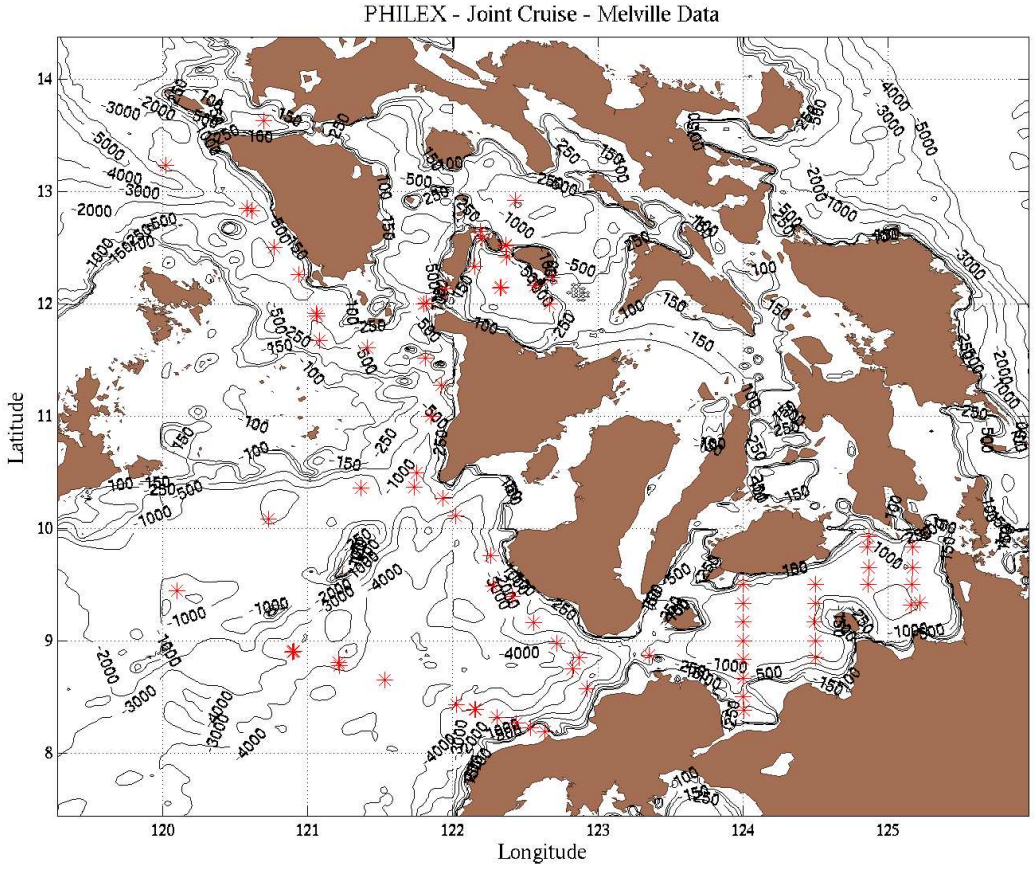

Figure C-26: Philippines Archipelago - Melville joint cruise Data (Winter 2008)

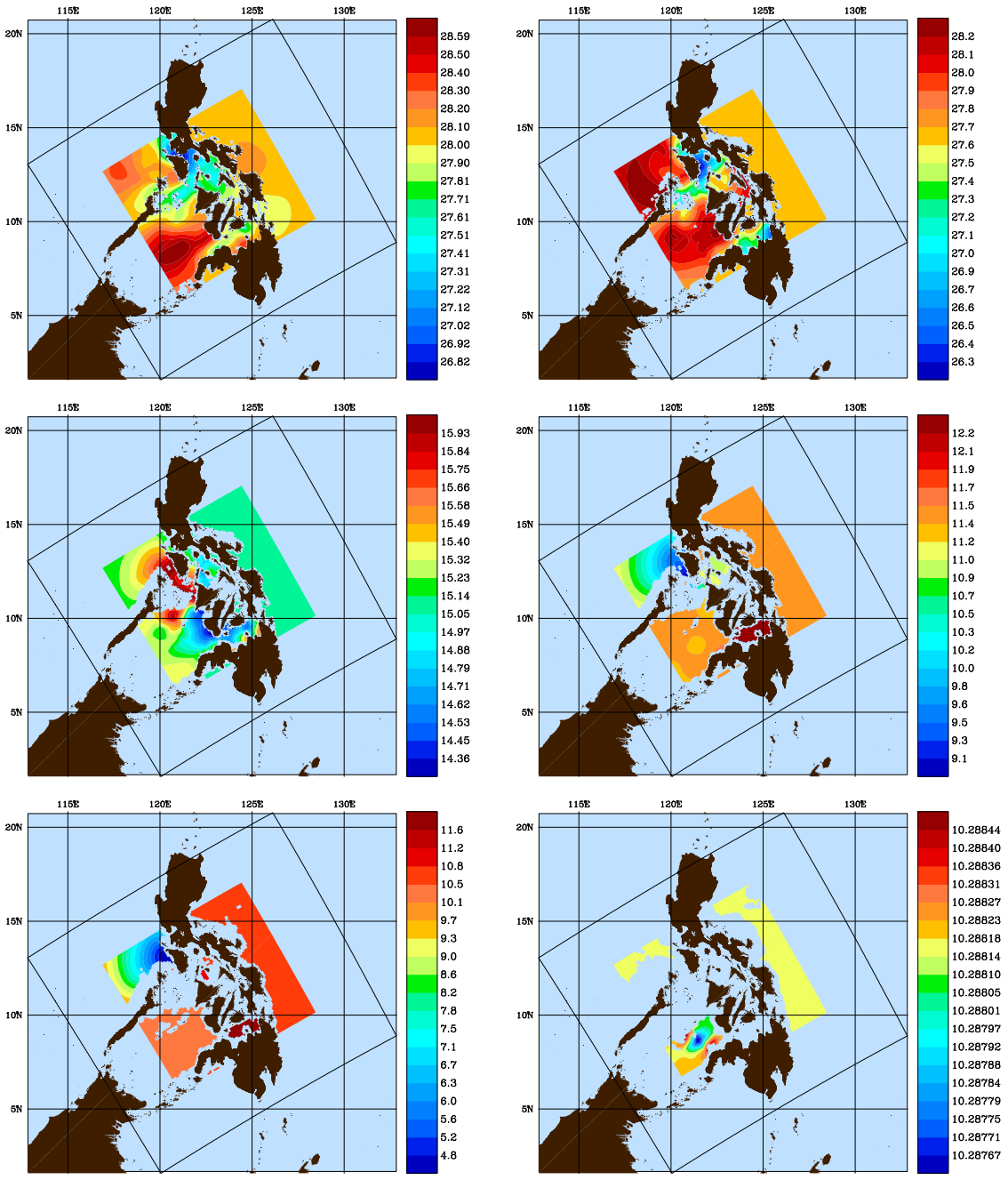

Figure C-27: Temperature (^{o}C) OA Fields using the FMM with Melville joint cruise data (Winter 2008) at Level: (Top - Left) 0m; (Top - Right) 40m; (Middle - Left) 200m; (Middle - Right) 450m; (Bottom - Left) 1000m; (Bottom - Right) 3000m

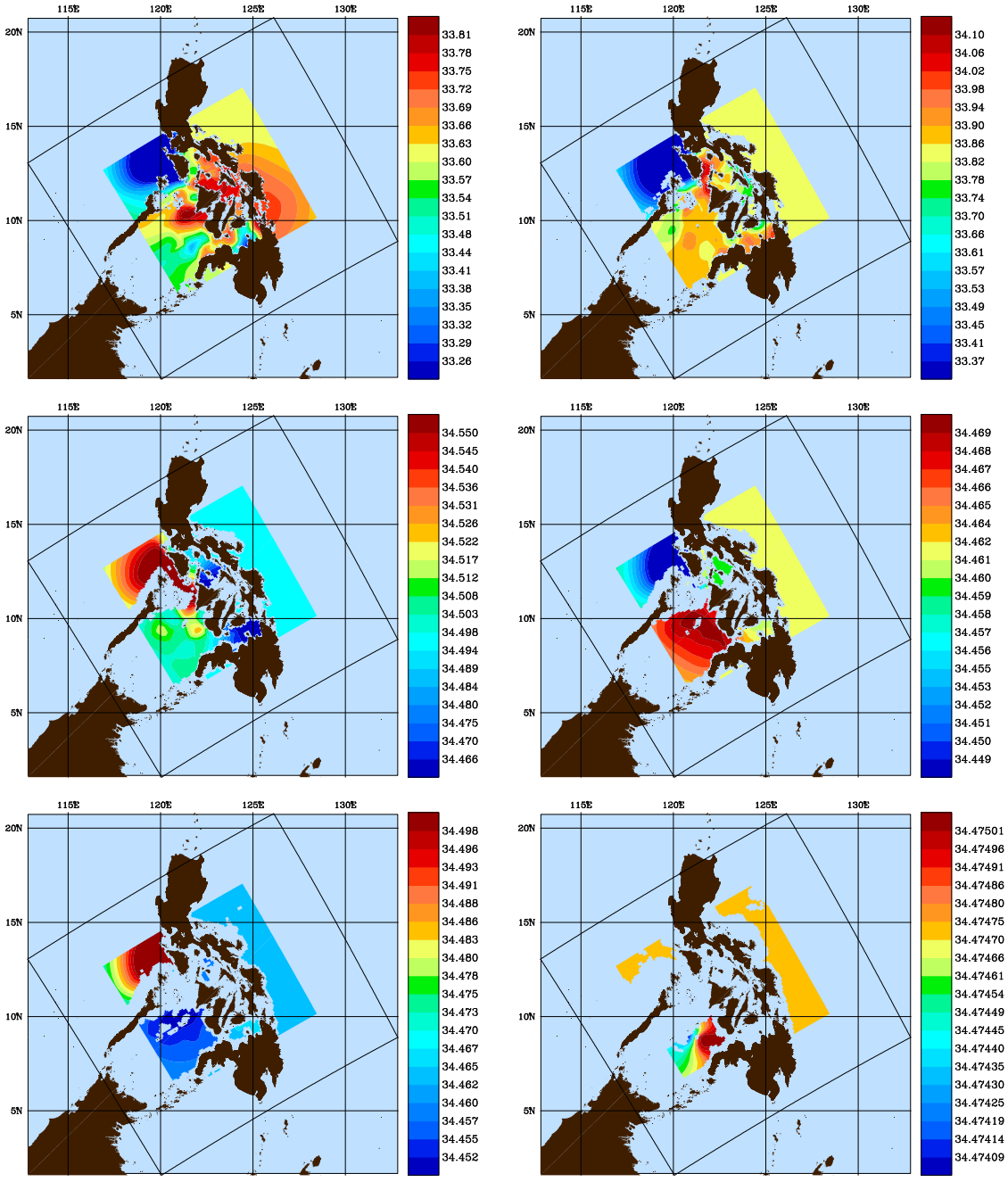

Figure C-28: Salinity (PSU) OA Fields using the FMM with Melville joint cruise data (Winter 2008) at Level: (Top - Left) 0m; (Top - Right) 40m; (Middle - Left) 200m; (Middle - Right) 450m; (Bottom - Left) 1000m; (Bottom - Right) 3000m

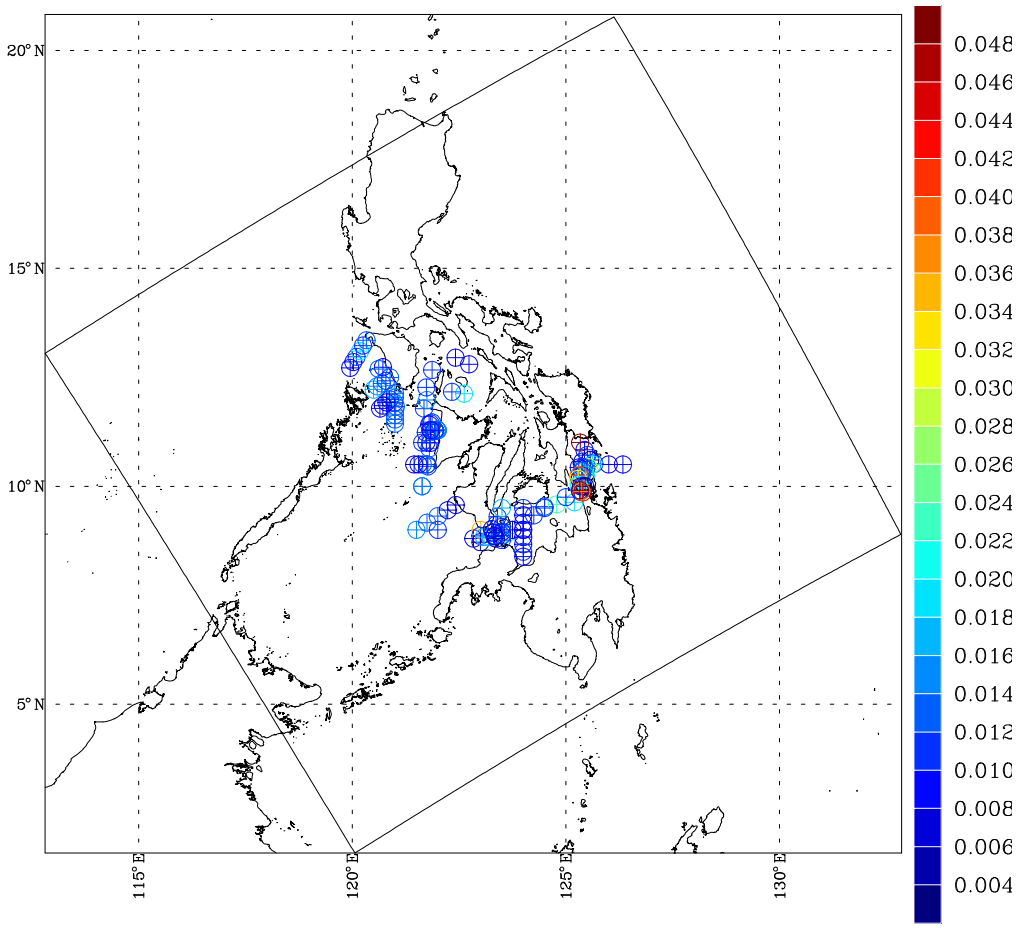

Figure C-29: Biology (chlorophyll) data in Philippines Archipelago

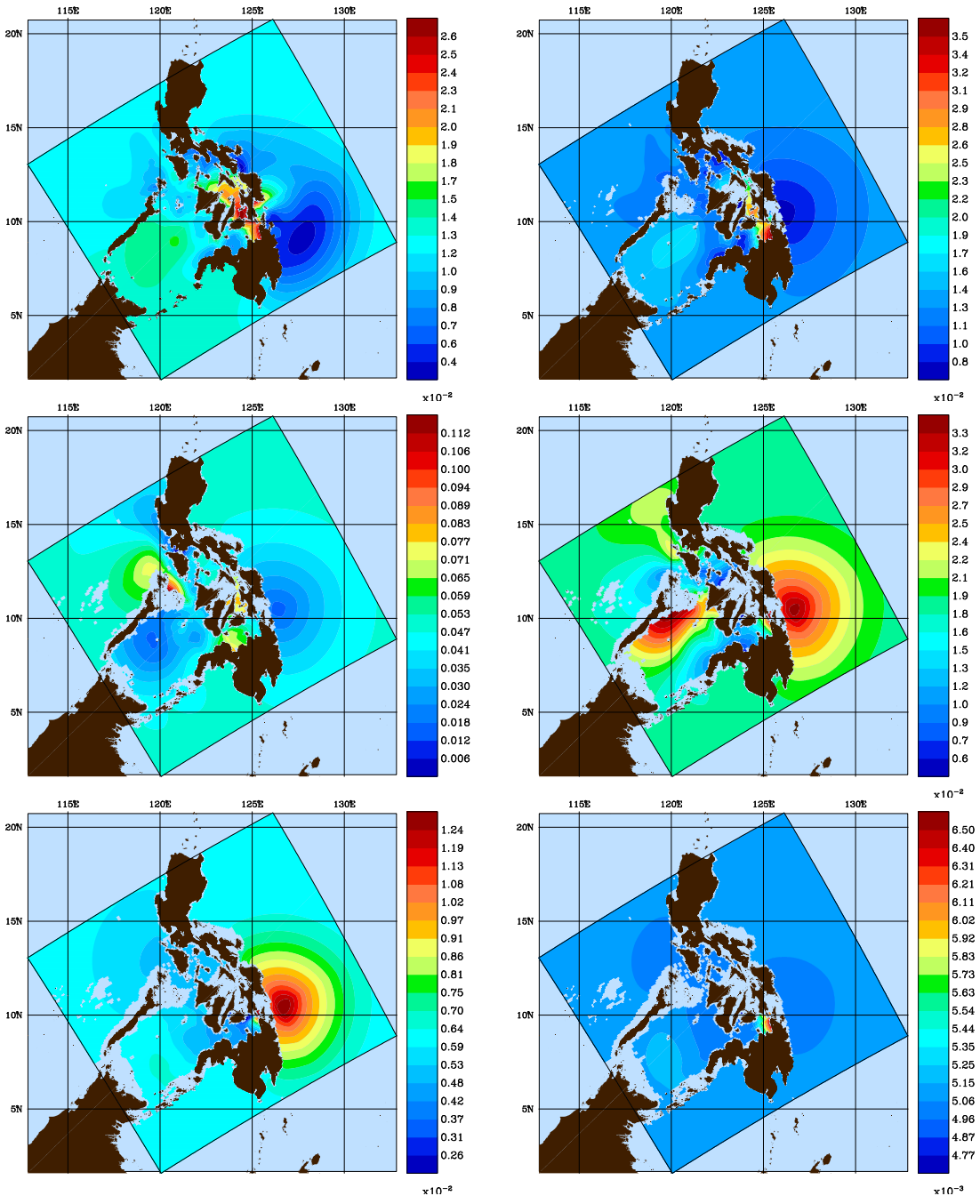

Figure C-30: Chlorophyll (μmol/Kg) OA Fields using the FMM at Level: (Top - Left) 0m; (Top - Right) 10m; (Middle - Left) 50m; (Middle - Right) 100m; (Bottom - Left) 160m; (Bottom - Right) 200m

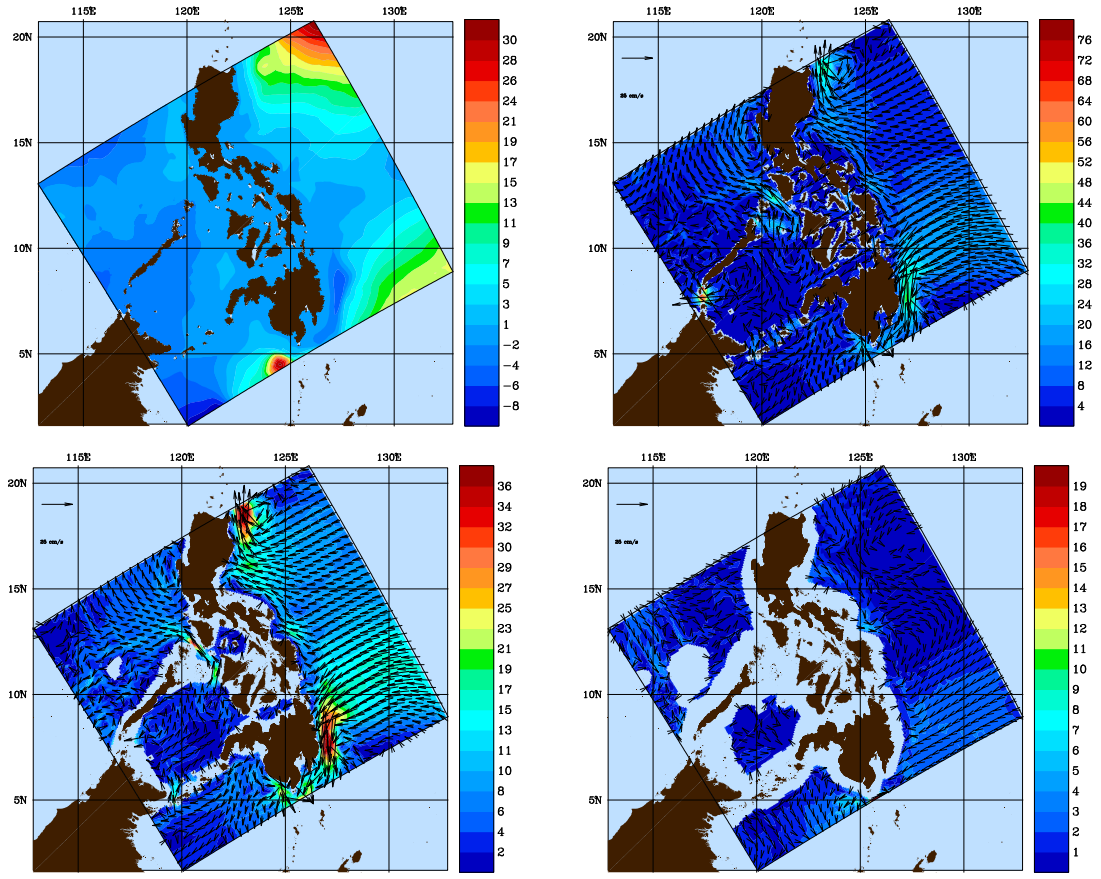

Figure C-31: Velocity estimation under geostrophic balance (weight functions based on the minimum vertical area) from field maps (WOA05) obtained using the FMM: (Top - Left) Streamfunction, Velocity at depths: (Top - Right) 0m; (Bottom - Left) 100m; (Bottom - Right) 1000m

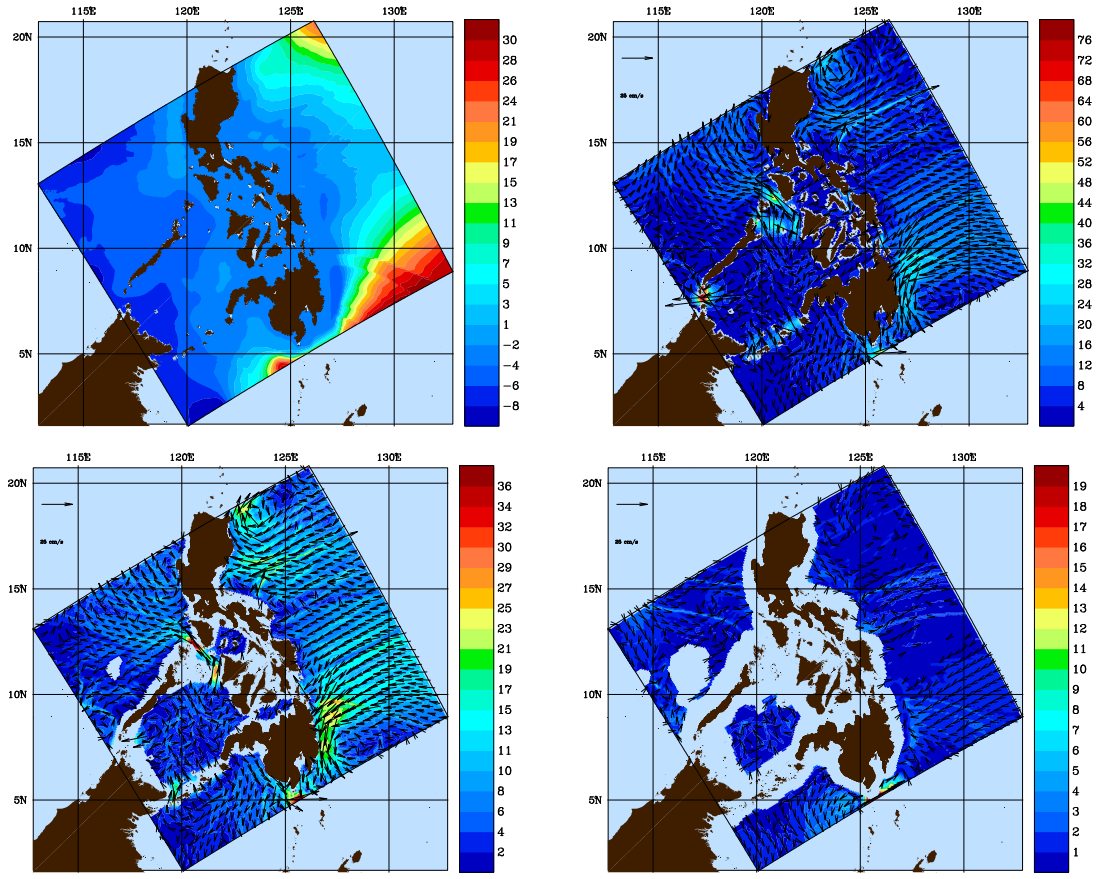

Figure C-32: Velocity estimation under geostrophic balance (weight functions based on the minimum vertical area) from field maps (WOA05) obtained using the SDE (Helmholtz equation) for field: (Top - Left) Streamfunction, Velocity at depths: (Top - Right) 0m; (Bottom - Left) 100m; (Bottom - Right) 1000m

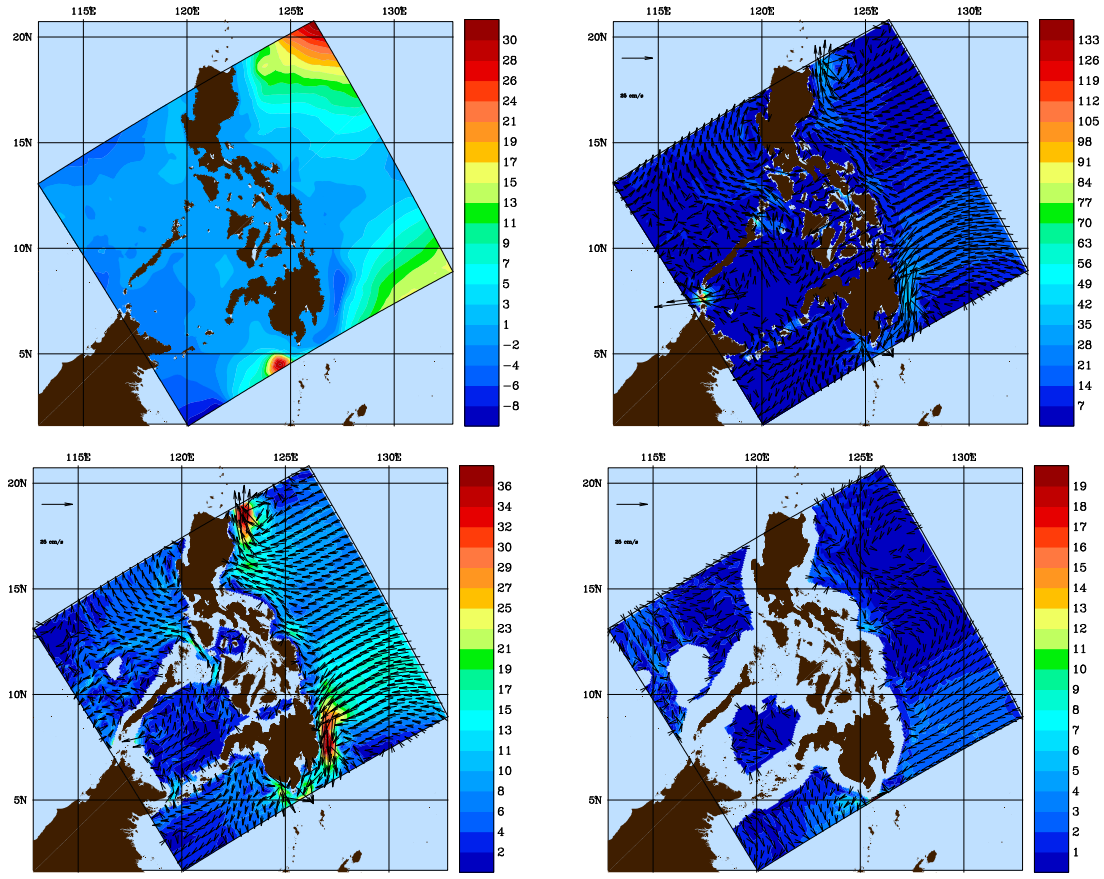

Figure C-33: Velocity estimation under geostrophic balance (weight functions based on the minimum distance) from field maps (WOA05) obtained using the FMM: (Top - Left) Streamfunction, Velocity at depths: (Top - Right) 0m; (Bottom - Left) 100m; (Bottom - Right) 1000m

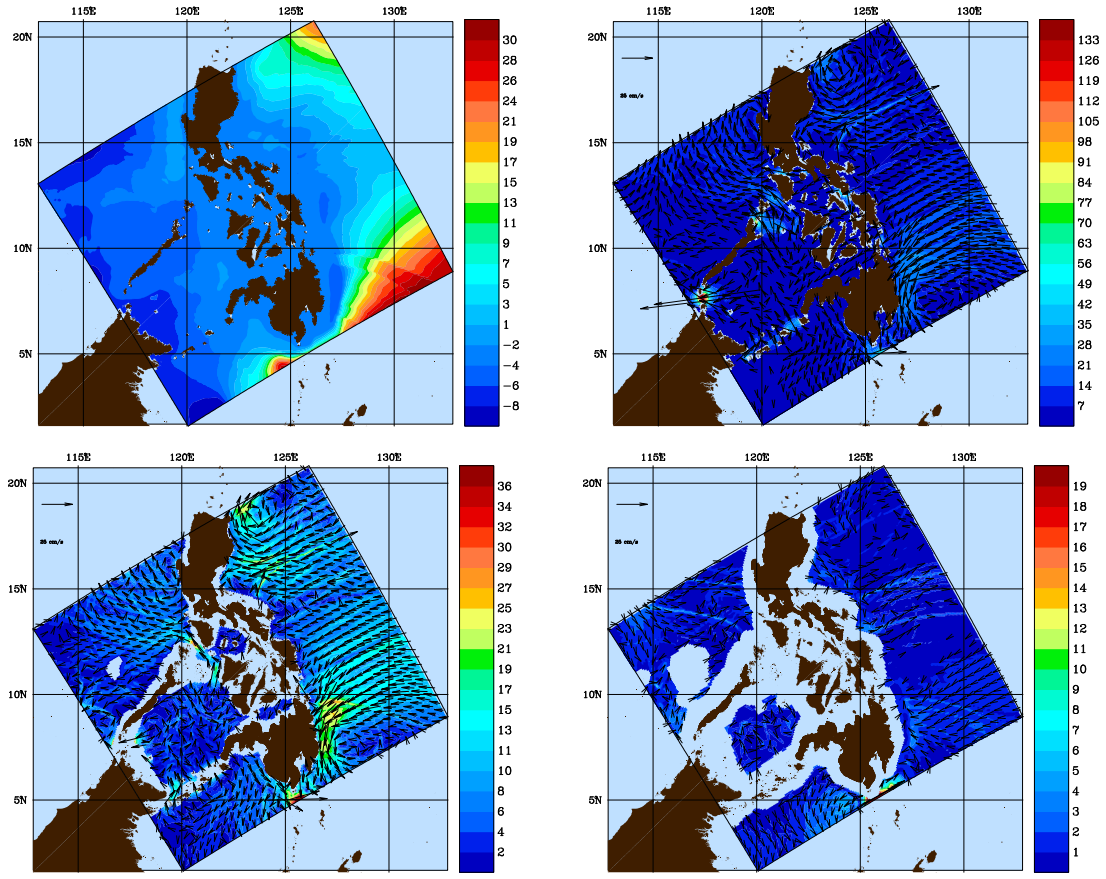

Figure C-34: Velocity estimation under geostrophic balance (weight functions based on the minimum distance) from field maps (WOA05) obtained using the SDE (Helmholtz equation) for field: (Top - Left) Streamfunction, Velocity at depths: (Top - Right) 0m; (Bottom - Left) 100m; (Bottom - Right) 1000m

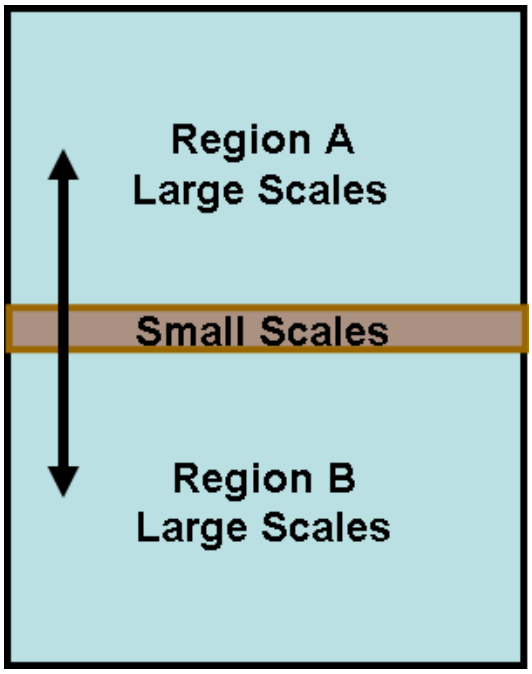

Figure C-35: Cartoon illustrating non-homogeneous scales in a continental shelf with a front having small scales in y-direction separating regions having large scales in y-direction

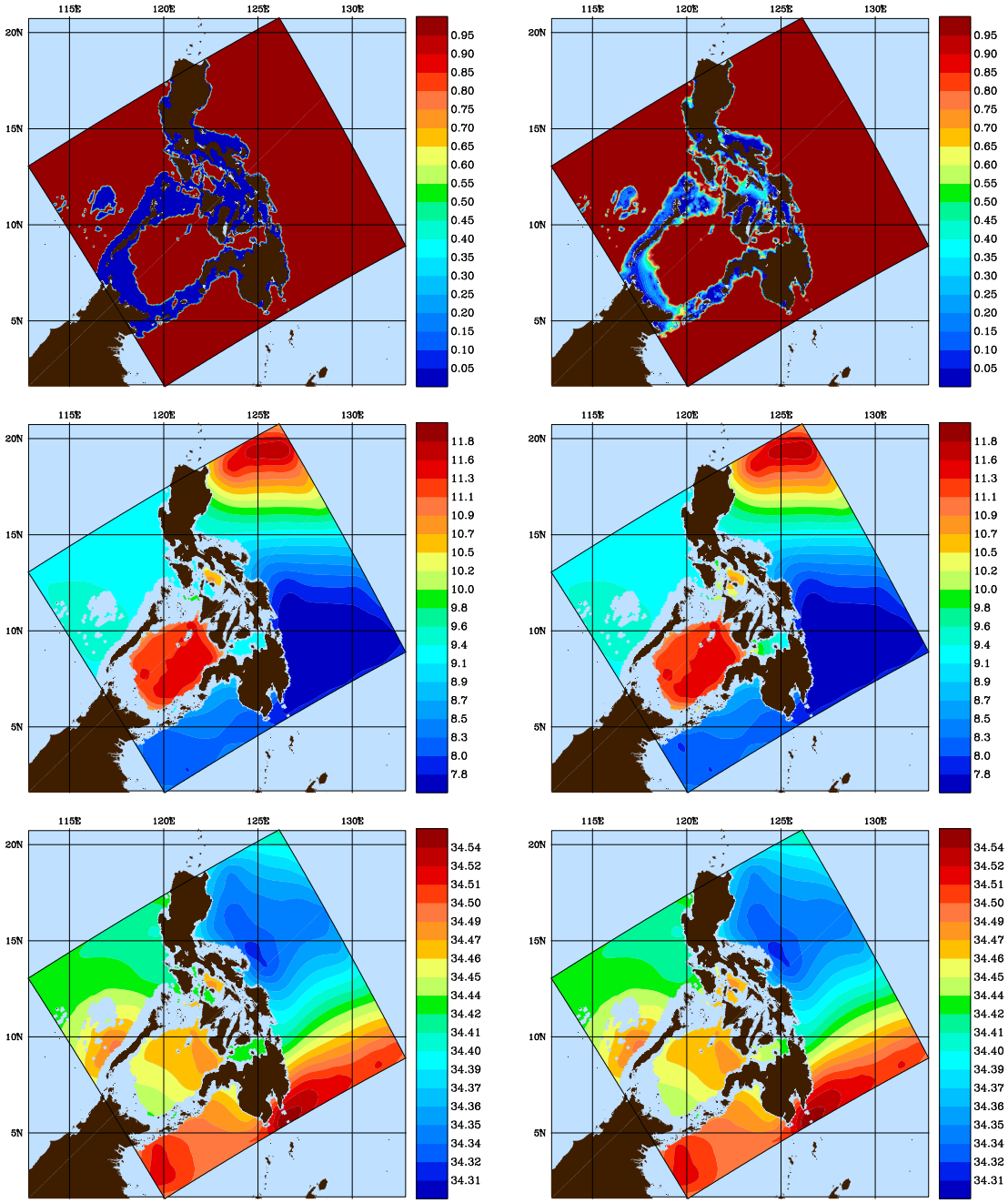

Figure C-36: Inclusion of bathymetry effects by modifying scalar speed function in Philippines Archipelago at a depth of 450m: (Top - Left) Regular scalar speed function (F1) with 0 for landforms and 1 for ocean; (Top - Right) Modified scalar speed function (F2) given by bathymetry / OA level; (Middle - Left) Temperature (^{o}C) field map based on F1; (Middle - Right) Temperature (^{o}C) field map based on F2; (Bottom - Left) Salinity (PSU) field map based on F1; (Bottom - Right) Salinity (PSU) field map based on F2

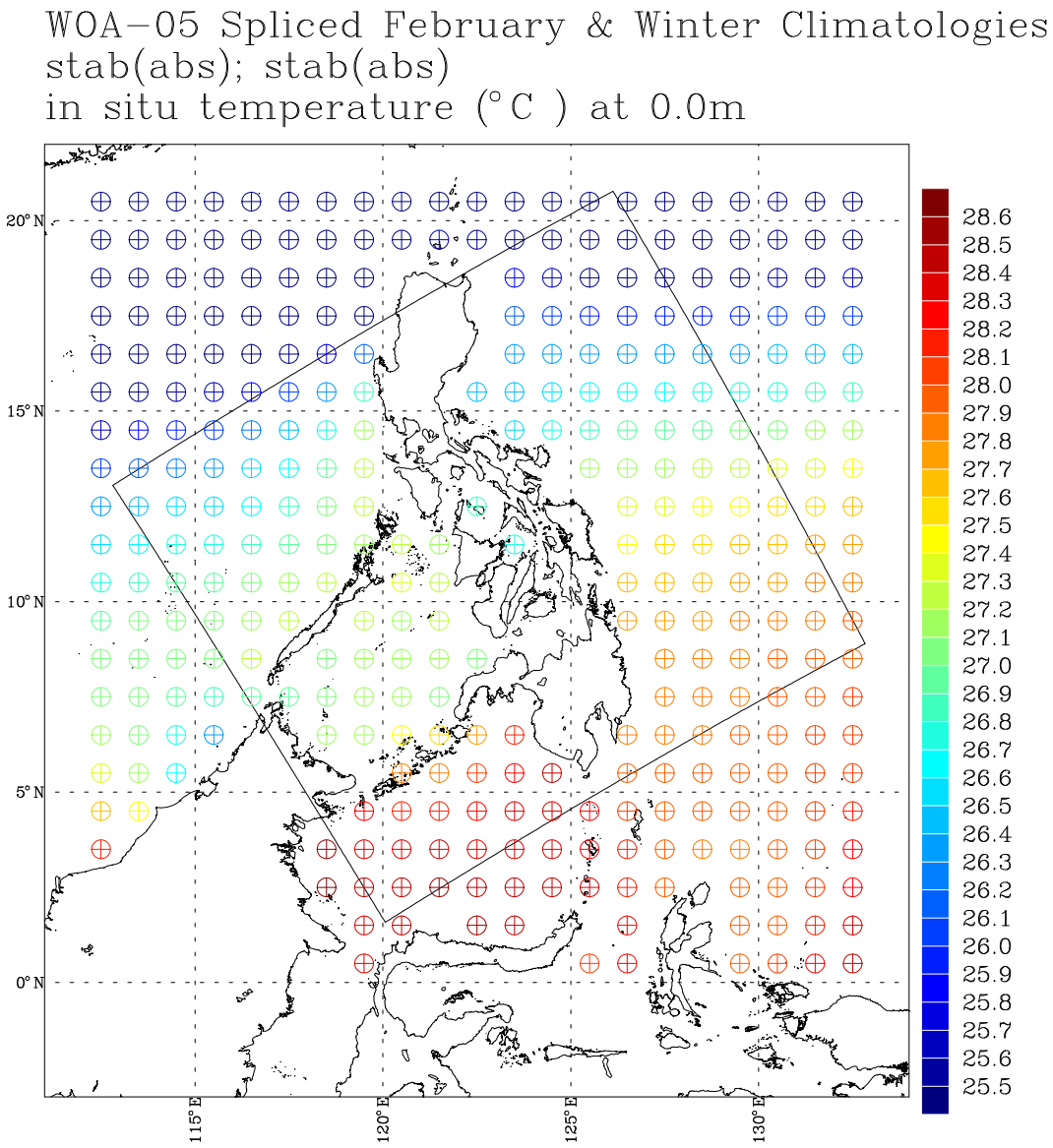

Figure C-37: World Ocean Atlas 2005 (Spliced February and Winter Climatology) in situ temperature (^{o}C) at 0.0m

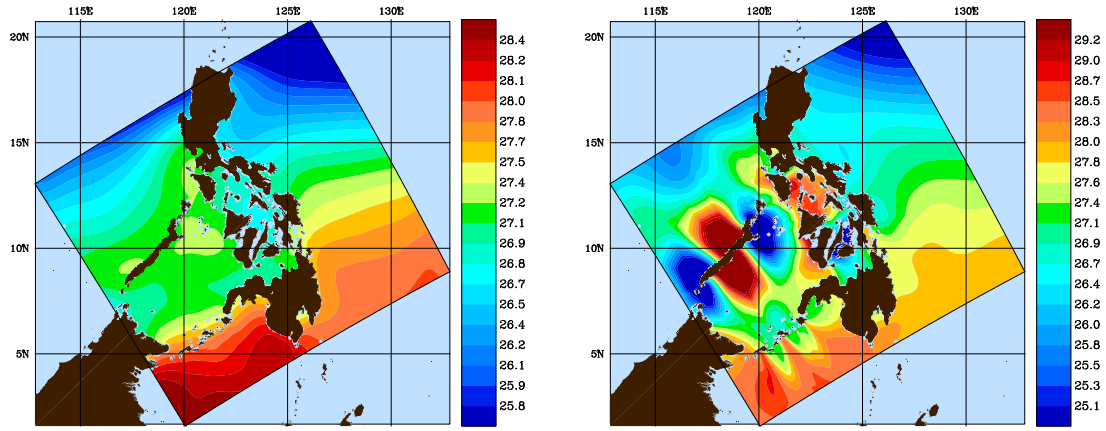

Figure C-38: Temperature (^{o}C) OA Fields using the Fast Marching Method at the surface (0m) using the following scales: (Left) $L_0 = 540Km$, $L_e = 180Km$; (Right) $L_0 = 1080Km$, $L_e = 360Km$

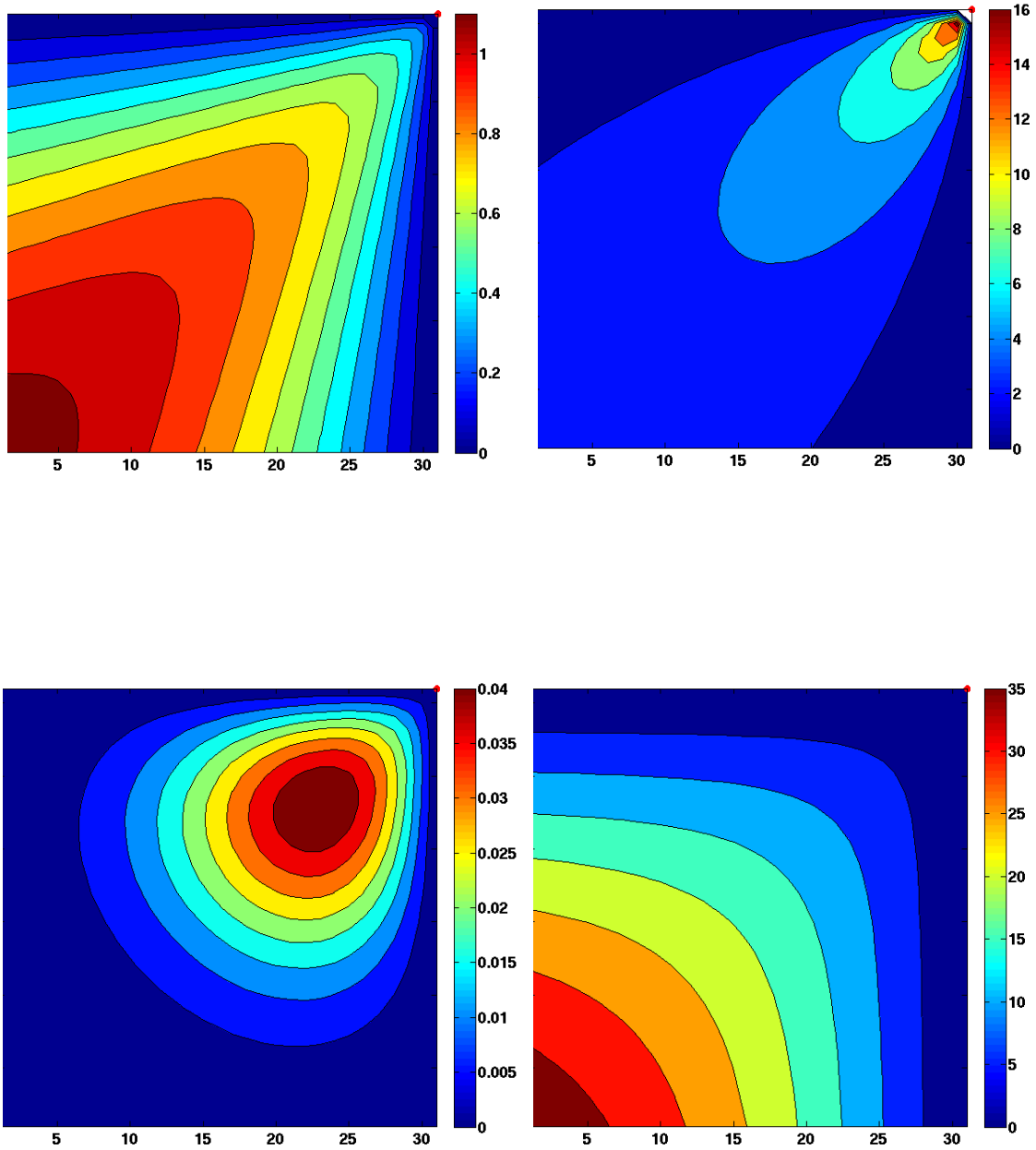

Figure C-39: Comparison between distance and correlation ($exp(\frac{-r^2}{2L^2}); L = 10$) obtained using the first order FMM and the Euclidean distance on a 30-by-30 domain without islands. (Top - Left) Difference in distance; (Top - Right) Normalized difference in distance; (Bottom - Left) Difference in correlation; (Bottom - Right) Normalized difference in correlation

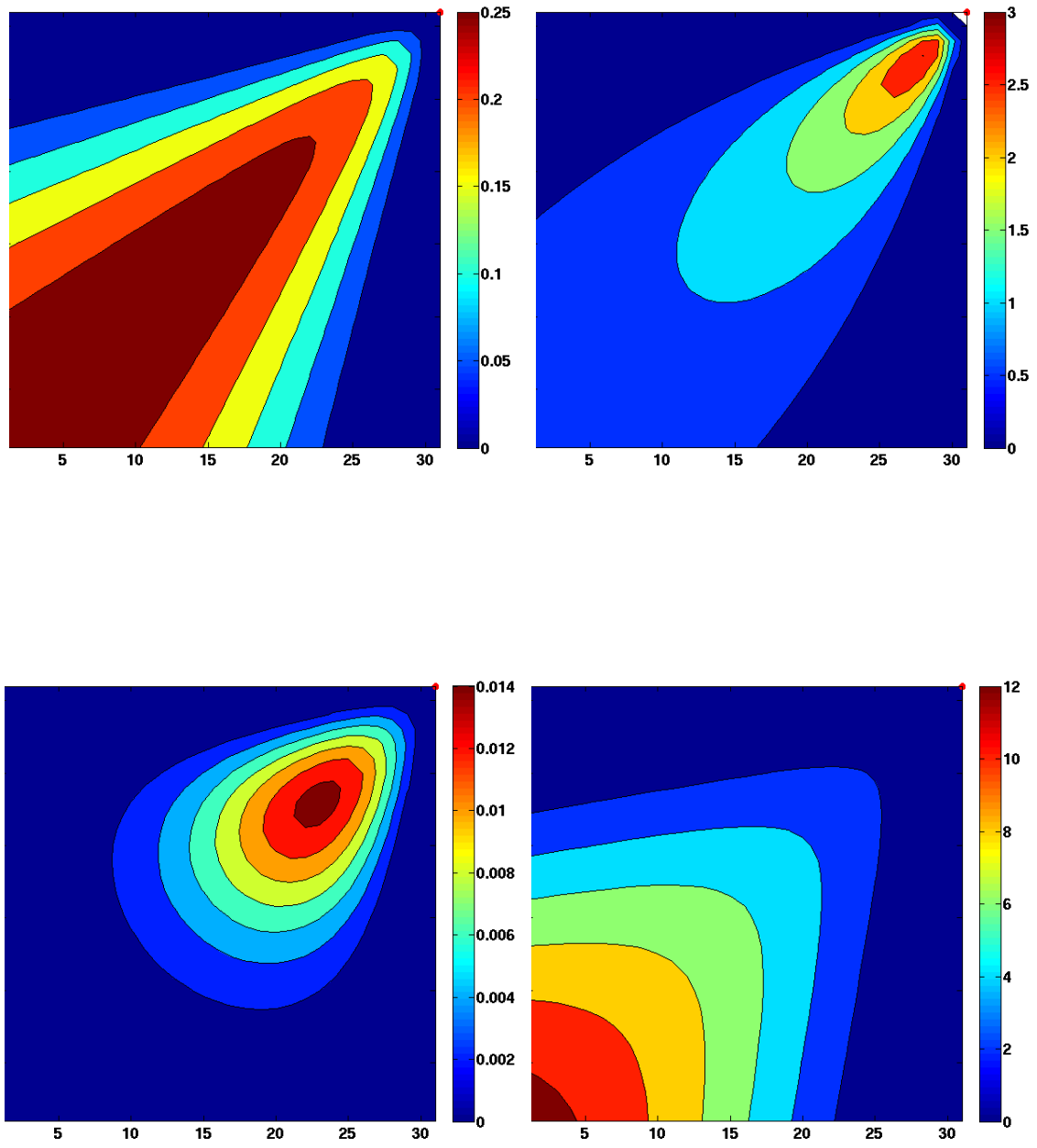

Figure C-40: Comparison between distance and correlation ($exp(\frac{-r^2}{2L^2}); L = 10$) obtained using the higher (second) order FMM and the Euclidean distance on a 30-by-30 domain without islands. (Top - Left) Difference in distance; (Top - Right) Normalized difference in distance; (Bottom - Left) Difference in correlation; (Bottom - Right) Normalized difference in correlation

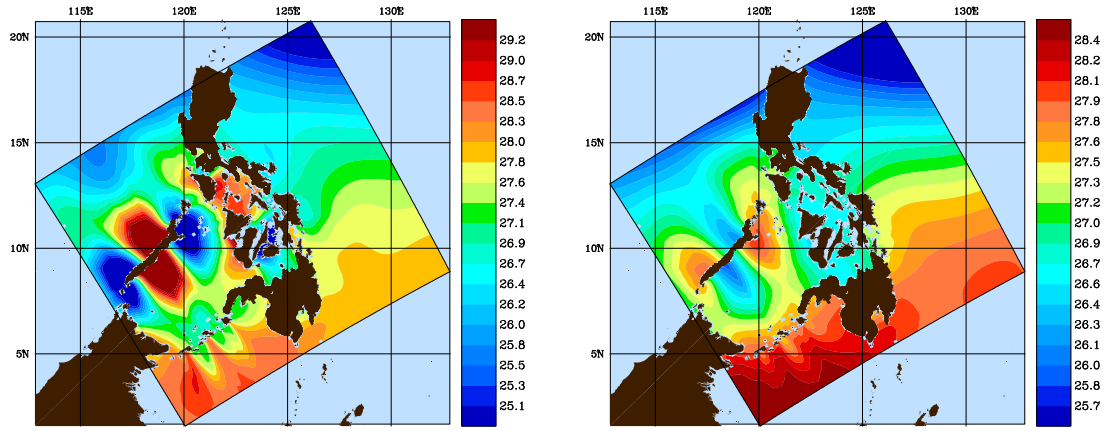

Figure C-41: Temperature (^{o}C) OA Fields at the surface (0m) (scales $L_0 = 1080Km$, $L_e = 360Km$) using: (Left) First Order FMM; (Right) Higher order FMM

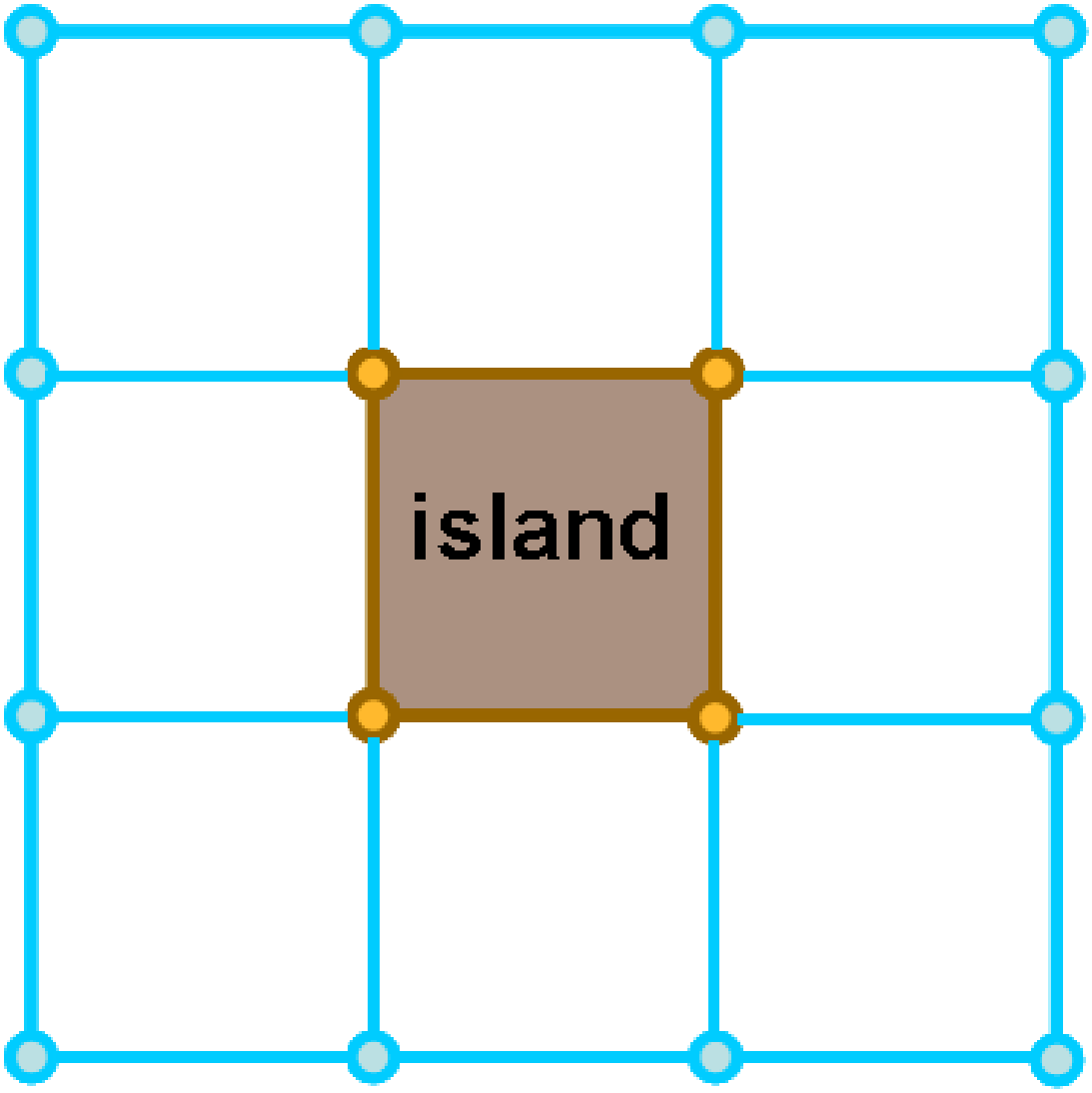

Figure C-42: Example of an idealized (multiply-connected) domain having an island

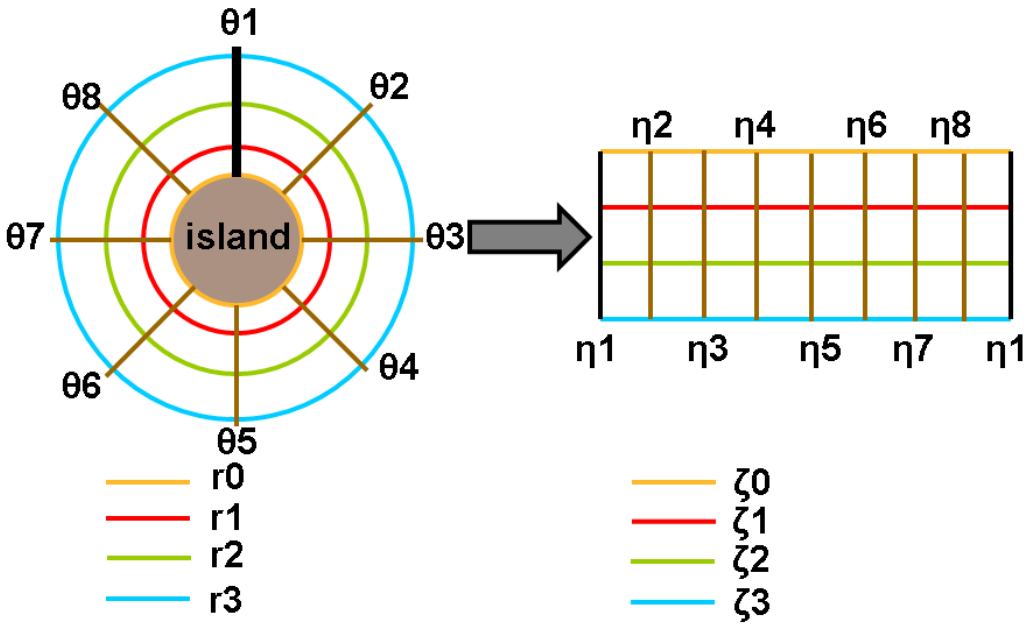

Figure C-43: Example illustrating the mapping and stretching in a domain with a circular island. Multiply-connected domain in the polar (r,θ) coordinates is mapped to a simply-connected rectangular domain in the curvilinear (ζ,η) coordinates.

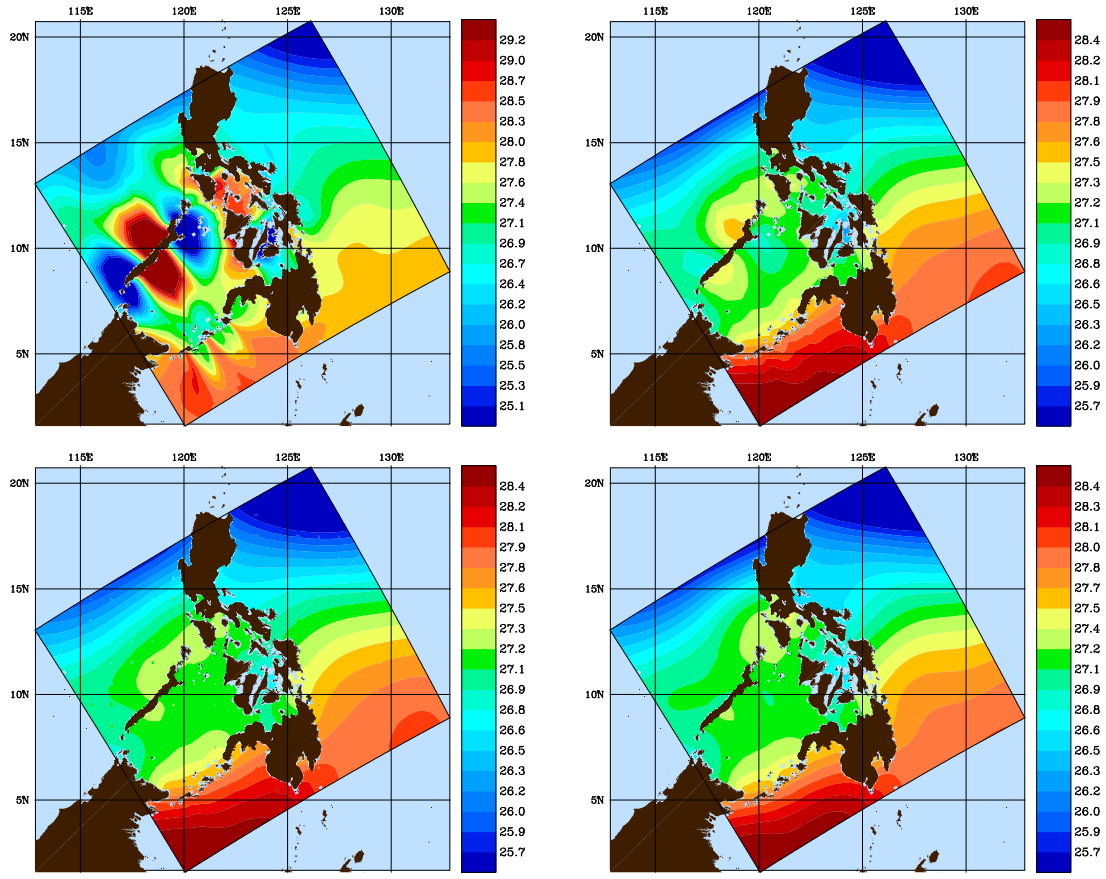

Figure C-44: Temperature (^{o}C) OA Fields at the surface (0m) (scales $L_0 = 1080Km$, $L_e = 360Km$) using: (Top - Left) FMM; (Top - Right) FMM and by discarding the problematic data; (Bottom - Left) FMM and by introducing process noise; (Bottom - Right) FMM and by dominant singular value decomposition (SVD) of a-priori covariance

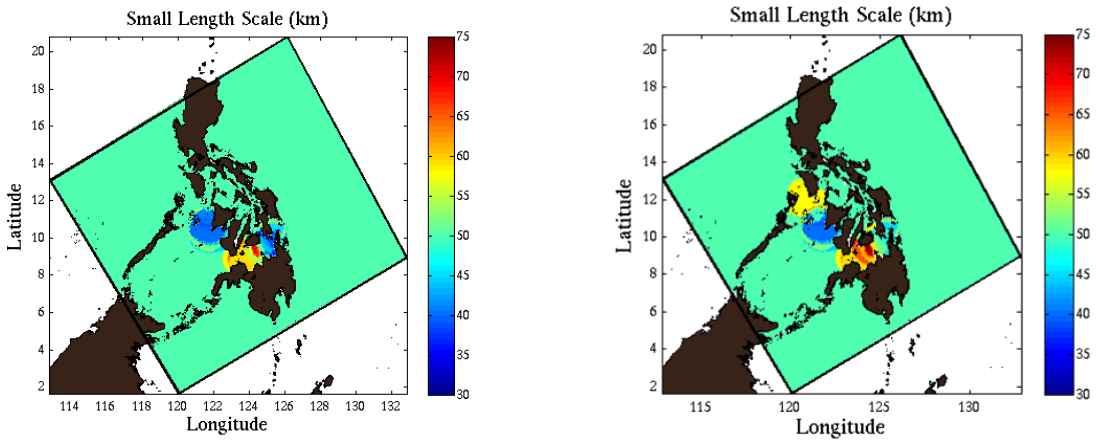

Figure C-45: Scale estimates for Philippines Archipelago from Melville exploratory cruise data (Summer 2007) on 26^{th} June 2007 (Left) and 15^{th} July 2007 (Right) using structure function

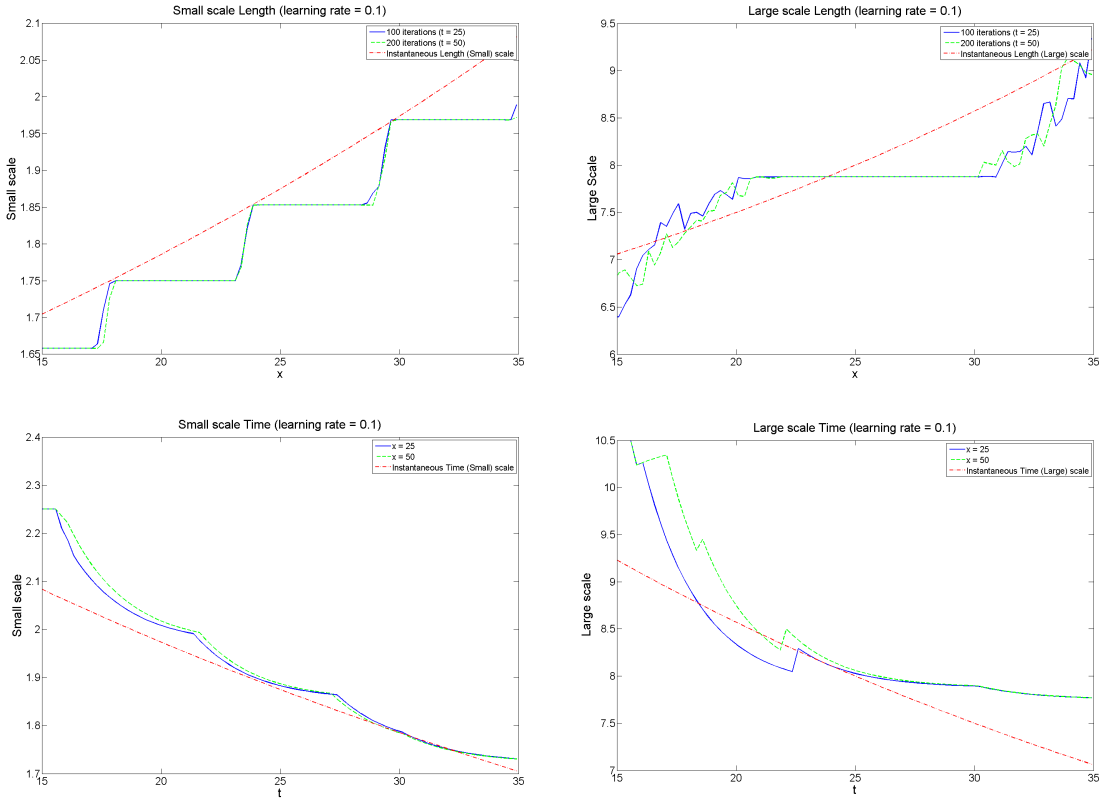

Figure C-46: Small and large length scales (Top) and time scales (Bottom) from the adaptive learning algorithm (learning rate = 0.1) based on STFT applied on the chirp signal data

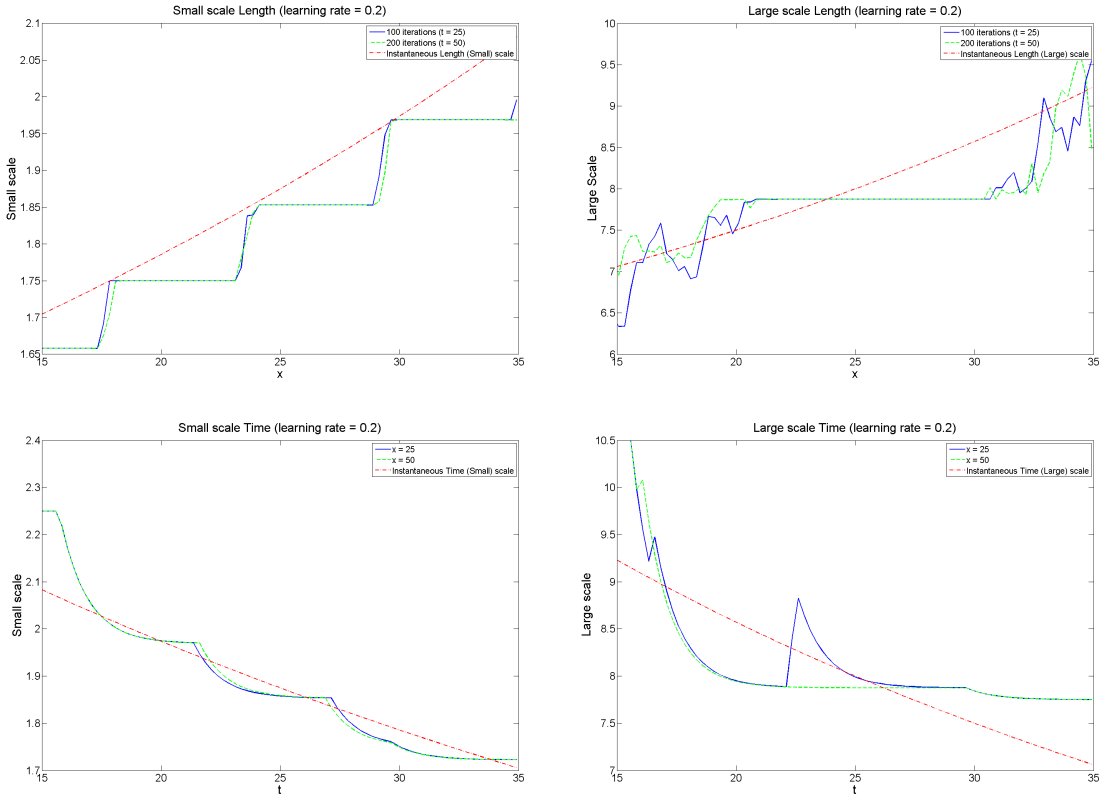

Figure C-47: Small and large length scales (Top) and time scales (Bottom) from the adaptive learning algorithm (learning rate = 0.2) based on STFT applied on the chirp signal data

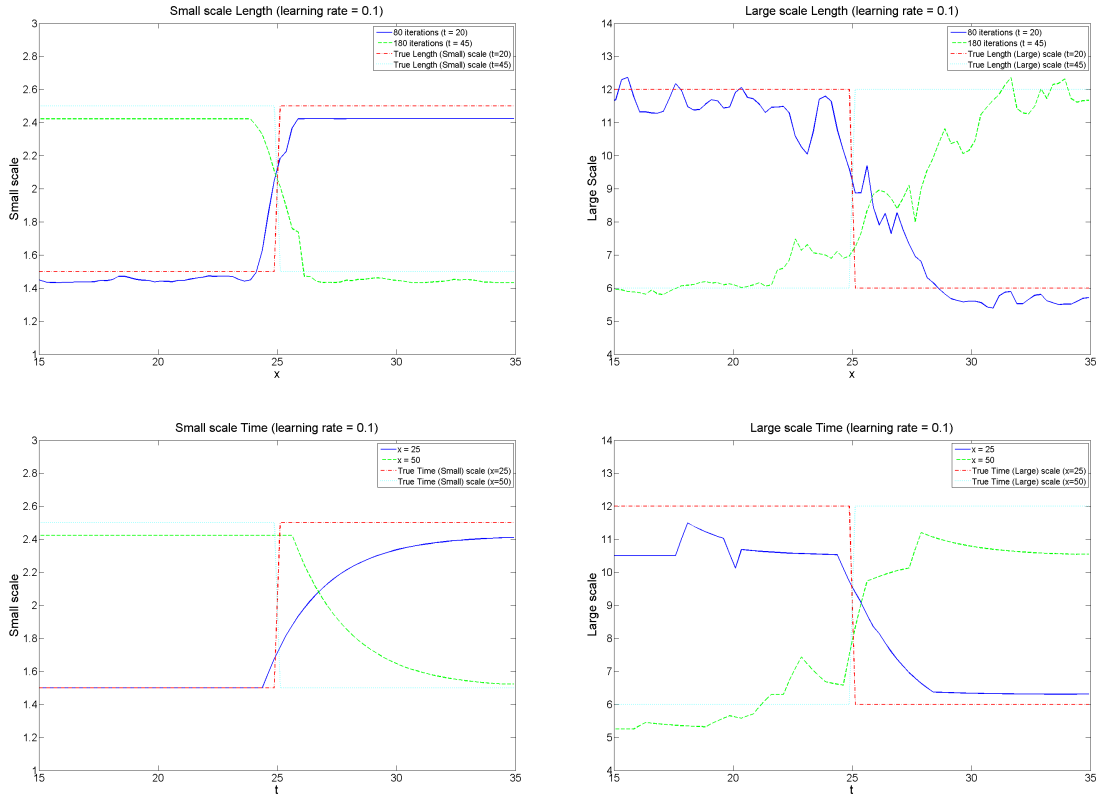

Figure C-48: Small and large length scales (Top) and time scales (Bottom) from the adaptive learning algorithm (learning rate = 0.1) based on STFT applied on Data Set 2

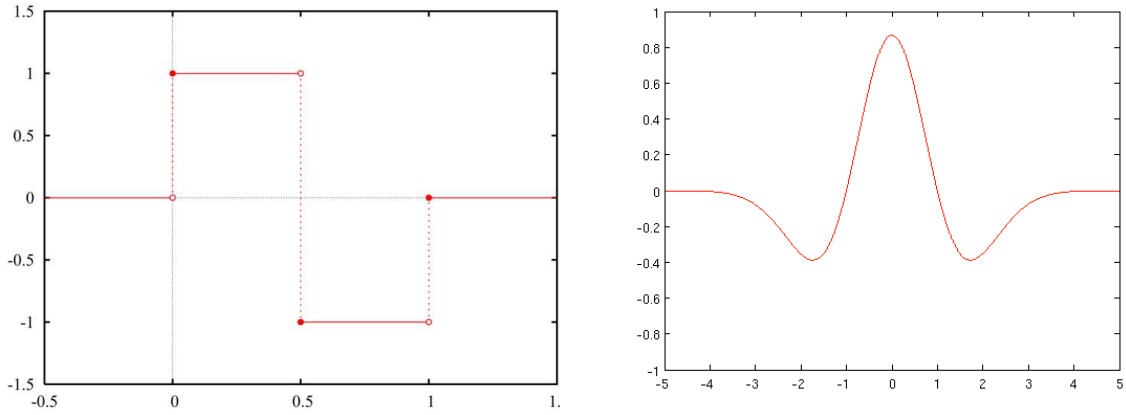

Figure C-49: Haar Wavelet (Left) and Mexican Hat Wavelet (Right) (Jansen and Oonincx, 2005)

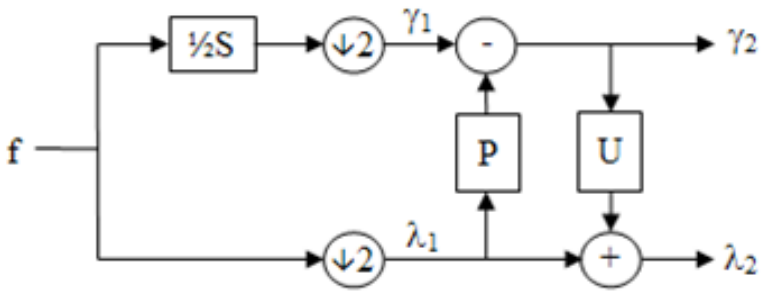

Figure C-50: Block diagram of second generation wavelet transform (Jansen and Oonincx, 2005)

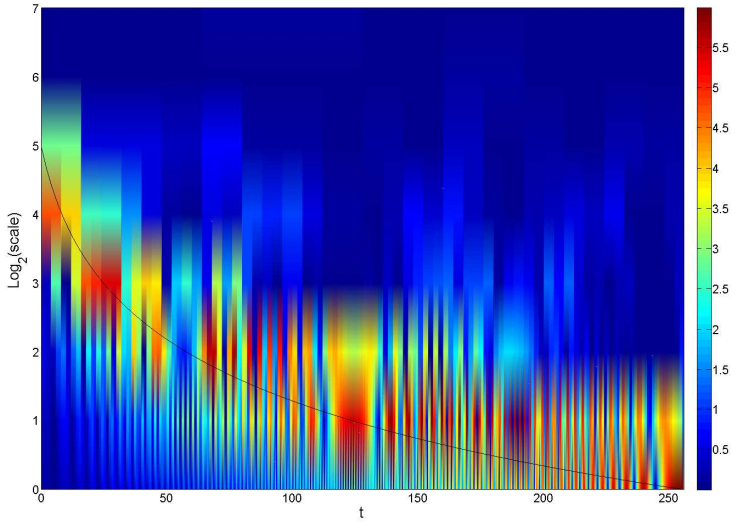

Figure C-51: Scale coefficients for idealized chirp signal using second generation wavelets (Lifting scheme corresponds to Haar Wavelet). Black line is the plot of instantaneous scale of the chirp signal varying with time.

Bibliography

Antonov, J. I., Levitus, S., Boyer, T. P., Conkright, M. E., OBrien, T. D., and Stephens, C. (1998a). World ocean atlas 1998 volume 1: Temperature of the atlantic ocean. *NOAA Atlas NESDIS 27. US Government Printing Office: Washington, DC.*

Antonov, J. I., Levitus, S., Boyer, T. P., Conkright, M. E., OBrien, T. D., and Stephens, C. (1998b). World ocean atlas 1998 volume 2: Temperature of the pacific ocean. *NOAA Atlas NESDIS 28. US Government Printing Office: Washington, DC.*

Antonov, J. I., Levitus, S., Boyer, T. P., Conkright, M. E., OBrien, T. D., and Stephens, C. (1998c). World ocean atlas 1998 volume 3: Temperature of the indian ocean. *NOAA Atlas NESDIS 29. US Government Printing Office: Washington, DC.*

Antonov, J. I., Locarnini, R. A., Boyer, T. P., Mishonov, A. V., and Garcia, H. E. (2006). World ocean atlas 2005, volume 2: Salinity, s. levitus (ed.). *NOAA Atlas NESDIS 62. US Government Printing Office: Washington, DC.*

Balgovind, R., Dalcher, A., Ghil, M., and Kalnay, E. (1983). A stochasticdynamic model for the spatial structure of forecast error statistics. *Monthly Weather Review*, 111:701–722.

Barnes, S. L. (1964). A technique for maximizing details in numerical weather map analysis. *Journal of Applied Meteorology*, 3:396–409.

Barnes, S. L. (1973). Mesoscale objective map analysis using weighted time series observations. *NOAA Technical Memorandum ERL NSSL-62.*

Barnes, S. L. (1994). Applications of the barnes objective analysis scheme, part iii: Tuning for minimum error. *Journal of Atmospheric and Oceanic Technology*, 11:1459–1479.

Battin, R. H. (1964). *Astronautical Guidance.* McGraw-Hill, New York.

Bertsimas, D. and Tsitsiklis, J. N. (1997). *Introduction to Linear Optimization.* Athena Scientific, Belmont, Massachusetts.

Bierman, G. J. (1977). *Factorization Methods for Discrete Sequential Estimation*. Academic Press, New York.

Boyer, T. P., Levitus, S., Antonov, J. I., Conkright, M. E., OBrien, T. D., and Stephens, C. (1998a). World ocean atlas 1998 volume 1: Temperature of the atlantic ocean. *NOAA Atlas NESDIS 30. US Government Printing Office: Washington, DC.*

Boyer, T. P., Levitus, S., Antonov, J. I., Conkright, M. E., OBrien, T. D., and Stephens, C. (1998b). World ocean atlas 1998 volume 2: Temperature of the pacific ocean. *NOAA Atlas NESDIS 31. US Government Printing Office: Washington, DC.*

Boyer, T. P., Levitus, S., Antonov, J. I., Conkright, M. E., OBrien, T. D., and Stephens, C. (1998c). World ocean atlas 1998 volume 3: Temperature of the indian ocean. *NOAA Atlas NESDIS 32. US Government Printing Office: Washington, DC.*

Boyer, T. P., Stephens, C., Antonov, J. I., Conkright, M. E., Locarnini, R. A., OBrien, T. D., and Garcia, H. E. (2002). World ocean atlas 2001 volume 2: Salinity, s. levitus (ed.). *NOAA Atlas NESDIS 50. US Government Printing Office: Washington, DC.*

Bresenham, J. E. (1965). Algorithm for computer control of a digital plotter. *IBM Systems Journal*, 4(1):25–30.

Bretherton, F. P., Davis, R. E., and Fandry, C. (1976). A technique for objective analysis and design of oceanographic instruments applied to mode-73. *Deep-Sea Research*, 23:559–582.

Brown, R. G. and Hwang, P. Y. C. (1997). *Introduction to Random Signals and Applied Kalman Filtering*. John Wiley & Sons, United Kingdom.

Burton, L. (2009). Modeling coupled physics and biology in ocean straits. *SM Thesis, Massachusetts Institute of Technology.*

Carter, E. and Robinson, A. (1987). Analysis models for the estimation of oceanic fields. *Journal of Atmospheric and Oceanic Technology*, 4(1):49–74.

Cebeci, T., Shao, J. P., Kafyeke, F., and Laurendeau, E. (2005). *Computational Fluid Dynamics for Engineers*. Springer.

Center, N. O. D. (2006). Operational oceanography group: Global temperature-salinity profile program. *U.S. Department of Commerce, National Oceanic and Atmospheric Administration, Maryland.*

Cho, Y., Shin, V., Oh, M., and Lee, Y. (1996). Suboptimal continuous filtering based on the decomposition of the observation vector. *Computers and Mathematics with applications*, 32(4):23–31.

Cossarini, G., Lermusiaux, P. F. J., and Solidoro, C. (2009). The lagoon of venice ecosystem: Seasonal dynamics and environmental guidance with uncertainty analyses and error subspace data assimilation. *Journal of Geophysical Research*.

Cressman, G. P. (1959). An operational objective analysis scheme. *Monthly Weather Review*, 87:329–340.

Daley, R. (1993). *Atmospheric Data Analysis*. Cambridge University Press.

Denman, K. L. and Freeland, H. J. (1985). Correlation scales, objective mapping and a statistical test of geostrophy over the continental shelf. *Journal of Marine Research*, 43:517–539.

Dolloff, J., Lofy, B., Sussman, A., and Taylor, C. (2006). Strictly positive definite correlation functions. *Proceedings of SPIE*, 6235.

Gamo, T., Kato, Y., Hasumoto, H., Kakiuchi, H., Momoshima, N., Takahata, N., and Sano, Y. (2007). Geochemical implications for the mechanism of deep convection in a semi-closed tropical marginal basin: Sulu sea. *Deep-Sea Research II*, 54:4–13.

Gandin, L. S. (1965). Objective analysis of meteorological fields. *Israel Program for Scientific Translations*.

Garcia, H. E., Locarnini, R. A., Boyer, T. P., and Antonov, J. I. (2006a). World ocean atlas 2005, volume 3: Dissolved oxygen, apparent oxygen utilization, and oxygen saturation, s. levitus (ed.). *NOAA Atlas NESDIS 63. US Government Printing Office: Washington, DC.*

Garcia, H. E., Locarnini, R. A., Boyer, T. P., and Antonov, J. I. (2006b). World ocean atlas 2005, volume 4: Nutrients (phosphate, nitrate, silicate), s. levitus (ed.). *NOAA Atlas NESDIS 64. US Government Printing Office: Washington, DC.*

Gordon, A. L. (2009). Philex: Regional cruise intensive observational period, leg 1 and 2 reports.

Grewal, M. S. and Andrews, A. P. (1993). *Kalman Filtering Theory and Practice*. Prentice Hall, New Jersey.

Haley, P. J. and Lermusiaux, P. F. J. (2009). In prep: Minimizing the inter-island transport.

Haley, P. J., Lermusiaux, P. F. J., Robinson, A. R., Leslie, W. G., Logoutov, O. G., Cossarini, G., Liang, X. S., Moreno, P., Ramp, S. R., Doyle, J. D., Bellingham, J., Chavez, F., and Johnston, S. (2008). Forecasting and reanalysis in the monterey bay/california current region for the autonomous ocean sampling network-ii experiment. *Deep Sea Research II*.

Hessler, G. (1984). Experiments with statistical objective analysis techniques for representing a coastal surface temperature field. *Boundary Layer Meteorology*, 28:375–389.

Jansen, M. and Oonincx, P. (2005). *Second Generation Wavelets and Applications*. Springer.

Lermusiaux, P. F. J. (1997). Error subspace data assimilation methods for ocean field estimation: Theory, validation and applications. *PhD Thesis, Harvard University*.

Lermusiaux, P. F. J. (1999a). Data assimilation via error subspace statistical estimation. part ii: Middle atlantic bight shelfbreak front simulations and esse validation. *Monthly Weather Review*, 127:1408–1432.

Lermusiaux, P. F. J. (1999b). Estimation and study of mesoscale variability in the strait of sicily. *Dynamics of Atmospheres and Oceans*, 29:255–303.

Lermusiaux, P. F. J. (2002). On the mapping of multivariate geophysical fields: Sensitivities to size, scales, and dynamics. *Journal of Atmospheric and Oceanic Technology*, 19:1602–1637.

Lermusiaux, P. F. J. (2007). Adaptive modeling, adaptive data assimilation and adaptive sampling. *Physica D*, 230:172–196.

Lermusiaux, P. F. J., Anderson, D. G. M., and Lozano, C. J. (2000). On the mapping of multivariate geophysical fields: Error and variability subspace estimates. *Quarterly Journal of the Royal Meteorological Society*, 126:1387–1429.

Lermusiaux, P. F. J., Lozano, C. J., and Anderson, D. G. (1998). On the mapping of multivariate geophysical fields: studies of the sensitivity to error subspace parameters. *Harvard Open Ocean Model Report No. 58, Harvard University*.

Lermusiaux, P. F. J. and Robinson, A. R. (1999). Data assimilation via error subspace statistical estimation. part i: Theory and schemes. *Monthly Weather Review*, 127:1385–1407.

Levitus, S. (1982). Climatological atlas of the world ocean. *NOAA Professional Paper 13. US. Government Printing Office: Washington,DC*.

Levitus, S. and Boyer, T. P. (1994). World ocean atlas 1994: Volume 4: Temperature. *NOAA Atlas NESDIS 4. US Government Printing Office: Washington, DC*.

Levitus, S., Burgett, R., and Boyer, T. P. (1994). World ocean atlas 1994, volume 3: Salinity. *NOAA Atlas NESDIS 3. US Government Printing Office: Washington, DC*.

Locarnini, R. A., Mishonov, A. V., Antonov, J. I., Boyer, T. P., and Garcia, H. E. (2006). World ocean atlas 2005, volume 1: Temperature, s. levitus (ed.). *NOAA Atlas NESDIS 61, U.S. Government Printing Office: Washington, D.C.*

Logoutov, O. G. (2008). A multigrid methodology for assimilation of measurements into regional tidal models. *Ocean Dynamics*, 58:441–460.

Lynch, D. R. and McGillicuddy, D. J. (2001). Objective analysis for coastal regimes. *Continental Shelf Research*, 21:1299–1315.

Maybeck, P. S. (1979). *Stochastic Models, Estimation and Control Vol. 1*. Academic Press, New York.

Osher, S. and Sethian, J. A. (1988). Fronts propagating with curvature-dependent speed: algorithms based on hamilton-jacobi formulations. *Journal of Computational Physics*, 79(1):12–49.

Papoulis, A. (1991). *Probability, Random Variables and Stochastic Processes*. McGraw-Hill.

Paris, C. B., Cowen, R. K., Lwiza, K. M. M., Wang, D. P., and Olson, D. B. (2002). Multivariate objective analysis of the coastal circulation of barbados, west indies: implication for larval transport. *Deep-Sea Research I*, 49:1363–1386.

Parrish, D. F. and Cohn, S. E. (1985). A kalman filter for a two-dimensional shallow-water model: Formulation and preliminary experiments. *Office Note 304, U.S. Department of Commerce, NOAA, NWS, NMC*.

Pedlosky, J. (1987). *Geophysical Fluid Dynamics*. Springer.

Plackett, R. L. (1950). Some theorems in least squares. *Biometrika*, 37(1-2):149–157.

Ruoy, E. and Tourin, A. (1992). A viscosity solutions approach to shape from shading. *SIAM Journal on Numerical Analysis*, 29:867–884.

Sedgewick, R. (1988). *Algorithms*. Addison-Wesley.

Selvadurai, A. P. S. (2000). *Partial Differential Equations in Mechanics*. Springer.

Sethian, J. A. (1996). A fast marching level set method for monotonically advancing fronts. *Proceedings of the National Academy of Sciences*, 93(4):1591–1595.

Sethian, J. A. (1999a). Fast marching methods. *SIAM Review*, 41(2):199–235.

Sethian, J. A. (1999b). *Level Set Methods and Fast Marching Method*. Cambridge University Press, Cambridge, United Kingdom.

Stacey, M. W., Pond, S., and LeBlond, P. H. (1988). An objective analysis of the low-frequency currents in the strait of georgia. *Atmosphere-Ocean*, 26(1):1–15.

Stephens, C., Antonov, J. I., Boyer, T. P., Conkright, M. E., Locarnini, R. A., OBrien, T. D., and Garcia, H. E. (2002). World ocean atlas 2001 volume 1: Temperature, s. levitus (ed.). *NOAA Atlas NESDIS 49. US Government Printing Office: Washington, DC.*

Sweldens, W. (1998). The lifting scheme: A construction of second generation wavelets. *SIAM Journal on Mathematical Analysis*, 29(2):511–546.

Takei, R. (2006). Dijkstra's and fast marching method for optimal path planning. *Report, University of California, Los Angeles*.

Williams, J. W. J. (1964). Algorithm 232 - heapsort. *Communications of the ACM*, 7(6):347348.

Wunsch, C. (1996). *The Ocean Circulation Inverse Problem*. Cambridge University Press, Cambridge, United Kingdom.

Xu, J., Lermusiaux, P. F. J., Haley, P. J., Leslie, W. G., and Logoutov, O. G. (2008). Spatial and temporal variations in acoustic propagation during the plusnet07 exercise in dabob bay. *Proceedings of Meetings on Acoustics (POMA), 155th Meeting Acoustical Society of America*, 4.

Yaglom, A. M. (1987). *Correlation theory of stationary and related random functions I.* Springer-Verlag.

Yaglom, A. M. (2004). *An Introduction to the Theory of Stationary Random Functions (Dover Phoenix Editions)*. Dover.